2-15-2019

Thermal management of photovoltaic panel using PCM for improved efficiency and power output

Joyjit Ghosal
University of Windsor

Thermal management of photovoltaic panel using PCM for improved efficiency and power output

by

Joyjit Ghosal

A Thesis

Submitted to the Faculty of Graduate Studies

Through Mechanical, Automotive, and Materials Engineering

In Partial Fulfilment of the Requirements for

The Degree of Master of Applied Science at the

University of Windsor

Windsor, Ontario, Canada

2019

Thermal management of photovoltaic panel using PCM for improved efficiency and power output.

by

Joyjit Ghosal

APPROVED BY:

_____

X. Nie

Department of Mechanical, Automotive and Materials Engineering

_____

G. Rankin

Department of Mechanical, Automotive and Materials Engineering

_____

A. Fartaj, Advisor

Department of Mechanical, Automotive and Materials Engineering

February 14, 2019

Declaration of Originality

I hereby certify that I am the sole author of this thesis and that no part of this thesis has been published or submitted for publication.

I certify that, to the best of my knowledge, my thesis does not infringe upon anyone's copyright nor violate any proprietary rights and that any ideas, techniques, quotations, or any other material from the work of other people included in my thesis, published or otherwise, are fully acknowledged in accordance with the standard referencing practices.

I declare that this is a true copy of my thesis, including any final revisions, as approved by my thesis committee and the Graduate Studies office, and that this thesis has not been submitted for a higher degree to any other University or Institution.

Abstract

Use of solar energy for electric power generation by means of photovoltaic (PV) cells have shown tremendous growth in recent years due to increased effort to decarbonise the economy as well as for sustainable growth of energy supply. However, low conversion efficiency has been a major issue for commercial application of PV system. Past research has shown that the conversion efficiency drops even further at high operating temperature. Various thermal management techniques to cool the PV cells have shown an increase in cell efficiency.

In this investigation, thermal regulation experiments are carried out to improve conversion efficiency and power output at high operating temperatures by using paraffin wax based phase change materials (PCM) as a means of thermal management of silicon PV cell. Phase change materials absorb a large amount of heat isothermally during phase change and keep the PV panel at lower temperature during change of phase. A PCM container is devised for retrofitting to commercial PV panel. Fins are fitted inside the container as well as on the external back surface to improve thermal conductivity of the PCM as well as enhance heat transfer away from the container. The effect of placing fins for enhancement of heat transfer from the PV to PCM and PCM to environment is studied. Results indicate a decrease in average cell temperature and an enhancement in efficiency by proposed configurations of fins. Results indicate a substantial drop in average cell temperature as compared to a reference PV cell with no PCM. An increase in cell voltage output and efficiency was also noticed.

Dedicated to –

To my beloved parents, Sujit Ghosal and Archana Ghosal for their love, support and sacrifice.

Acknowledgement

At the very outset and foremost I would like to express my most sincere gratitude and thanks to my supervisor Dr. Amir Fartaj for kindly providing me the opportunity to work on this thesis project and for being a guiding light throughout the course of this thesis. His utmost patience, perseverance, resourcefulness and tireless supervision have made possible the completion of this project. It has been an absolute honour to have worked with him which has taught me a great deal about impeccable professional and honourable conduct as well invaluable knowledge about engineering concepts and principles.

I would also like to thank my thesis committee members Dr. Gary Rankin and Dr. Xueyuan Nie for their critical review and valuable advice. I would like to extend my gratitude to Dr. Farid Bahiraei for his valuable suggestions. Special thanks to Dr. Shahram Fotowat for his valuable insights and assistance with the experimental setup at various stages of the work. I would also like to thank Serena Askar for her valuable suggestions and help.

Last but not least, I would like to thank the Department of Mechanical, Materials and Automotive Engineering for Graduate Assistantship (GA) opportunity, special thanks to the secretarial services of Ms. Angela Haskell and all faculty and staff members of the Department of Mechanical, Materials and Automotive Engineering and the Faculty of Graduate Studies for their help.

Table of Content

List of Figures

List of Tables

Nomenclature

A	Frontal area of PV, PCM (m^2)
B	Bias error in measurement
C_P	Specific heat at constant pressure (J/kg/K)
G	Intensity of incident radiation (W/m^2)
G_T	Total global radiation
h_1	Heat transfer coefficient (PV front surface) ($W/m^2/K$)
h_2	Heat transfer coefficient (PV back surface), ($W/m^2/K$)
I	Current (Ampere)
I_{sc}	Short circuit current (Ampere)
k	Thermal conductivity (J/m/K)
L	Latent heat of fusion/solidification (J/kg)
m	Mass (kg)
P	Power (Watt)
P_{out}	Electrical power output of the PV panel
P_{in}	Power input to the PV panel (Watt)
P_m ,P_{max}	Power at maximum power point (Watt)
q	Heat flux (W/m^2)
R	Thermal resistance , Electrical Resistance
R_L	Load resistance
T	Temperature (K)
$T_{ambience}$	Ambient temperature (K)
$T_{surrounding}$	Temperature of the surrounding environment (K)
T_m	Melting temperature (K)
t	Time (Seconds)
V	Voltage (Volt)
V_{oc}	Open circuit voltage (Volt)

Symbols for Uncertainty Analysis

$B_{parameter}$	Total bias error in the parameter based on elemental bias errors, B_1 , B_2 , B_3.
$P_{parameter}$	Precision error in the parameter
$U_{parameter}$	Uncertainty associated with a parameter

Greek Letters

α_s	Absorptance of panel for solar radiation (dimensionless)
τ_{pv}	Transmittance of PV panel top layer(dimensionless)
ε_{glass}	Emissivity of glass top cover of PV (dimensionless)
η	Conversion efficiency of PV panel (dimensionless)
β	Temperature coefficient of PV conversion efficiency (%/K)
γ	Temperature coefficient of power of PV panel (%/K)
ρ	Density (kg/m^3), Reflectivity (dimensionless)
Δx	Thickness of PV cell component layer (m)
Δt	Time step (Seconds)
σ	Stephen-Boltzmann constant (W/m^2/K^4)

Subscripts

amb.	Ambient
m, max	Maximum
i	i-th layer in PV cell
ref	Reference condition
equiv.	Equivalent

Abbreviations

BIPV	Building Integrated Photovoltaic cell
CAAGR	Compound Annual Growth Rate
CSP	Concentrated Solar Power
EVA	Ethylene Vinyl Acetate
Gt	Giga ton
IEA	International Energy Agency
MT	Million Ton
m.p.	Melting point (^{0}C)
Mtoe	Million ton of oil equivalent
OECD	Organisation for Economic Cooperation and Development
PCM	Phase Change Material
PV	Photo-Voltaic
PV/T	Photovoltaic-Thermal
RSS	Root Sum Squares
STC	Standard Test Condition
WEO	World Energy Outlook

Chapter 1: Introduction

1.1. Background

Generation and use of energy form the backbone of modern civilisation. However, increased awareness about global warming and its harmful effects on the environment has reinvigorated the interest to pursue sustainable clean growth. This has prompted research on improving existing renewable energy technologies as well as developing new technologies for energy generation. Paris Agreement on climate change is in force from Nov. 2016. This agreement is essentially an agreement about one of the most relevant issues of modern times - that of climate change and energy security. Growth in energy-related CO_2 emissions stalled completely in 2016 (Figure 1.1). It has been made possible due to increase in conversion efficiency of conventional energy sources and chiefly due to expanded use of renewable energy the world over.

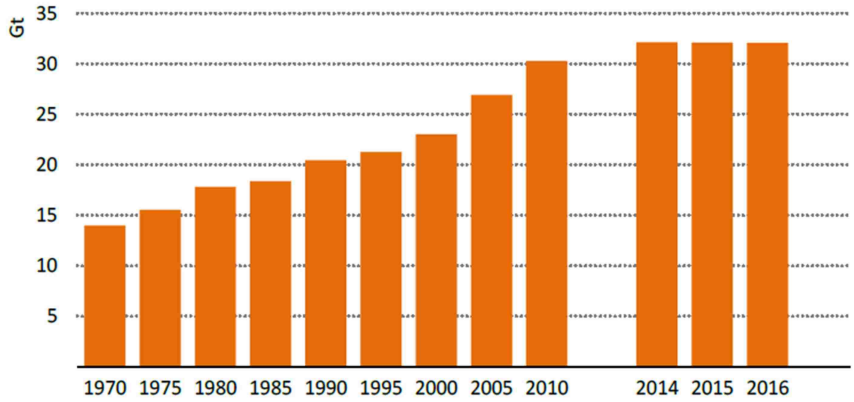

Figure 1.1 Global energy related CO_2 emission [1]

International Energy Agency (IEA) has projections of electricity generation growth through 2040 by fuel type (annualized growth rate = 2.0%) as furnished in Table 1.1. It is observed that the contribution from renewable energy sources increases from about 6% to slightly over 10%, but overall the generation mix is not substantially different to what it is now.

Some European countries announced plans to phase out coal-fired power completely [1]. They include France (by 2023), the United Kingdom (by 2025) and Finland (by 2030). The United Kingdom and France both proposed an outright ban on sales of new diesel and gasoline vehicles by 2040 [1].

Likewise, Canada also responded to reduce greenhouse gas emission in line with the Paris agreement. On October 3, 2016 the Government of Canada proposed the pan-Canadian framework on clean growth and climate change. Two important core objectives of the framework are to meet Canadian emission targets and to promote innovation and growth by increasing sustainable technology development. A direct consequence of the framework is the carbon pricing due to be implemented in 2018.

Table 1.1 World primary energy demand by fuel in the new policy scenario (Mtoe)[1]

	2000	2014	2020	2025	2030	2035	2040	CAAGR* 2014-2040
Coal	2 316	3 926	3 906	3 955	4 039	4 101	4 140	0.2%
Oil	3 669	4 266	4 474	4 577	4 630	4 708	4 775	0.4%
Gas	2 071	2 893	3 141	3 390	3 686	4 011	4 313	1.5%
Nuclear	676	662	796	888	1 003	1 096	1 181	2.3%
Hydro	225	335	377	420	463	502	536	1.8%
Bioenergy**	1 026	1 421	1 543	1 633	1 721	1 804	1 883	1.1%
Other renewables	60	181	339	478	643	835	1 037	6.9%
Total	10 042	13 684	14 576	15 340	16 185	17 057	17 866	1.0%

*Compound average annual growth rate. ** Includes the traditional use of solid biomass and modern use of bioenergy.

Estimated capacity additions in various sectors of energy generation in the year 2016 through 2040 are shown in Figure 1.2. The correponding capacity addition during the period 2010-2016 is also shown for comparison. It is observed that capacity addition from coal power was 65 GW during 2010-2016 in 6 years. However, during the period of 2016-2040, in 24 years, the projected estimate is shown to come down to only 16 GW. The corresponding figures for renewable enrgy are 128 GW and 160 GW. Out of the renewable energy capacity addition, solar PV capacity addition in the period 2016-2040 has been projected to be an astounding 74 GW compared to the value of 39 GW during 2010-2016.

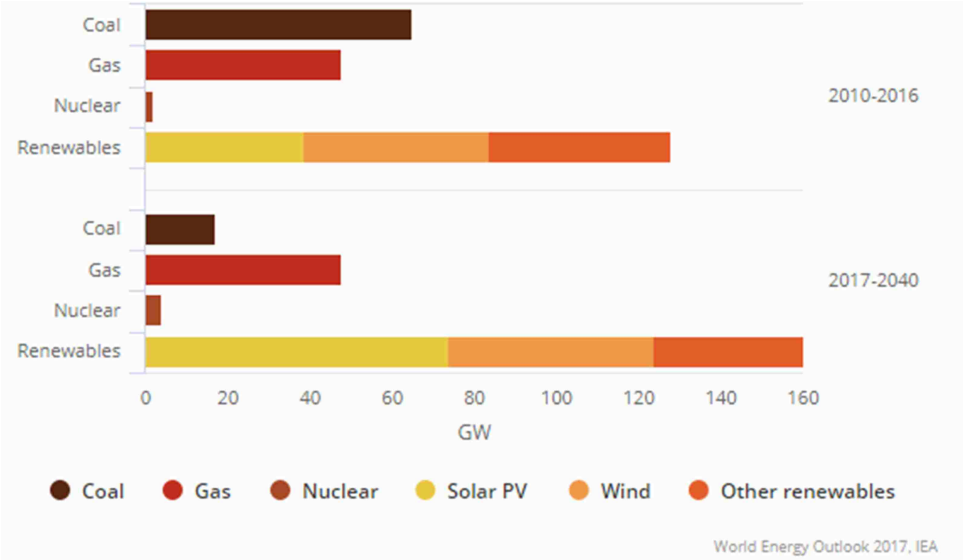

Figure 1. 2 Global Average Net Capacity Addition by type of Energy Source [1]

By 2040, The world power generation capacity mix in the new policy scenario (Figure 1.3) indicates a staggering 26% of the total generation coming from the combined solar and wind power alone with almost equal share of each.

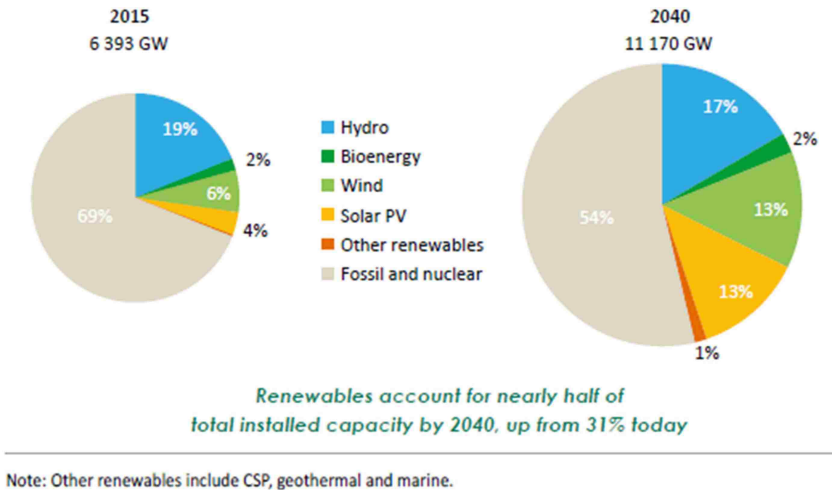

Figure 1.3 Present and projected world power generation capacity mix [1]

A major milestone was achieved in 2015, when the renewable energy industry had a capacity addition, exceeding more than from fossil fuels and nuclear fuel. It is predicted that the total renewable energy generation will reach 5170 GW in 2040 and become the largest source of electricity supply before 2030.

1.2 Solar Power Scenario and Photovoltaic (PV) Cell

Among renewable energy sources, solar energy has traditionally being viewed as one of the most promising of all sources. Solar PV annual additions surpassed those of wind power for the first time in 2015, with more than 70 GW coming on line, some 50% higher than the previous year. PV's share of global electricity will reach 16% by 2050 with a projected PV capacity of 4600 GW. Impetus for current and projected rapid growth is due to large scale cost reduction of PV cells (Figure 1.4), thanks to the rapid development in cell technology.

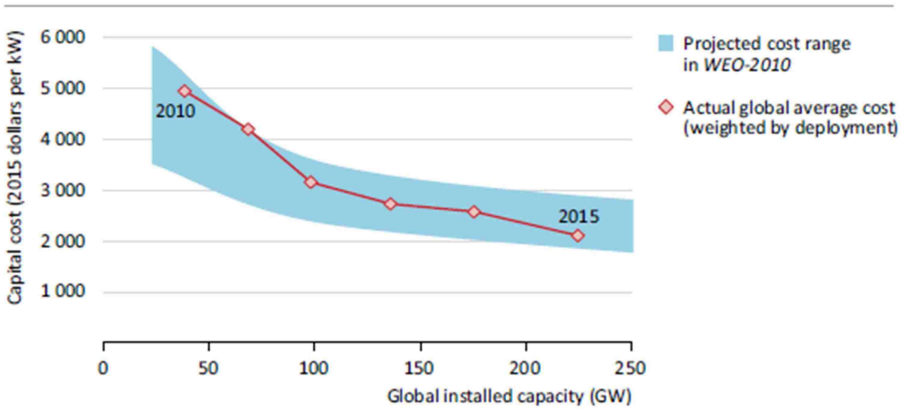

Figure 1.4 Projected and actual global weighted average capital costs for solar PV, 2010-2015[1]

1.2.1 Working principle of a PV cell

Solar photovoltaic energy conversion is a direct conversion process which generates electrical energy from light energy. According to quantum theory, light is made up of packets of energy called *photons*. The energy of photon depends only upon the frequency of the light as given by Planck's equation,

$E=hv$ ...(1.1)

where, h is Planck's constant and v, the frequency.

Frequency and wavelength (λ) of radiation are connected by the following equation.

$v=c/\lambda$ ..(1.2)

where, c is the velocity of light in vacuum.

And hence, Equation 1.1 can also be written as

$E=h\ c/\lambda$ .. (1.3)

Thus, Planck's Law states that that emitted radiation is directly proportional to the frequency or inversely proportional to the wave length.

Visible photons, incident on a material, excite electrons bound to the solid up to higher energy levels where they are freer to move. This phenomenon is known as the photoelectric effect. Albert Einstein explained this phenomenon using quantum theory. While photoelectric effect acts on a single conducting plate ejecting out electrons, the photovoltaic effect takes place at the interface of two semiconducting materials and electrons accumulate along the boundary creating a voltage.

Albert Einstein discovered that blue or ultra-violet light excites electrons to escape from the surface of a metal. Normally, when light is incident on matter, energy of photons excites electrons to higher energy states within the matter, but the excited electrons quickly fall back to their ground state. To prevent this from happening in a photovoltaic device, built-in asymmetry (P- and N-type semiconductor materials placed together to form the electrode terminals for external circuit) the photoelectric effect takes place at the interface.

In a photovoltaic cell, two semiconducting materials are fused to create what is called a P-N junction. Commonly, a single material, such as Silicon, is doped with different chemicals to create this junction. If Antimony is doped into Silicon, an N-type semiconductor is created, while doping with Boron makes a P-type semiconductor. Electrons that are knocked out of their orbits accumulate near the P-N junction and increase the voltage across it.

P-type material pulls the excited electrons from the interface (depletion layer), where, before electrons go back to their ground state and feeds them to the external circuit. Consequent holes in the conduction band move towards N type material and receive the electrons back through the external circuit with load thus producing D.C. electrical power as shown in Figure 1.5 (a & b).

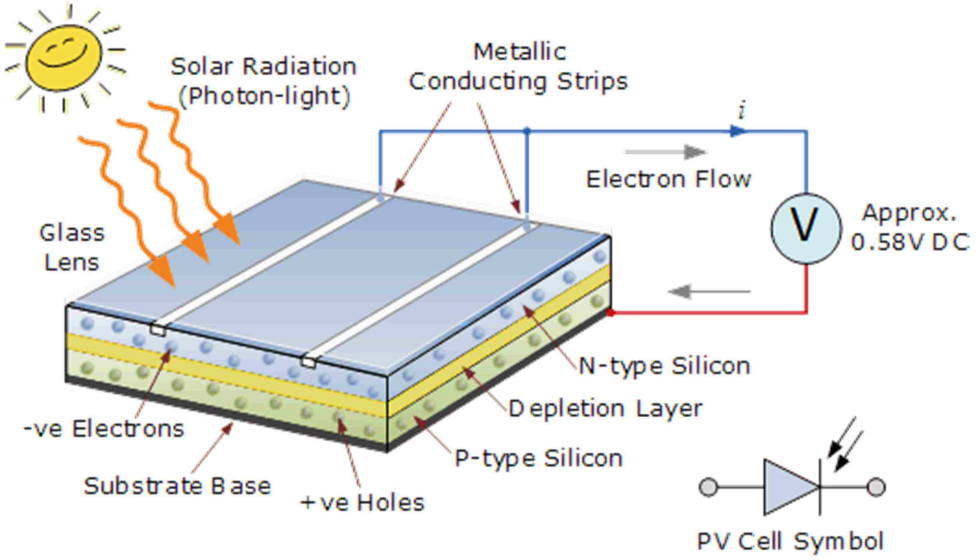

(a)

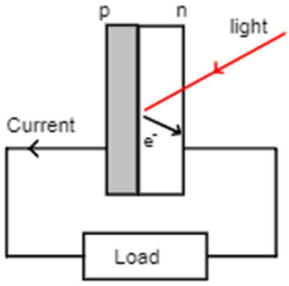

(b)

Figure 1.5 Working principle of a photovoltaic cell [2]

1.2.2. Effect of incident light spectra on the efficiency of a solar cell

Figure 1.6 depicts the spectrum of radiation reaching the earth. It produces a spectrum of emitted radiation with a distribution similar to a blackbody at a temperature of 5778 K. This is the temperature of the Sun. Area of the curve under each category represents the intensity of radiation for each. Thus, visible and infrared (IR) regions account for most of the Sun's energy.

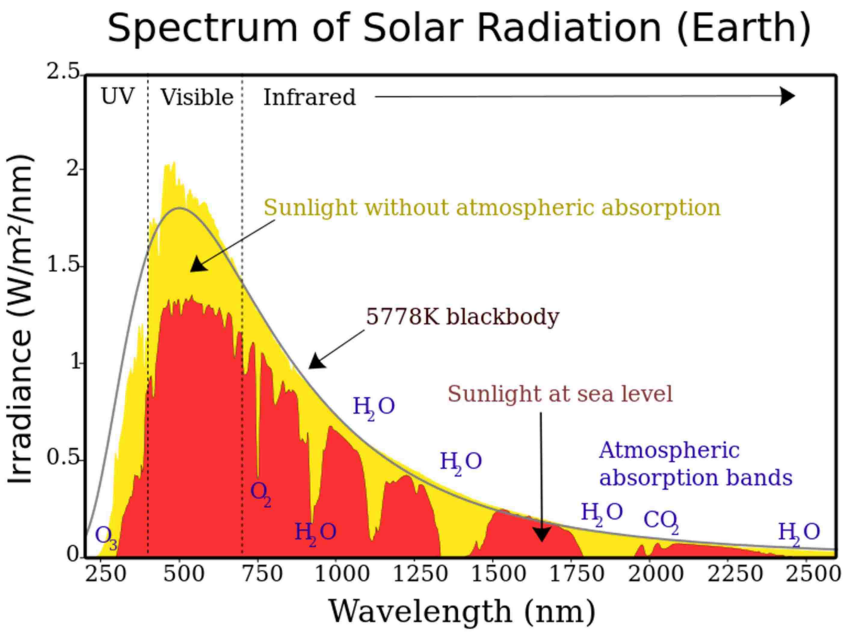

Figure 1.6 Spectral intensity distribution in solar radiation [3]

In course of its passage through the atmosphere, some of the light energy with specific energy bands is lost due to absorption by gases, mainly CO_2 and water vapour (Figure 1.6). It is also observed that Ultraviolet (UV) range spans from 100 – 400 nm. Visible range of light spans 380-780 nm, while infrared (IR) wavelength ranges from 700 nm to 1000000 nm (or 1 mm).

Photovoltaic effect is sensitive to frequency, ν (or in other words, wavelength, λ) of the incident radiation (Equations 1.1 and 1.3) and hence responds better to sunlight in some zones of the spectrum than the others. After being incident on a conducting material, photons collide with the electrons in the outer shell in the individual atom and if possess sufficient energy, knock them out. Free electrons then circulate through the material.

Planck's law shows that the energy of the photons is inversely proportional to their wavelength. Shorter wave length thus implies higher energy levels of photons. Sunlight comprises a whole spectrum of radiation, but only those with a short enough wavelength will produce the photoelectric or photovoltaic effect. This means that not all part of the solar spectrum is useful for generating electricity.

The threshold energy to knock an electron out of its orbit and into the conduction band is known as the band gap for the semiconductor.

For a voltage to develop across the P-N-junction, the incident radiation must exceed the band gap energy, E_g, which is equal to 1.78×10^{-19} joules. From Plank's equation 1.3, the wavelength of light corresponding to this energy becomes,

$\lambda = hc/E_g = 1110$ nm (frequency $v = c/\lambda$, h= Plank's constant)

Thus for enough energy of photon for photoelectric effect, the wavelength of radiation should be less than or equal to 1110 nm. A photon with a wave length of 600 nm, for example, possesses energy of 3.31×10^{-19} Joules and is more than the band gap energy. The visible light spectrum occurs between 400 and 700 nm, so the bandwidth wavelength for silicon solar cells covers all of the visible range and a part of infrared zone. Thus, it is observed that all of the visible light, UV radiation and some part of the infrared radiation cause the photovoltaic effect for generating electricity. Radiation with a longer wavelength will not be able to produce photovoltaic electricity.

1.3 Electrical performance of solar cell

The electrical performance of a solar cell which acts as a current generator like a battery is broadly assessed through its voltage-current (V-I) characteristics, power-voltage (P-V) characteristics and efficiency. Efficiency of a PV cell is quoted as corresponding to the maximum power condition in the P-V characteristics (Figure 1.7) as given by

$$Efficiency = \frac{Maximum\ power\ output}{Incident\ radiant\ energy\ rate\ \ in}$$

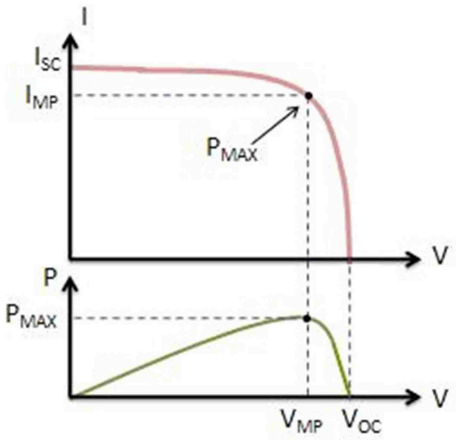

Figure 1.7 Electrical characteristics of a PV cell [4]

All the characteristics are shown for the standard test conditions. Standard test conditions are defined as the solar irradiation of one kilowatt (kW) per square metre, a module temperature

of 25^0C and a solar irradiation incident angle of 45 degrees. When a cell is subjected to incident radiation it attains a temperature established by the thermo-physical properties of the cell (heat absorption by the cell), incident radiation and ambience where an energy exchange process with the surrounding takes place. There are several factors that affect efficiency and operation of PV system. They are as follows.

- Absorbed irradiance,
- PV cell temperature
- PV cell technology
- Ancillary equipment

However, the efficiency of a PV cell varies only negligibly with incident radiation but mostly on operating temperature of the PV. Figures 1.8 and 1.9 show the typical variation in I-V and P-V characteristics of a silicon PV cell in dependence of incident radiation while Figures 1.10 through 1.12 show typical variation in I-V, P-V and efficiency characteristics of a typical silicon PV cell as a function of cell operating temperature. These trends are already established in literature.

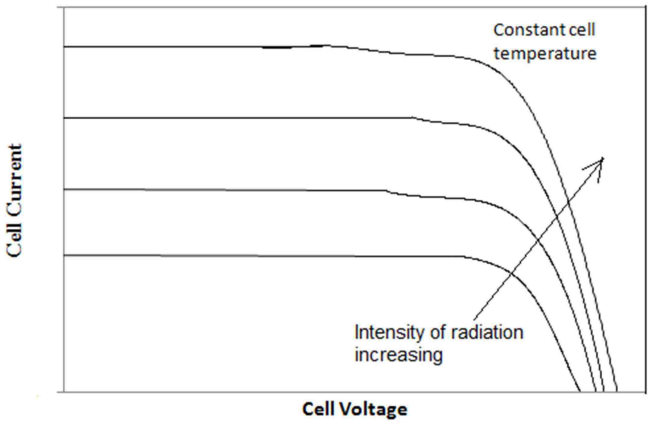

Fig. 1.8 Typical V-I characteristics of the solar PV array due to change in incident radiation intensity at constant cell temperature

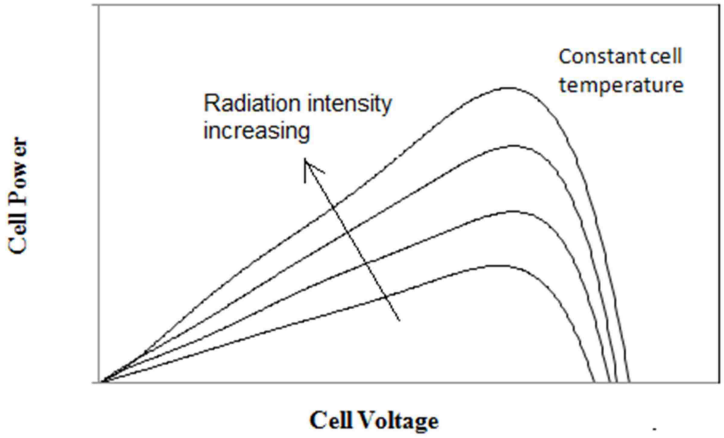

Figure 1.9 Typical P-V characteristics of the solar PV array due to change in incident radiation intensity at constant cell temperature

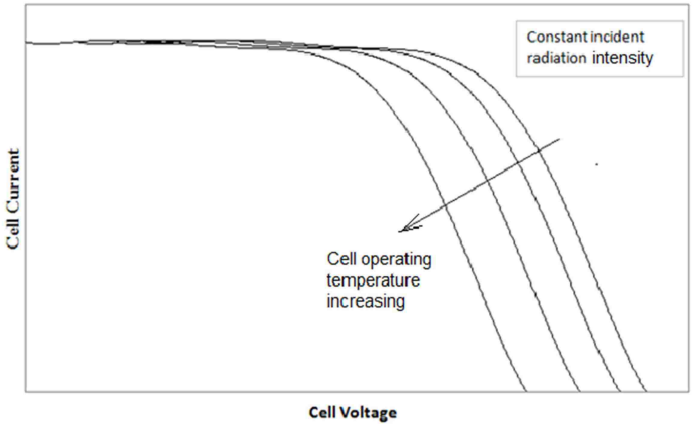

Figure 1.10 Typical V-I characteristics at different cell operating temperature

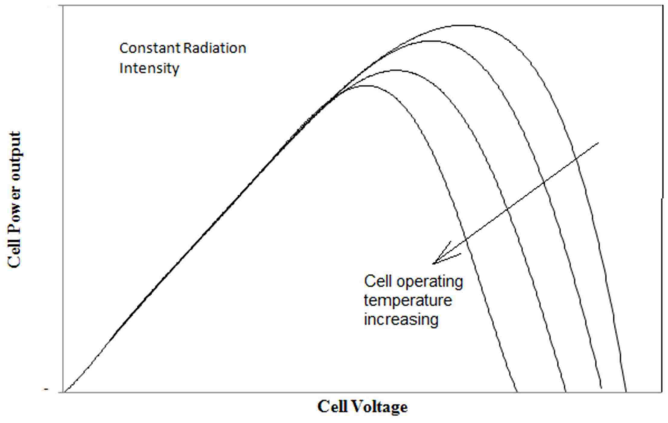

Figure 1.11 Typical P-V characteristics at different cell operating temperature

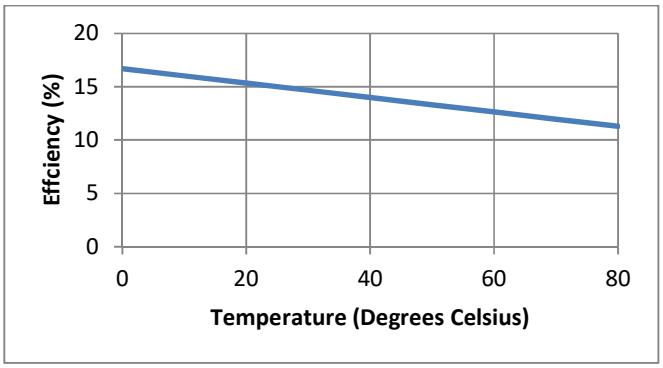

Figure 1.12 Typical variation of cell efficiency in dependence of cell operating temperature

1.4 Thermal management of PV cell

Low conversion efficiency of silicon solar cells (15-20%) had been a major stumbling block for its economic use for power generation in the past. The solar energy conversion efficiency of PV panels depends on the three factors [5] namely, solar cell materials, operating temperature and solar radiation intensity (to a lesser extent). In general, the availability of solar radiation, as a natural resource is beyond human control. There is a huge research focus; therefore, on exploring the other two options namely development of newer solar cell materials and maintaining low operating temperatures to improve conversion efficiency. Solar cell operation concerns the ability of semiconductors to convert sunlight (photons) into electricity by exploiting the photovoltaic effect. However, only a fraction of the absorbed solar radiation is converted into electrical energy, the rest being absorbed inside and also dissipated as heat to the outside environment. The maximum possible efficiency is determined by the band-gap of the material. Only those photons which possess energy levels higher than the band-gap yield the photovoltaic effect. Those below are absorbed an dissipated as heat and all excess active photon energy is also absorbed and dissipated as heat [6]. Cell temperature rises on two accounts namely,

1. Electrons and holes indirectly recombine to their original state when they encounter an impurity or defect in the crystal structure or interface releasing thermal energy

2. Absorption of infra-red radiation due to incident irradiation leads to sensible heating of the cell

Experimental work in References [7, 8, and 9] establishes that high cell operating temperature reduces the efficiency of a crystalline silicon PV cell at a rate of 0.40-0.65% per deg Celsius rise above the nominal cell operating temperature of 25^0C. The operating temperature of a PV can be as high as 80^0C at higher incident radiation intensity. At higher cell temperature, saturation current increases while the voltage developed decrease but the product decreases due to higher degree of voltage decrease compared to increase in current resulting in a decrease in power output [9].

The expression for variation of conversion efficiency in dependence of cell operating temperature is given in [10] as

$$\eta\,(T) = \eta_{ref}\,[1-\beta\,(T-T_{ref})] \qquad ..(1.4)$$

Where T_{ref} is reference/characteristic temperature (25^0 C); η_{ref} is the solar cell efficiency under reference temperature (usually, 10-18 %, 12% on an average); and β is the temperature-coefficient of efficiency, the average value of about 0.45% /K.

A similar expression for PV power output variation with temperature is given in [10] as

$$P = G_T\,\tau_{pv}\,\eta_{ref} A\,[1-\gamma\,(T-T_{ref})] \qquad ..(1.5)$$

In which G_T is the global solar radiation, τ_{pv} is the transmittance of the PV cell outside layer, A is the area of solar cell and γ is temperature coefficient of power usually in the range of 0.22-0.71% /K.

In case of Building Integrated PV (BIPV), Krauter et al [8] reports that the temperature rises to such an extent that a further decrease of 9.3% in power output occurs compared to a non-integrated PV.

This stresses on the need for effective temperature regulation for PV in general and BIPV in particular. Importance of the topic thus, as expected, has attracted research workers world-over and a host of literature is currently available related to thermal management of PV cell.

Research has amply shown that thermal management of the Solar PV cell by lowering cell operating temperature improves the cell efficiency [11]. The main objective of thermal regulation is to control temperature to values as low as possible. The PV/thermal (PV/T) technology was developed for this purpose, where, PV panels and heat extraction components are integrated into a single module [12]. The concept was originally proposed by Kern and Russell [13] in the nineties in the last century. Both active and passive cooling techniques

have been used for the purpose. Figure 1.13 describes various methods of thermal management.

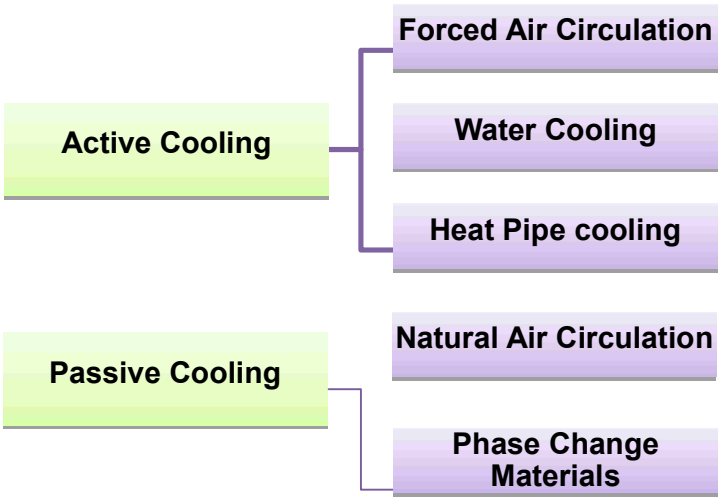

Figure 1.13 Methods for thermal management of PV cell

1.4.1 Passive and Active cooling techniques

The *passive cooling method* depends on the three basic heat transfer mechanisms: natural convection, conduction and radiation. Due to less paraphernalia and cost, it is commonly used for the cooling of PV cells particularly in Building-Integrated Photovoltaic Cell (BIPV) application. A duct or air channel behind the PV panel or its mounting system takes heat away through natural circulation or stack effects due to buoyant flow caused by the warming of the external air due to heat transfer from the rear of hot surface of the PV panel. PV panel back surface gets heated up by the heat conducted through the bulk of the PV panel. The front surface of the PV also removes heat through natural convection and radiation exchange with the surrounding. The process of heat transfer is explained in Chapter 3.

Heat pipe cooling is another option in passive cooling. A heat pipe (Figure 1.14) is a heat-transfer device that combines and utilizes both direct conduction transfer and phase change phenomenon to transfer heat between a source and sink. At the hot interface of a heat pipe a liquid comes in contact with the heat source through a thermally conductive solid surface and

turns into a vapour by absorbing heat from that surface. The vapour then travels along the heat pipe at the cold interface by buoyancy, rejects its latent heat to the sink via conduction heat transfer across the cold interface, condenses back into the liquid form and returns to the hot interface either through capillary action, centrifugal force, or gravity, and the cycle repeats. Due to the very high heat transfer coefficients for boiling and condensation, heat pipes are highly effective heat transfer devices.

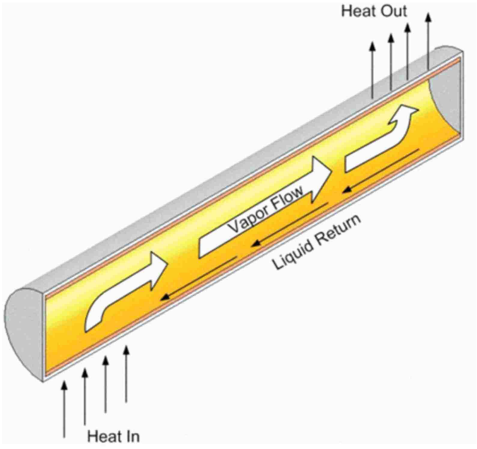

Figure 1.14 Working principle of a heat pipe [14]

Active approach is primarily a forced convection heat removal employing a pump or a fan. As a consequence, this approach leads to better thermal regulation and increased PV efficiency compared to the passive approach and has better control as well. But this approach involves the parasitic pumping power and maintenance too, thus offsetting somewhat the benefits reaped otherwise. However, this can be cost effective if the heat removed can be utilised in the building services.

1.4.2 Phase Change Materials for thermal regulation of PV cell

A novel approach to passive cooling is to use phase change materials (PCM) which employs the principle of absorbing/releasing high latent heat while keeping the temperature of the material substantially same during the phase change process. Fortunately, a wide choice of PCM is available to suit different applications. Different types of PCM available can be categorised as shown in Figure 1.15.

Two of the very commonly used PCMs are Paraffin and Salt Hydrate. Table 1.2 and 1.3 furnish typical values for these two types of PCM.

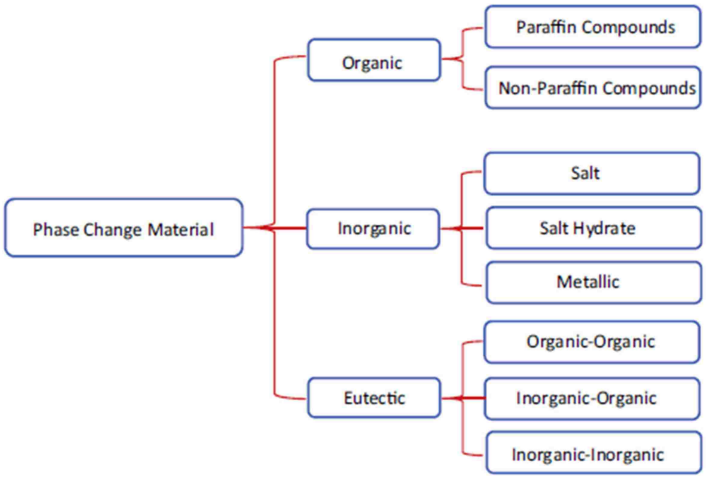

Figure 1.15 Classification of PCM [10]

Table 1.2 Comparison table for typical organic, inorganic and eutectic PCM

Organic (Wax Paraffin)	**Inorganic (Salt Hydrate)**	**Eutectic of the two**
Low cost	Moderate cost	Sharp melting point
Chemically inert and stable	High volumetric energy storage density (180-300 MJ/m^3)	Low volumetric energy storage density
Self-nucleating	Higher thermal conductivity (0.6 W/m ^{0}C)	Limited available material property data
No phase segregation	Non flammable	
Recyclable	Low volume change	
Available in large temperature range	Sub cooling	
Flammable	Phase segregation	
Low thermal conductivity (0.2 W/m ^{0}C)	Corrosion of container material	
Large volumetric energy storage density (90-200 MJ/m^3)		

Table 1.3 Thermophysical properties of a two representative phase change materials

Material	**Salt Hydrate**	**Paraffin**
Thermal conductivity (W/m ^{0}C)	0.60	0.2
Specific heat capacity (kJ/kg ^{0}C)	2.0	2.0
Density (kg/ m^3)	1500	802
Viscosity (kg/m.s)	0.00184	0.003
Solidus temperature (^{0}C)	27	38
Liquidus temperature (^{0}C)	32	43
Latent heat of fusion	200	140
Material source	*Rubitherm (SP-29)l*	*Rubitherm (RT-42)l*

In the past, PCM has been used in many applications as a thermal storage device and for controlling temperature. They have been used in electronic cooling, human body temperature control, refrigeration system, mobile phone, Li-ion battery, to name a few. Integrating PCM with a PV have shown promising results for efficiency enhancement and have engaged the attention of scholars. A typical PV-PCM system is shown in Figure 1.16, following Huang et al [15]. It consists of a metal PCM container, to the front wall of which the back of the PV cell is attached. Heat from the PV cell is absorbed by the PCM and dissipated away to the environment through the back metal plate wall of the PCM container. As a matter of fact, this heat from the back plate can be gainfully utilised for building heating with BIPV system or, during summer, the heat can be absorbed by the PCM from the environment through back plate to keep the environment cool during the night time when sun light is not available for power generation. However, a major problem with PCM is that they have, in general, quite low thermal conductivity. Researchers have used different techniques like placing fins of different configuration, forming metal cells within PCM, mixing highly conducting nano-particles, wire mesh etc.

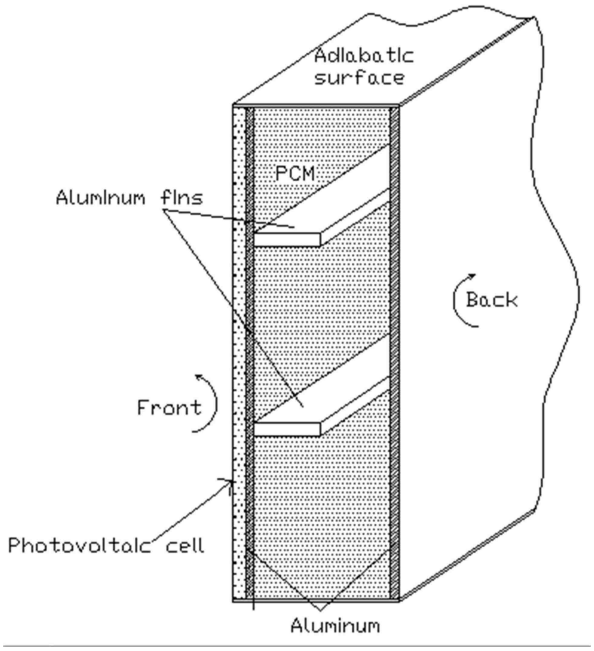

Figure 1.16 A scheme of a typical PV-PCM system with transverse fins

1.5 Motivation

The great promise and projected growth of PV cell use combined with government level effort to promote this device for clean power generation has prompted the rapid research growth in the field. It is already noted that by 2050 solar PV technology and system along with wind power will be a major share in global electricity generation.

An advantage of the PV solar energy is that the solar panels are modular in nature and can be connected (in a combination of series and parallel connection) together in such a way that exactly the required quantum of power is delivered. This feature is referred to as "custom made" energy. The reliability and low operations and maintenance costs, as well as modularity and expandability, are enormous advantages of PV solar energy in many rural applications. There are two billion people mostly in rural parts of the world that have no access to electricity and the solar electricity may help them develop their life in a most cost effective manner. Bringing solar electricity to these people represents a huge market potential. Some companies and people have realised that solar electricity can fetch economic benefit now and this fact is probably the real driving force to a widespread development and deployment of the PV solar energy which is further reinforced by government level incentives and efforts towards green energy.

PV power from solar energy is clean, inexhaustible and environment friendly. Development of such a system is considered at present very pertinent with a social contribution. Lot of research is still going on in various aspects of PV technology such as cell material, smart grid integration, integration with wind power, thermal management and manufacturing, among others. One of the important design criteria in the development of an effective solar cell is to maximize its photon to electricity conversion which is adversely affected by rise in cell operating temperature. As such, an open area of active research is thermal management of a PV cell to limit temperature rise. The thermal regulation of PV is the broad area of the current thesis. PCM is a very exciting candidate for thermal management of PV cell and lots of issues are currently hotly researched.

Phase change materials have been used for many applications including medical applications for effective thermal management. However, it is only recently, over the last decade that it is investigated as a viable means for temperature control of a PV panel. A major stumbling block for use of PCM for solar PV application is its very low thermal conductivity. Among

many other techniques, effect of fins placed inside the PCM container for enhancing heat transfer away from the PV cell is very hotly researched. .

It follows that a PV-PCM system, although investigated by many researchers, still requires more study, particularly with respect to placement of fins inside the PCM container. Against this backdrop that it was thought very timely to undertake possible research activity to investigate into the promising field of thermal regulation of PV cell by Phase Change Materials (PCM) using finned containers with modified fin arrangements and with a design suitable for retrofitting.

Chapter 2: Literature Survey and scope of present work

A host of literature is available as to thermal regulation of solar panels. They may be broadly categorised as i) work in the field of conventional passive cooling, ii) Active cooling and iii) cooling with PCM. Both experimental and numerical works have been undertaken while many works relate to mathematical model development. Among research work in the field of PV-PCM system, enhancement of thermal conductivity of PCM has engaged attention of many researchers and various methods of conductivity enhancement like putting conducting fins, wire mesh, nano particles inside PCM have been investigated with promising results.

2.1 Passive cooling of PV module

Yang et al [16] investigated the thermal regulation performance of a PV-wall with air duct using a simulation model (PVWALL-1.0). Brinkworth et al. [17] presented a 'loop analysis' approach to estimate the flow rate in naturally ventilated PV system, Commercial CFD software TRNSYS was also used to investigate thermal regulation performance in Batagiannis and Gibbons [10] and Brinkworth et al. [17]. Fossa et al [18] studied an ANSYS model of natural convection in a PV module channel. A recent innovation by Yun et al [19] used ventilated photovoltaic facade in building as a heating device during winter and natural cooling duct during summer.. The results indicate that the temperature of the ventilated PV module rose to a maximum of 55.5^0 C compared to 76.7^0 C without ventilation resulting in 15% enhancement in PV efficiency. Heat pipe cooling is another passive cooling method, which delivers heat via working fluid circulation as described in Chapter 1. Anderson et al. [20] experimentally studied the heat pipe cooling of concentrated PV cells. A copper heat pipe passively removed the heat from a PV cell, which was subsequently rejected to ambient air through natural convection

2.2 Active approach of PV cooling:

Active approach cooling consists in forcing water or air over the PV cell by pump or fan. Brogren and Karlsson [21] used forced cooling by water circulating over the cells. The results showed that the power generated was twice the power possible by the conventional system in addition to a high thermal energy stored in the water. A similar cooling system where a water film was flowing over the front of the module was studied by Krauter S [22]. The temperature of the PV module was lowered significantly resulting in an efficiency

improvement by 10.3%. In a novel design, Wilson et al [23] employed gravity-fed cooling water instead of water pump and was flown over the back surface of the PV module. A quick fall in temperature from 62^0 C to 30^0 C was noticed and an increase of 12.8% in efficiency could be achieved.

Another approach to active PV thermal regulation is to employ forced air circulation.. Fans are employed to force circulating air through channel. However, systems with heat extraction by air circulation suffer due to the small thermal conductivity, low density and small heat capacity of air. As a result, heat transfer augmentation measures become necessary. Tonui and Tripanagnostopoulos [24] compared performance of natural and forced air circulation. He used fins for heat transfer augmentation. However, parasitic pumping power and maintenance issues are the disadvantages of an active cooling system.

2.3 PV-PCM system for thermal regulation

An innovative approach to passive cooling is to use phase change materials (PCM).. Incorporating PCM in a container and putting it at the back side of a PV panel to take away heat from the PV panel is showing promising results for efficiency enhancement. The principle behind this approach employs the capability of PCM in absorbing/releasing high latent heat while keeping the temperature of the material substantially same during the phase change process. They offer a wide choice of phase transition temperature which facilitates a lot of control on the temperature of the cell. A good review on applications of PCM for energy storage in solar thermal power plant is given in Ben and Li [25]

Figure 2.1 from Hasan et al [7] illustrates how solar panel temperature responds to a PV-PCM system compared to one without PCM. The PV-PCM system it remains much below the PV reference cell temperature for a long period of time of approximately 10 hours, which is a duration long enough for a sunny day when the intensity of sunlight is substantial and active. However, it is observed that given sufficient time, cell temperature for a PV-PCM system becomes equal to the steady state temperature of the PV reference cell and has still a rising trend and can thus shoot beyond the steady state temperature of the PV reference cell.

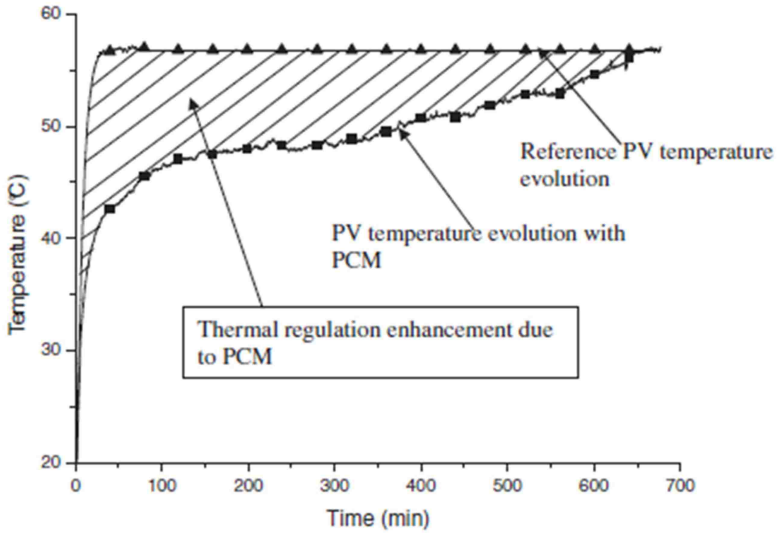

Figure 2.1 Thermal regulation of PV operating temperature by using PCM [7]

Huang [15] and Huang et al [26, 27, 28, and 29] have carried out extensive work in the direction, both experimentally and numerically. Their pioneering research has shown great promise for a PV-PCM system. Huang et al [28,30] investigated performance with different PCMs. Further, they have used and studied different configurations of fins (Figure 1.16) for enhancement of effective thermal conductivity of PCMs. Effects of molten PCM fluid flow through the bulk of PCM by buoyancy driven flow, the phenomenon of segregation of crystals during re-solidifications, hysteresis due to cycling of solidification-melting and the effect of Rayleigh number on heat transfer were investigated in Huang et al [29, 30]. Maiti et al [31] studied incorporating PCM to the back of a V-troughed PV module. Tan [32] used PCM to study its effects on a concentrated solar collector. The results indicate improved system reliability and enhancement of electrical output power. Recently, Karthik et al [33] investigated thermal regulation of Building Integrated PV system (BIPV) using Glauber's salt as PCM. Various parameters such as power generation, module surface temperatures and electrical efficiency are analysed. The experimental results show that with BIPV- PCM, the cell temperature reduced by up to 8^0C and electrical efficiency increased by 10% compared to the reference BIPV module.

Atkin and Farid [34] investigated, among others, effect of placing aluminium fins on the external surface of PCM containers. They found that placing external fins reduced the peak temperature.

2.4 Mathematical models and simulation

In the domain of simulation and mathematical models, a host of articles is available for reference. 1-D finite difference model for A PV-PCM system was developed in [32] and Smith et al [35]. to predict the thermal and electrical performance of the system under different parametric conditions A finite volume based numerical simulation model of non-linear transient 2-D temperature field was developed and implemented by Huang et al. [36]. Conjugate heat transfer was later incorporated while solving the Navier-Stokes equations and Energy equation in [26, 27]. The natural flow arises out of buoyancy in the solid-liquid PCM system. A 3-D numerical model for the purpose was later developed by Huang et al in [26, 36]. A CFD model with an enthalpy approach has been used to model the heat and mass transfer in a PV-PCM system by Biwole et al [38, 39]. More simulation work has been conducted recently. A 2D Ritz-Galerkin model was proposed by Sarwar et al. [40] to simulate the heat transfer phenomena within the PV-PCM system. Park et al [41] developed a transient heat transfer model for the energy simulation program TRNSYS. They predicted power output and the energy conversion efficiency of PV-PCM modules. The commercial package COMSOL MULTIPHYSICS was first used by Cellura et al [42] for analysing a PV-PCM system. The simulation results demonstrate an obviously enhanced energy generation efficiency of the PV-PCM system, when compared with the reference PV system. Their group also developed a finite difference model capable of describing the behaviour of the PV-PCM system as in Ciulla et al [43] and Lo Brano et al [44, 45] and the models were validated against field measurements. In addition, Tanuwijava et al. [46] investigated, via CFD simulations, the heat transfer and thermal management performance of microencapsulated PCMs for PV applications under the conditions of variations of intensity of daily solar radiation.

Hasan et al [47] made a comparison between the numerical results, with calculations from a finite difference model and the experimental results obtained from a test facility under different climatic conditions. The average differences between them were less than 7% vindicating the validity of the proposed thermal model. The shaded area in Figure 2.1 represents the thermal regulation enhancement component of the PV-PCM system.

The 2D numerical simulation model in [36] predicted that the PV-PCM system can maintain a PV module temperature below 38˚C for one and half hours. The experimental tests by Hasan et al [47] showed that the PV surface temperature remained below 40˚C for approximately 6 hours, if PCMs are used.

2.5 Enhancing thermal conductivity of PCM

To obtain desired thermal regulation, the PV–PCM system applications need to achieve quick PV panel thermal dissipation. Unfortunately, PCMs, in general, have poor thermal conductivity. A realizable solution is to increase the typically low PCM thermal conductivity by some synthetic methods. Most scholars have relied on the insertion of fins embedded in the PCM and fitted onto the PCM containers. The effects of fin spacing, widths and fin types on system performance were examined, in detail, by Huang et al. [28]. The effect of different fin configurations on heat transfer improvement was examined using numerical simulation in [27]. The use of conductive fins, mesh or encapsulation inside the PCM layers to enhance PCM heat conductivity has been described in Malvi et al [49]. It was found that an increase in PCM conductivity by 10% can enhance PV output by 3%. Through laboratory tests, Hasan et al. [47, 48] observed that the temperature of a PV module could be reduced to 25^0 C for a reasonable duration of time by enhancing the PCM thermal conductivity. More number of fins in addition reduced thermal stratification, leading to a more uniform temperature distribution in the PV–PCM system [30, 36]. Fins improve heat transfer into the bulk of the PCM and encourage thermal homogeneity, but they can also pose barriers to free fluid flow, and thus convective heat transfer in the melted PCM may be reduced [27]. Further, the duration of thermal control decreases as the volume of PCM is reduced by the mass of metal fins as in Huang [50] and Huang et al [30]. The increased weight of the metal fins for thermal control capacity is another potential problem [30]. However, both these effects may be reduced by using very thin fins. In addition, the fins increase heat resistance due to the formation of bubbles under the fins during PCM melting [29]. Fortunately, these effects are not very significant. This research topic, therefore, suggests further experimental and numerical study [29].

2.6 Materials selection

There is much literature on PCM applications for thermal energy storage and quite a good account is can be found in Jeon et al [51], Khudhair et al [52], Kurnia et al [53], Regin et al [54] and Zalba et al [55]. Hasan et al. [56] reviewed the performances of various PCMs used in BIPV thermal control. The selection criteria for a suitable PCM for its different thermal properties including its melting point, latent heat of fusion and thermal conductivity and different designs and configurations for integration of PV and PCM have been reported. Hasan et al [57, 58] and Makki et al [59] analysed the characterization of organic, inorganic and PCM eutectics incorporated with PV panels. The temperature regulation effect of five different PCMs on solar cell performance was experimentally evaluated at three incident radiation intensity levels. The latent heats of fusion of the five PCMs varied between 170 and 240 kJ/kg while the melting temperatures ranged from 21^0 to 30^0 C. Hasan et al. [48], by using the temperature history method (THM), discovered that some potential PCMs were unable to extract latent heat during the discharge process due to low solidification temperatures, while the eutectics of fatty acids, such as Capric–Lauric and Capric–Palmitic, exhibited good performance. Karthik et al [33] used Glauber's salt for their experiment with BIPV. The suitable container volume requirement for PCMs so that it can keep a low PV temperature for a longer period of time has also been investigated by Hasan et al [60].

Research into PV–PCM systems has very largely been concerned with system configuration development, simulation models, prototype experiments and electrical and thermal performance evaluation. The topic is still in the research and development phase, and so far there are few real life applications in practice. However, in spite of the great potential for improved thermal regulation, poor thermal conductivity of PCM and problem of integrating them into existing PV systems remain a concern and needs further attention. To enhance thermal conductivity, many methods like internal fins, metal wire matrix, nano-particles have been used with promising results. However, literature clearly suggests that the research topic of thermal conductivity and heat transfer through fins requires further experimental and numerical study.

2.7 Summary of literature survey

From the literature survey it is clear that PV-PCM system has been hotly researched in the past and present decades. However, there is considerable scatter on the results in the literature. Many issues are still open for further investigation. After careful examination of the available literature, it was observed that majority of the studies were deficient in an innovative test set-up in terms of PCM containment and resemblance to actual outdoor conditions during thermal studies. The need was felt for devising a suitable PCM containment which would seamlessly retrofit at the back of the solar panel and could easily be dismantled to change the PCM for experiment purpose at the same time. Further, the previous works focused more on the fluid dynamics behaviour of the PCM and their thermal management capabilities. Electrical performance improvement was tangentially linked to the extent of thermal regulation enhancement rather than experimentally quantifying thermal management enhancement and electrical performance improvement in tandem. Also, the experimental setup varied considerably across studies and this fact had considerable impact on the results.

As evident from the literature survey, fluid flow within the container is inhibited to some extent possibly due to the transverse orientation of the fins forming thermal stratification of the PCM. It is thought that longitudinal orientation of fins could improve the flow due to natural convection within the PCM. However, from the literature survey, no work with longitudinal orientation of fins could be observed to be used by early researchers. In this study, longitudinal fins are used for the purpose of enhancing the natural convection of melt pool over the hot surface of the back of the PV cell as well as in bulk of the melt pool of PCM.

It is also observed from literature survey that the research on PV-PCM system comprised an enclosed PCM container with PV foil pasted over the front plate of the container. Fins were fitted on the inside (i.e. PCM side) of the front plate extending into the PCM bulk but not touching the back plate of the PCM container (Figure 1.16) as in References [15,28]. This arrangement transfers heat from the PV foil directly to the internal fins. In turn, it heats up the PCM in the bulk, thereby improving the initial thermal regulation particularly at the initial phase of heating and phase transformation of PCM by increasing the effective thermal conductivity. However, it has two possible ramifications First, the completely enclosed container system cannot be fitted for the very large number of existing PV set up and secondly, during the liquid PCM heat up period throughout the bulk of the PCM when the

PCM has fully melted, the fins do not contribute at all to the transfer of heat from the liquid PCM to the back plate because they do not extend up to the back plate thus reducing the heat dissipation from the PCM to the ambience through the back plate during later part of PV heating.

Heat is dissipated away from PV-PCM system from the front PV surface and outside surface of the PCM container back plate. Enhancing heat dissipation from the back plate can be increased by placing external fins. However, no work has been noticed during the literature survey which combines internal fins with external fins. In the present work, therefore, the combination of these two types fin configurations are devised to be investigated (Figure 4.4). In the present investigation, thus, internal fins starting from the back plate and external fins at the outside of the back plate (Figure 4.4) thus complement each one's function.

It was also observed from the literature survey that all the thermal regulation investigations comprised an energy analyses which were carried out on a 'dry' basis i.e. the PV cell was not connected to any load. The electrical energy output along with its changing value (due to changing operating temperature) during the course of thermal experiment would change the temperature condition of the cell and hence energy analysis for predicting the thermal performance should incorporate electrical output.

In the light of the above, the following can be summarised:

i) Tremendous growth of solar PV technology over the last few years as a means to generate clean energy has given impetus for research in this area, the world over.

ii) Thermal management of PV panels has shown encouraging results in improving conversion efficiency at high operating temperature.

iii) Most of the analyses in thermal management with PCM have focussed on temperature regulation without any consideration of concurrent electrical power output which would influence the predicted energy budget and temperature response.

iv) Low thermal conductivity of PCM remains a challenge. Although usage of PCM shown encouraging results, its full potential can only be realised by improving its low thermal conductivity. Although work has been done on this aspect, other methods particularly different configurations of fins within the PCM container is worth investigating.

2.6 Objectives:

In the light of literature review, therefore, thermal regulation is experimentally investigated in the present study. using a PV-PCM system with fins inside and outside the PCM container designed for retrofitting. The main objectives of the thesis are as follows.

i) To study the deterioration in electrical performance of PV cell with rise in temperature under a constant incident radiation heat flux.

ii) To study the enhancement of passive heat transfer and thermal regulation in a PV panel using phase change material.

iii) To investigate the effect of different fin configurations in longitudinal orientation (placed both within and outside) in the PCM container on the time evolution of PV panel temperature as well as on electrical power output in both PV/PCM and finned PV/PCM system.

iv) To study the energy budget for the systems under study incorporating electrical power output during thermal regulation study.

v) To design and develop a solar panel thermal test set-up with data acquisition system and related instrumentation.

vi) To design a PCM container suitable for retrofitting to commercially available solar panels.

The above-mentioned objectives are achieved through an experimental investigation of thermal regulation of a commercial PV cell. Heat bulbs are used to simulate both the visible and infrared portion of sunlight. A commercially available PCM with a melting temperature of 28 ^{0} C is used for thermal regulation of the panel. To facilitate retrofitting of PCM container, a container open at the front is designed, which is fitted at the back frame of an existing PV panel. In doing so no fins could be fitted to the back surface of the PV panel. Instead, fins are fitted on the inside of the back plate of the PCM container. As already discussed, the fins are fitted in longitudinal orientation (Figure 4.4).

Chapter 3: Theoretical Background and Energy Balance

In this chapter, a theoretical background for the present work and the energy exchange process for both the PV and PV-PCM system with the surrounding are analysed. The energy analysis is carried out to assess the rates of heat absorption and heat loss by the PV reference system as well as PV-PCM system due to the incident radiation. This energy budget information is essential in gaining more insight into the phenomenon of thermal regulation of a PV-PCM system. A steady state heat conduction analysis for the PV and PV-PCM system is also carried out to assess the heat transfer capability of PCM for thermal regulation.

In earlier studies, energy balance analysis considered only the thermal energy exchange of the PV system. However, the concurrent electrical load as output should be included in the analysis as it would alter the overall energy balance. For this, the power (set by rheostat for maximum power condition) generated by the cell during the entire duration of the thermal experiment is needed to be found out. In the present investigation for temperature response of the PV cell under the influence of constant incident irradiation, the maximum power load setting was made prior to the thermal regulation experimentation. During the process of heating, the maximum power output and hence conversion efficiency decreases due to higher operating temperature. Thus, establishing a correlation of conversion efficiency with temperature is required to determine the maximum electrical power output at each instant of time during the experimentation, the incident radiation energy input being known. In the present investigation, a separate dedicated experimentation for electrical parameter characteristics is carried out for different steady state temperature conditions for the purpose. The correlation is later plugged into the energy balance equation to calculate electrical power output at any instant of time corresponding to the instantaneous temperature condition of the PV cell as obtained from experiment.

In the next sections to follow, the basis of experimentation for electrical characteristics is discussed with steps for calculating conversion efficiency followed by the energy conservation analysis.

3.1 Background of electrical measurements

Figure 3.1 shows a typical current vs. voltage (V-I) and power vs. voltage (P-V) characteristics of a solar cell. The important electrical parameters of a PV cell include open circuit voltage, short circuit current, maximum power output and panel efficiency which determine the electrical performance of the PV cell. A short description of these quantities is presented as follows.

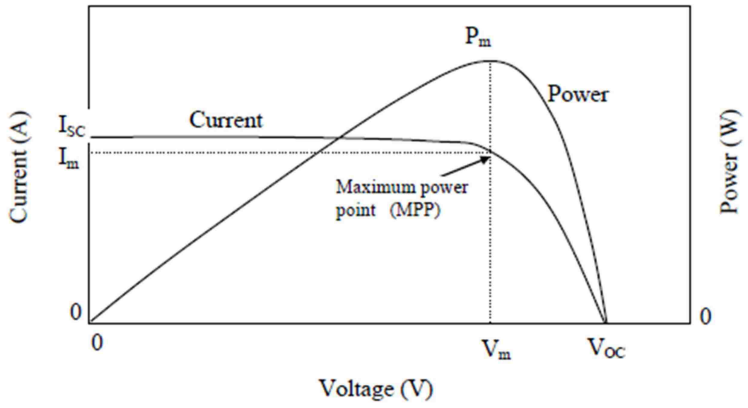

Figure 3.1 V-I and P-V characteristics of a PV cell [61]

a) Short circuit current (I_{sc}):

Short circuit current is the current drawn when the terminals of the PV cell are connected together with only a very short length of very low resistance conductor (ideally the cell terminals brought together and joined) i.e. with almost zero external resistive loads. At this condition, since external load resistance (R_L) is zero, the voltage potential (V_{output}) used up for driving current (I) through external load resistance (R_L) is zero ($V_{output} = R_L * I = 0$). All the voltage developed by the cell is consumed to overcome the internal resistance. The output power is thus also zero.

b) Open circuit voltage (V_{oc}):

The voltage developed when the terminals are isolated and kept open (infinite load resistance of air) is called the open circuit voltage V_{oc}. Under this condition, there is no current through the cell and hence no internal voltage loss. Thus the full

voltage developed is available for any possible external load. Also power output at this condition is zero. For this, voltage across the terminals of the cell is measured when there is no electrical load in the cell. This voltage depends upon the techniques of manufacturing and cell operating temperature but not fairly on the intensity of light and area of exposed surface. Normally, open circuit voltage of solar cell ranges from 0.5 to 0.6 volt.

c) Maximum or Peak power (p_m):

It is the maximum electrical power one solar cell can deliver at its standard test condition. The P-V curve is obtained from V-I data using the relationship P=VI. On the V-I characteristics of a solar cell, maximum power will occur at the drooping point of the characteristic curve. It is shown in the P-V characteristics of solar cell by P_m (or P_{max}). To get a comparative picture of the efficacy of different thermal regulation measures adopted in the present investigation, plots of variation of maximum electrical power output with time are presented in Chapter 5.

d) Panel efficiency :

The efficiency also called the conversion efficiency of a PV panel is defined as the ratio of the maximum electrical power output to the incident radiation power input to the cell. It is expressed in percentage. Mathematically, efficiency of a solar cell is expressed as

$$\eta(T) = \frac{Maximum\ eletrical\ power\ output}{Input\ incident\ radiation} = \frac{P_m(T)}{G*A} \qquad ..(3.1)$$

where, T is the PV cell temperature, G is the intensity of incident radiation, P_m is the maximum or peak power output as extracted from P-V characteristics under given conditions and A is the frontal area of the panel.

The V-I characteristic of a PV panel under an applied load forms the basis of its electrical performance. In the present investigation, the V-I characteristic of the PV panel under investigation is obtained for different electrical load conditions at a specific steady state temperature. The process is then repeated for a series of steady state temperatures to obtain

V-I characteristics at each steady state temperature. From the V-I characteristics, the P-V characteristics are plotted. The maximum power output values are extracted from the P-V characteristics. The conversion efficiencies (corresponding to maximum power values) at each steady state temperature is calculated using Equation 3.1 with measured values of incident radiation (G). Electrical characteristics as obtained in the experimentations are presented in detail in Chapter 5. A temperature correlation of conversion efficiency was obtained by a best fit straight line obtained from the plot of efficiency with temperature. This correlation was subsequently used to calculate the electrical power output of the PV cell at different transient temperatures (measured through DAQs) for the entire time duration for each specific set of thermal regulation experimentation. As already stated, electrical power output calculation forms an integral part of energy budget analysis.

3.2 Temperature coefficient and conversion efficiency correlation

The electrical characteristics (open circuit voltage, short circuit current, peak power and efficiency) of PV cell vary with cell operating temperature as already shown in Figure 1.8 through 1.12. However, for the purpose of energy balance and thermal regulation studies, all changes in electrical parameters may be represented finally through the efficiency parameter which is a function of temperature.

The cell efficiency as a function of temperature is given by,

$$\eta(T) = \eta_{ref}\left[1 - \beta\left(T - T_{ref}\right)\right] \quad ..(3.2)$$

where, η_{ref} is the cell efficiency at some reference condition of temperature (T_{ref}) and irradiance which is usually the Standard Test Condition (STC) and β is the temperature coefficient of efficiency for the cell obtained from experiment.

Usually, STC refers to a PV cell temperature of 25^0C and solar irradiance of 1000 W/m^2. The value of η_{ref} is supplied by the cell manufacturer. Thus, the conversion efficiency can be computed if the temperature coefficient β is known.

Temperature coefficient of efficiency, β is given by

$$\beta = \frac{1}{\eta_{ref}}\frac{d\eta}{dT} \text{ ,} \quad ..(3.3)$$

The value of the temperature coefficient, β, can thus be calculated from the slope $\frac{d\eta}{dT}$ of the plot of η vs. T.

Normally, the temperature coefficient value will be supplied by the cell manufacturer and forms the basis of a comparative assessment of temperature dependence of cell efficiency for different cells. Generally, for a polycrystalline solar cell, temperature coefficient is about -0.5%/K. This means the panel will lose half of one percent of its power for every degree temperature rise. In absence of any specific data, an average value of 0.45%/K can be assumed as the temperature coefficient of a solar cell.

In the present study, efficiencies at four different steady state temperature conditions were determined from electrical and irradiation measurements by using Equation 3.1. Variation of the efficiency with temperature T is then plotted from the experimental data. A best fit linear correlation of the form, $\eta = a + bT$, is obtained which yields the slope of the curve $\frac{d\eta}{dT}$., which is the coefficient b in the linear correlation above. The slope being known, the value of the temperature coefficient β is found using equation 3.3. Efficiency value at any temperature can then be calculated from equation 3.2. However, for the purpose of calculating the electrical power output as a function of temperature as used in the energy conservation analysis; instead of using the Equation 3.2, the correlation of the form (η = a + bT) is more convenient to use. The temperature coefficient β is found only for the purpose of comparing with standard values and any possible deviation therein has been discussed in Chapter 5.

Once efficiency is known, the electrical energy output at any temperature for a given irradiance input can be easily found out from Equation 3.1. The details of electrical measurements are discussed in Chapter 4. The results of the related experimentation and the correlation obtained are presented in Chapter 5.

3.3 Energy exchange and conservation analysis for the PV panel

The energy exchange analysis requires the description of the layers of material forming the PV cell along with radiation and convection properties of the cell surfaces..

3.3.1 Composition of a typical silicon PV cell

A silicon PV cell is composed of various layers, which have their own unique purpose and function.

The PV panel chosen for the present investigation is the ACOPOWER polycrystalline silicon PV. There are five main layers in this PV panel including two layers of EVA similar to the components as given in Reference [37] and presented in Figure 3.1. A brief description of each layer is given below:

1. *Glass top* - Tempered glass is used for UV ray protection and physical damage protection and coated with Anti Reflection Coating (ACR). The glass used in PV panels is ultra-clear with a high transmittance for solar radiation.

2. *EVA (Ethylene Vinyl Acetate*) *layer* - PV cells are sandwiched between EVA sheets which are optically transparent and help adhesion to the top glass layer and the bottom material. It also provides barrier to entry of moisture into the cell and ensures electrical isolation from rest of the panel material as well.

3. *Photovoltaic (PV) Cell* – Polycrystalline silicon PV cells have been used in the PV panel under investigation. Thickness for such PV cells typically ranges from 200-300 μm.

4. *Polymer back sheet (Tedlar Foil)* – It is a white coloured plastic sheet. Tedlar film is the Dupont trade name made of a film of Polyvinyl Fluoride (PVF), poly ethylene terephthalaye (PET). This layer is photostable and provides additional moisture protection and electrical insulation.

Tedlar foil along with the glass layer on the front side is the key barriers against damaging external factors, most importantly water, vapour and dirt. Relevant thermo-physical properties of the layers and numbering of the layers are furnished in Table 3.1.

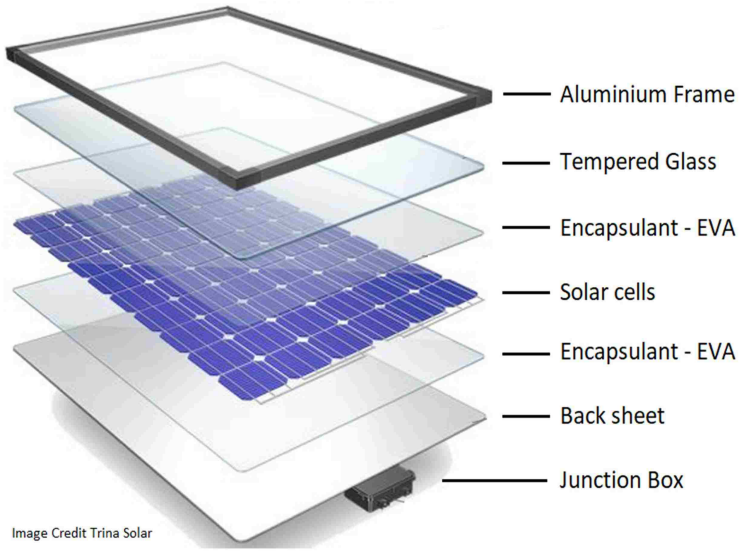

(a)

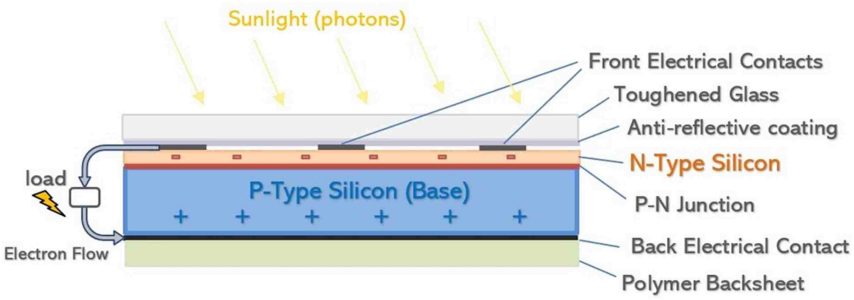

(b)

Figure 3.2 Different layers composing a PV cell [62]

Table 3.1 Relevant properties of a cell component material [37] and PCM used

Layer	Material of the layer	Thermal conductivity ,k (J/m/K)	Specific heat, C_p , (J/Kg/K)	Density, ρ (kg/m^3)	Thickness, Δx (m)
1	Glass	1.81	500	3000	0.003
2	EVA	0.35	2090	960	5×10^{-4}
3	PV material	148	677	2330	2.25×10^{-4}
4	EVA	0.35	2090	960	5×10^{-4}
5	Polymer back sheet (Tedlar foil)	0.2	1250	1200	1×10^{-4}
6	PCM	0.18 (typical) for liquid paraffin wax [15]	2400 (liquid)	300-400 (liquid)	0.02

3.3.2 Radiation and convection properties of the surface

PV cell surface receives incident radiation. Its surfaces dissipate heat convection heat transfer (forced as well natural) from the surfaces to the surroundings. Only natural convection is considered as forced convection is practically absent within the laboratory where the experiment was carried out. The surfaces also have a net low temperature long wave radiation radiation exchange with the surrounding environment. Table 3.2 furnishes the important radiation and natural convection properties of the PV cell surfaces, required for the analysis. The reflectance property of a typical silicon PV solar cell is shown in Figure 3.3. It is observed that the approximate average value of reflectance in the wave length range of 450 nm to 1000 nm (visible and IR zone which form most of the incident energy) is only about 0.025 which can be neglected for the purpose of present analysis.

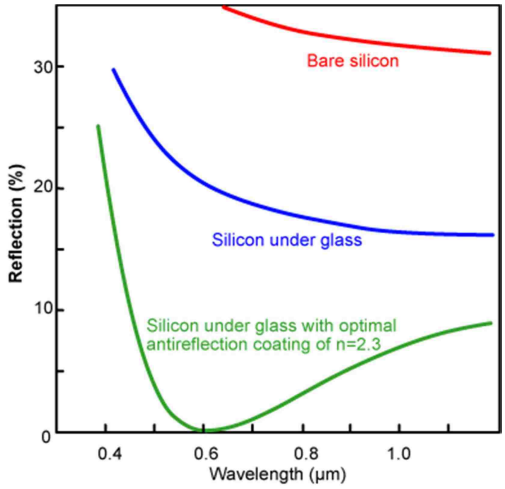

Figure 3.3 Reflectivity property of a PV cell top surface for different wavelengths of incident radiation [63]

Table 3.2 Relevant Convection and Radiation quantities

Parameter	Symbol	Value
Heat transfer coefficient (top surface) [64]	h_1	8.0 W m^{-2} K^1
Heat transfer coefficient (bottom surface) [64]	h_2	2.0 W m^{-2} K^1
Absorptance of cell for solar energy[36]	α_s	1.0
Emissivity of glass[36]	ε_{glass}	0.95
Reflectance of PV cell top surface	ρ	0.0
Stephen Boltzmann-constant	σ	5.67 x 10^{-8} W m^{-2} K^4

3.3.3 Energy analysis

Figure 3.4 shows a PV cell cross section used for the conservation analysis. The energy quantities involved are all shown for the sake of completeness. However, some of them are neglected as detailed under the assumption part below. The layers are numbered following Figure 3.3. The analysis is essentially the same for the PV-PCM system as well. The energy conservation analysis for the PV has been developed as follows.

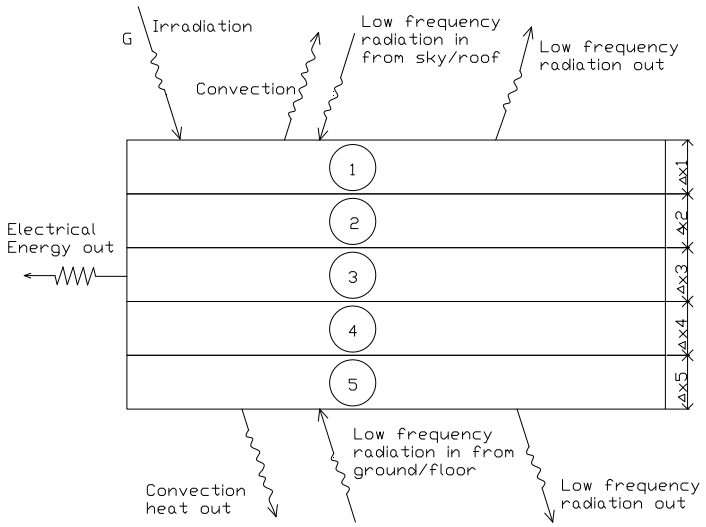

Figure 3.4 Energy exchange, heat transfer and layer components in PV cell

Incident radiation falls onto the front side (PV front) of the system. All the incident radiation is absorbed (no reflection assumed because of anti-reflection coating on the glass top cover of a PV cell). The absorbed radiation consists of visible and other electromagnetic (mostly infrared for the present experiment) radiation. A part of the absorbed energy is converted to electrical energy while the rest appears as thermal energy inside the PV and heats it up (sensible heating for the PV cell). The PV cell loses heat both at the front and back surfaces as convection and radiation heat to the surrounding media. It also absorbs radiation heat from its surroundings. When the PV is connected to electrical load, it also gives up energy in the form of electrical energy. Following are the assumptions for the energy conservation analysis.

Assumptions

1. The four side surfaces of the PV cell system other than the front and back surfaces have negligible surface areas and any heat transfer through these surfaces is not considered and they are thus adiabatic.
2. There is no forced convection (air circulation velocity inside the laboratory is taken to be insignificant) and only natural convection is considered.
3. The back surface of the cell is just away from the table on which the PV holding frame is kept and hence there is practically no radiation exchange nor any convection heat dissipation from the back surface. As such, it is already observed (Table 3.2) that the bottom/back surface heat transfer coefficient is much less than the top surface heat transfer . Heat transfer only from the top front surface is considered.
4. The property values remain substantially constant for the entire range of temperature change during heating.
5. Any reflection of incident radiation from the front surface is neglected.
6. Electrical load is applied throughout the heating process.
7. The radiation exchange with the surrounding and convective loss takes place only at the top surface of the PV cell.
8. The absorptance of the PV cell (α_s) for solar radiation is assumed unity.
9. The surrounding is assumed to be a black body for radiation exchange.
10. The surrounding space completely encloses the PV cell so that view factor of the surrounding for the radiation energy coming from the cell is unity.

The basis of the radiation exchange quantities and view factor for the purpose are detailed in Appendix A.

The general energy conservation of the PV panel (Figure 3.4) can be written as

Rate of change of energy of the system(rate of heat absorption)
$$= \text{Rate of energy in} - \text{rate of energy out}$$
= Rate of energy in – (net heat loss+ electrical power out)

Net heat loss consists of net radiation exchange loss and convection loss from the surface of the PV cell. Heat losses are considered only for the top surface of the panel for reasons stated earlier.

Mathematically, the above conservation expression can be written as,

$$Rate\ of\ heat\ absorption = A\left[\alpha_s G - \epsilon_{glass}\left(\sigma T_{surface}^4 - \sigma T_{surrounding}^4\right) - h_1\left(T_{surface} - T_{ambience}\right) - \eta\alpha_s G\right] \quad \ldots (3.4)$$

The first term within on the RHS of equation 3.4 represents the incident irradiance absorbed by the cell, the second term within parentheses is the low temperature long wave radiation energy loss from the PV top surface due to net radiation exchange with the surrounding environment, the third term within the parentheses denotes the natural convection loss from the top surface and the last term represents the electrical energy rate out of the PV cell. Dividing both sides by the frontal area (A) of the cell would make all the terms in the form of energy flux (J/s/m^2 or W/m^2). A balance of these energy fluxes goes to change the internal energy flux (heat flux absorbed) and hence temperature of the PV cell will change.

For the purpose of radiation exchange, the surrounding environment is taken to be a black body. Hence, to compensate for this assumption, the temperature of the surrounding is taken a little lower than the ambient temperature [65]. However, for all practical purposes, the deviation is not much and in the present analysis, $T_{surrounding}$ is taken to be equal to $T_{ambience}$ without introducing significant error in the value of the radiation emitted by the surroundings.

3.4 Heat loss rate and heat absorption rate for a PV cell

For the present study, the energy absorbed by the PV and the heat loss rates are investigated. The calculations are directly derived from the basic energy conservation principle as described in Article 3.3 and Equation 3.4. The sum of the second and third terms in Equation 3.4 represents the heat loss at any point of time. Calculation of RHS expression of the equation would yield the heat absorption by the cell.

RHS of Equation 3.4 can be calculated if the following quantities are known.

1. Temperature of the solar cell
2. The incident radiation
3. Electrical efficiency
4. The relevant radiation and convection properties

In the present investigation, the first three quantities are all known as part of the experimentation. The radiation and convection parameters are taken from standard published sources.

3.4.1 Heat loss rate

The heat loss rate or heat flux out through the surface is found out directly by calculating the losses from the front/ top surface of the PV reference cell.

The basic heat loss terms are already incorporated in the energy balance equation as in Equation 3.4. Collecting all the heat loss terms in Equation 3.4, the following heat loss equation is obtained.

Net heat flux out = Radiation flux out +Convection flux out

$$=[\sigma\epsilon_{glass}\left(T_{surface}^4 - T_{surrounding}^4\right) + h_1[T_{surface} - T_{ambience}\,] \quad ..(3.5)$$

3.4.2 Heat absorption rate

Heat absorption flux is found out by subtracting the sum of energy fluxes out (electrical power out plus heat dissipation out) from the incident energy rate (G) received by the PV-reference cell and follows from Equation 3.4. With absorptance of glass top of the cell for solar radiation $\alpha_s = 1$, the following equation is obtained for the purpose.

$$Heat\ flux\ absorption\ rate = \left[G - \epsilon_{glass}\,\sigma\left(T_{surface}^4 - T_{surrounding}^4\right) - h_1\left(T_{surface} - T_{ambience}\right) - \eta G\right] \quad ..(3.6)$$

It may be noted that the second and third terms in Equation 3.6 representing the net heat loss has already been calculated in Equation 3.5 as in Article 3.4.1 and can be directly used in Equation 3.6. The incident energy is obtained from the measurement in the experiment using pyranometer. The flux of electrical energy or electrical power per unit area [$\eta\ (T)\ x\ G$] at the particular temperature, T, at any instant of time, required in Equation 3.6 is obtained from the correlation of conversion efficiency with temperature already developed for the purpose from the experiment involving measurement of electrical parameters for efficiency as described in

Article.3.2. The surface temperatures are those obtained from thermal experiments with the PV reference panel only.

Results of the heat loss and heat absorption quantities for PV reference panel are presented in Chapter 5.

3.5 Energy analysis for a PV-PCM system

The energy balance and energy budget analysis for a PV-PCM do not pose any additional complexity and essentially, the RHS of the Equation 3.4 is replaced by the term 'heat absorption rate' because in case of a PV-PCM system, the heat absorption term comprises both sensible heat of the PV as wells as PCM and also the latent het absorbed by any part of PCM undergoing phase change. The same set of Equations 3.4 through 3.6 are used also for a PV-PCM system where only different values of surface temperature ($T_{surface}$) for the PV top surface obtained from experiments with PV-PCM system shall be used for calculations. This is because energy balance is made on an overall basis at the macro level concerning the surface quantities and the bulk energy quantities for a control volume and thus independent of the internal constituents of the matter. The assumptions for the analysis are same as in case of a PV cell.

A 3-D solid model view of the proposed PV-PCM system is shown in Figure 3.5. The energy exchange process for the system is shown in Figure 3.6.

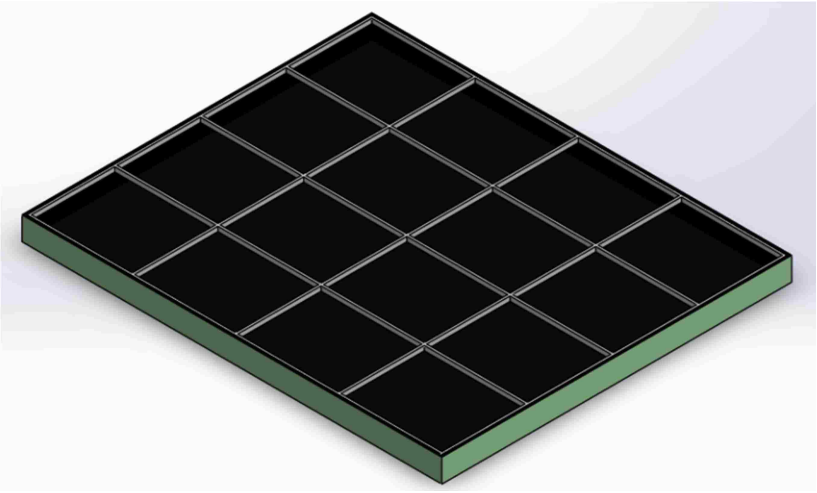

Figure 3.5 Solid model view of the PV-PCM system for the present investigation

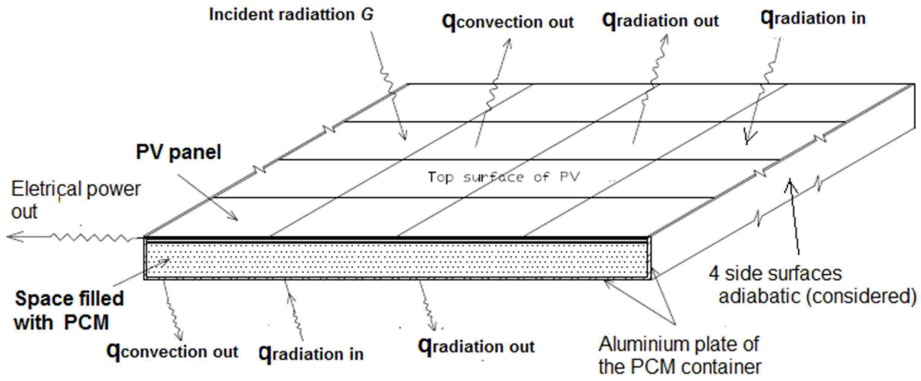

Figure 3.6 Energy exchange model of a PV-PCM system

The heat loss rate and heat absorption rate for a PV-PCM system are identically calculated using Equations 3.5 and 3.6 respectively, using the experimental values of instantaneous PV cell temperature ($T_{surface}$) and incident radiation (G) for the PV-PCM system. The results obtained are presented in Chapter 5.

3.6 Steady state of heat conduction through the PV and PV-PCM system

Ease of conduction heat flow for given thermal boundary conditions under steady state are indicated by thermal resistance. This section presents a simplified analysis of heat conduction phenomenon through both the PV reference panel as well as PV-PCM system for an understanding of the comparative heat flow condition through the bulk of the two systems. To this end, 1-D heat conduction (in the direction of the depth of the systems) model has been used, which simplifies the resistance analysis while achieving the objective of obtaining a picture of comparative performance in heat flow for the systems using the same assumption of 1-D heat flow in both the cases. This assumption considers negligible heat transfer from the four side surfaces of the PV/PV-PCM systems, area being much smaller for the four side surfaces and depths being much smaller compared to the other dimensions as shown in Figures 3.5 and 3.5. The length and height of the working area of the present PV panel are 292.9 mm and 317.5 mm (Chapter 4), respectively while the depth of the PV cell and the PV-PCM combination are only 4 mm (Table 3.1), typically, and 24 mm, respectively. As discussed in Chapter 2, simple 1-D analysis has been used in literature work [32, 35] as well for understanding the essential features of heat conduction through a PV-PCM system

3.6.1 Steady state analysis through thermal resistance network

Thermal resistance concept is very useful for steady state heat conduction analysis within a body. To simplify analysis but essentially indicating The following analysis in If a solid has two different temperature conditions (T_1 and T_2,) at the two ends (for 1-D conduction), Fourier's law of heat conduction relates the heat flux with the temperature difference and thickness as

$$q_x = k\frac{T_1 - T_2}{\Delta x},\ [T_1 > T_2] \qquad ..(3.7)$$

Where, q_x is the heat flux in x-direction, k is the thermal conductivity of the solid and Δx is the thickness of the solid. However, for steady state heat conduction only, the heat flow through the solid remains constant for any position of x so that Δx can be arbitrarily large.

Equation (3.7) can be rewritten as

$$q_x = \frac{T_1 - T_2}{\frac{\Delta x}{k}} \qquad ..(3.8)$$

Comparing Equation 3.8 with Ohm's law ($I = \frac{V}{R}$), the quantity $\frac{\Delta x}{k}$ can be taken as the resistance, R, of a thermal circuit within the solid, the current I through the resistor R is equivalent to heat flow, q_x , through the solid and potential difference V is equivalent to the temperature difference, (T_1-T_2). This analogy makes steady state analysis for a composite slab easy as the concepts of series and parallel resistances with the use of equivalent resistance comes very handy. The elementary circuit for Equation 3.8 is shown in Figure 3.7.

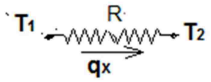

Figure 3.7 Resistance element for steady state heat flow through a body

The resistance R, in Figure 3.7, is given as,

$$R=\frac{\Delta x}{k} \qquad ..(3.9)$$

Thus, if the resistance, $\frac{\Delta x}{k}$, is low, the heat flow for a given temperature difference is high and conversely for a given heat flow (incident radiation for the present case), the temperature

difference across the solid (PV cell for the present case) is very small - both the situations indicate ease of heat flow.

3.6.2 Steady state resistance analysis for a PV and PV-PCM system

For a composite like the PV cell and following Figure 3.4, the resistance circuit can be drawn as in Figure 3.8. For a PV-PCM system an additional resistance R_6 (due to PCM), in series is to be added. For simplicity, the electrical power flux out is not considered.

The resistance for each layer, in series, sum up to the equivalent resistance as follows.

$$R_{eqiv.} = \sum_{i=1}^{5} R_i \quad ..(3.10)$$

where, individual resistance of the i-th layer of the PV panel, $R_{i,}$ is given by

$$R_i = \frac{\Delta x_i}{A k_i}. \quad ..(3.11)$$

The steady state heat conduction equation for the PV resistance circuit as in Figure 3.7, can be written as,

$$q_x = \frac{T_1 - T_2}{R_{equiv}}, \quad ..(3.12)$$

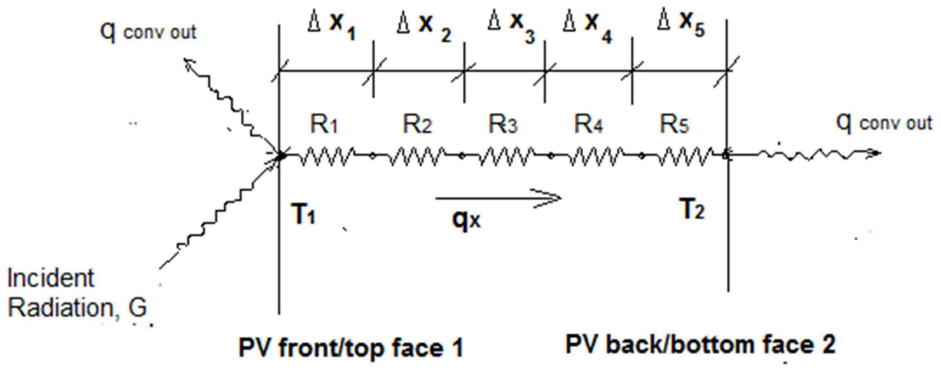

Figure 3.8 Steady state resistance circuits across a PV cell indicating energy flow

From continuity of heat flux at nodes 1 and 2, the following equation can be used to determine the heat flux flow through the bulk of the PV/PV-PCM system.

$$q_x = G - q_{conv.out_1} = q_{conv.out_2}\ , \quad ..(3.13)$$

The calculations for the temperature difference (T_1-T_2) between the front and back surface of PV and PV-PCM systems using Equations 3.12 and 3.13 are furnished in Appendix B. The resistance for the PV-PCM system is observed to be quite high hindering heat flow through the PV-PCM system. Thus, for a PV-PCM system to be effective in thermal regulation, additional means of conductivity improvement for the PCM is imperative. Incorporating internal fins within the PCM is one of the viable means to this end. Further, external fins at the back surface of the PCM container in conjunction with internal fins also promise better thermal regulation for the system. In the present investigation, different configurations of internal and external fins are therefore studied as a promising option for effective thermal regulation.

Chapter 4: Experimentation – The Set Up and Methodology

4.1 The experimental set up and scheme of experimentation

The principal objective of the experiment has been to investigate enhancement of thermal regulation and electrical output of a PV cell through limiting the operating temperature rise in the cell, by using PCM in conjunction with heat transfer enhancing elements of fins. A series of experiments were conducted to investigate the laid down objectives and can be divided into four stages. Firstly, detailed electrical measurements were carried out under steady state conditions to obtain the efficiency correlation with temperature. During thermal investigation study also, the panel was always put under electrical load. To this end, necessary electrical circuitry was constructed to study the deterioration of relevant electrical parameters of the PV panel with high operating temperature. Continuous electrical loading on the PV and PV-PCM system during thermal regulation experiment was also applied through the circuit arrangement, Secondly, the rise in the panel operating temperature for a reference PV cell only was studied under a constant heat flux. The third part of the experiment consisted of the thermal regulation investigation using PCM as a PV-PCM system under a constant electrical load output setting. Finally, different arrangements of fins were incorporated into the PV-PCM system to study the improvement of the thermal conductivity of the PCM.

The experimental system consists of the following components.

1. A PV panel
2. A frame structure for housing the PV panel and also the PV-PCM system and the lamp system
3. PCM container with arrangement for longitudinal fins fitted both on the internal and external surface of the back plate of the container
4. A halogen lamp system to generate incident radiation on the PV panel
5. Instrumentation for measurement including a variable load bank (rheostat) for applying electrical load
6. Data acquisition system
7. Phase Change Material (PCM)
8. A circulating fan

An aluminum frame is constructed which holds the solar panel and has cleats to facilitate holding the panel at different heights thus controlling the distance between the panel and light

source.. A PCM container which contains the PCM is designed and fabricated and fitted at the back of the cell. The overall layout and scheme of the experimentation is shown pictorially in Figure 4.1. An overhead lamp system produces illumination providing the incident irradiation. Temperature of the PV panel, incident radiation, current and voltage generated by the panel are measured for the purpose of the study to achieve the objectives of the experimentation.

The photovoltaic power generated is measured through ammeter-voltmeter combination. Panel temperatures are measured through nine thermocouples fitted on the top surface of the panel. The temperature data are continuously logged to the computer through data acquisition system. Incident radiation intensities are also measured at nine locations on the panel by using pyranometer.

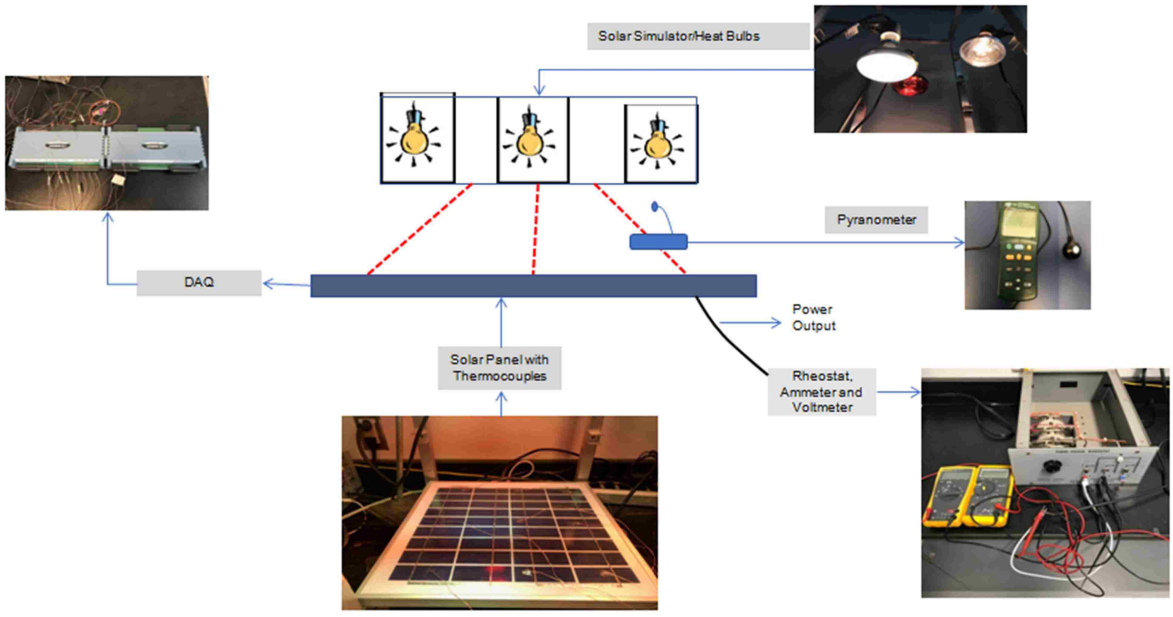

Figure 4.1 A photo schematic of the experimental set up

Each of the components of the experimental set up is discussed in some details in the following sections.

4.1.1 Solar panel

A commercially available polycrystalline silicon type solar panel of size as shown in Figure 4.2 has been used for the study. Figure 4.2(b) along with the dimensions are as provided by the manufacturer.

A moderately high peak power of the panel is chosen so that the range of power obtained is relatively high for better power variation resolution obtainable for the power data points.

The specifications of the panel are as follows.

Test conditions: 1000W/m^2, 25^{0}C (Standard Test Conditions, STC)

Peak power (P_m):	15 W
Peak circuit voltage (V_{oc}):	21.7 V
Short circuit current (I_{sc})	0.95 A
Voltage at peak power (V_m)	17.5 V
Current at peak power (I_m)	0.87 A
Overall panel size [From manufacturer drawing, Figure 4.2(b)]:	(370.8 mm x360.mmx17.8 mm)
Actual Panel Area (as measured);	0.093 m^2 (292.9 mm x317.5 mm)

Thus, efficiency at maximum power point under standard test condition (η_{ref}) is calculated as

η_{ref} = 15/(1000x0.0.093) x100 = 16.09 %

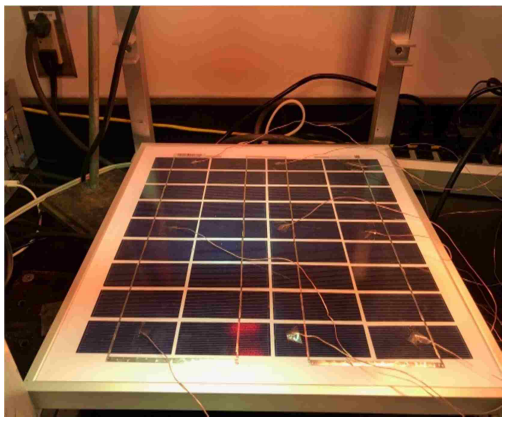

(a)

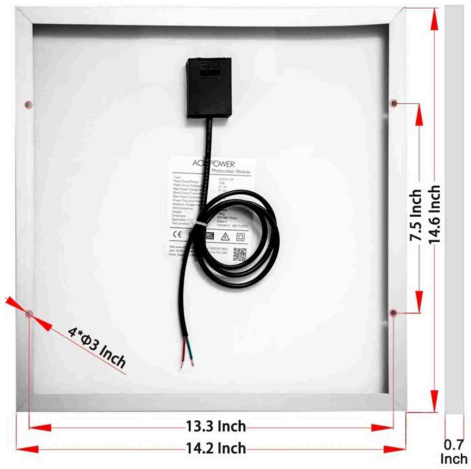

(b)

Fig. 4.2 Solar panel showing (a) the locations of thermocouple in the front side and (b) major dimensions and electrical leads at the back side

4.1.2 Frame structure

The frame structure has been conceived and designed to achieve the following objectives:

i. It should hold a commercially available solar panel of some size securely with provision for fixing it at different heights to vary the incident radiation

ii. It should have place for mounting lamps conveniently

iii. It should facilitate placement of different instruments

iv. It should be rigid enough to withstand accidental push during working

The experimental set up has been designed and fabricated as shown in Figure 4.3. The frame members are made of aluminum box sections mutually interlocked with Allen screws. 1”x1” Intermediate channel cleats are provided along the column legs of the frame for placing the PV panel at different heights, if required, as well as for placement of wire mesh screens to control the amount of radiation reaching the solar panel, if required.

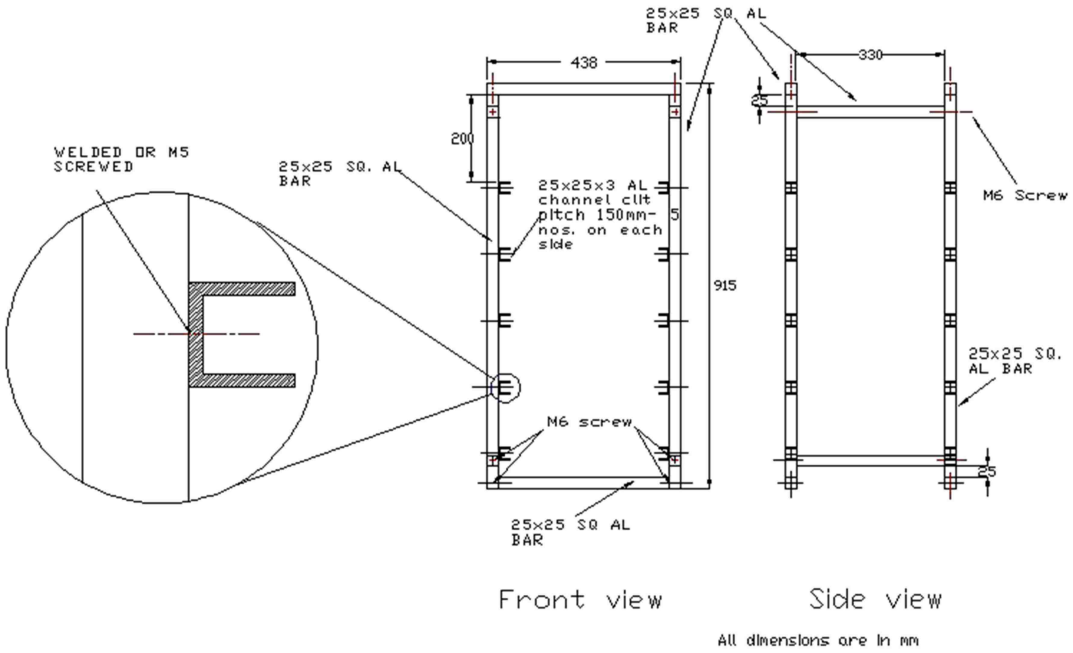

(a)

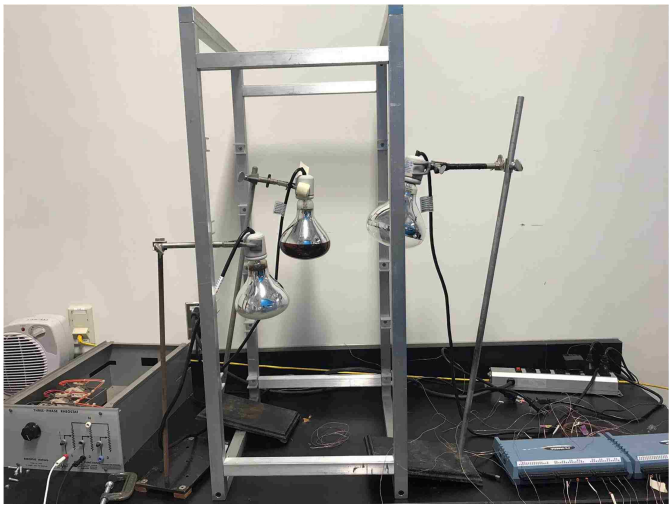

(b)

Figure 4.3: The fabricated frame structure for holding PV and PV-PCM system

4.1.3 PCM container

The PCM container conceived is very much like a hat with cornice to be fitted with the back of the solar panel. The container is filled with PCM through a pouring arrangement fitted with a ball valve. The material of construction is aluminum with good ductility. The thickness is chosen as 1.6 mm to provide sufficient strength at the same time allowing for ease of bending during fabrication. The depth of the container is taken as 20 mm for the case at hand. This is so chosen because many of the previous researchers have used this depth for PCM so that comparison of results is possible. Also literature indicate that the time to come to a steady state value with this depth of PCM is about 3-4 hours which is considered quite practicable for laboratory experimentation duration and measurement

Aluminum straight fins (1 mm thick) are so designed for fixing with the back plate that they can be fitted or removed very easily either from inside or outside of the back plate by suitable screws as shown in Figure 4.4. Figure 4.5 shows the PCM container with external fins as also the experimental set up with PV-PCM system placed in the frame structure.

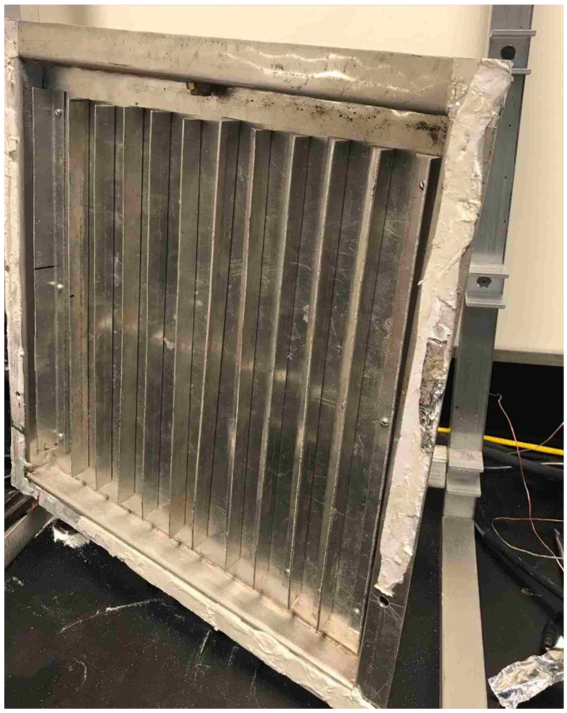

(a)

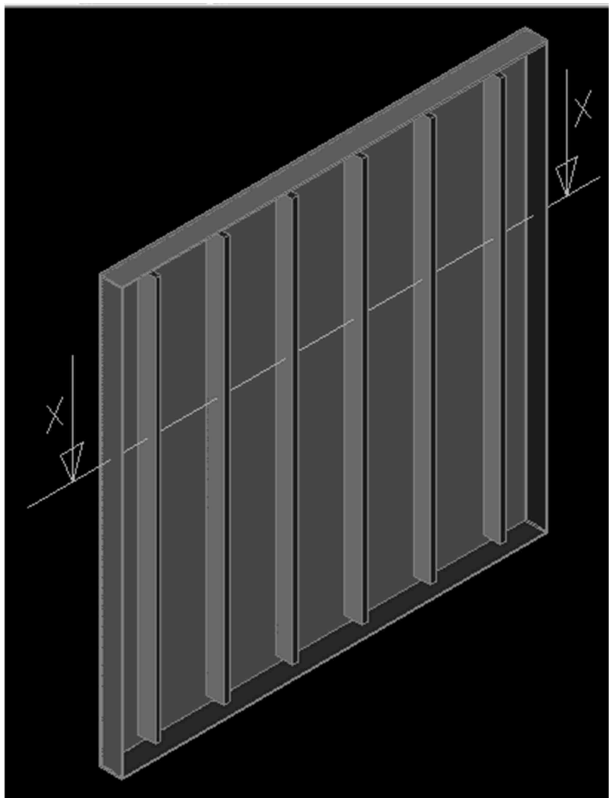

(b)

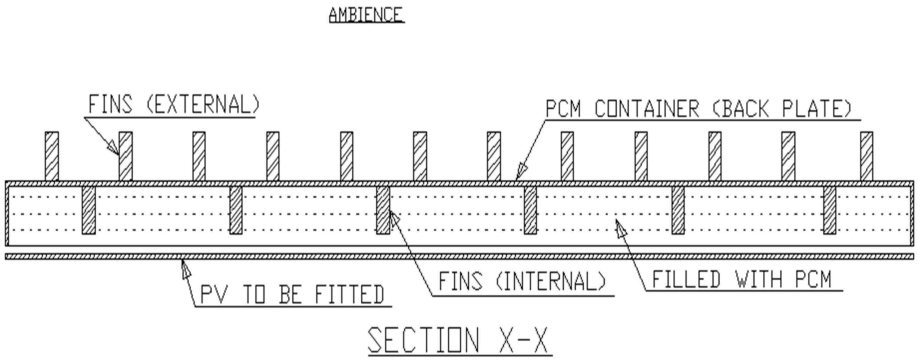

(c)
(Fin thickness exaggerated**)**

Figure 4.4: (a) The PCM container in vertical position with 12 internal fins (b) a 3-D solid model with 6 fins and (c) a sectional top view of the container with fin arrangement

(a)

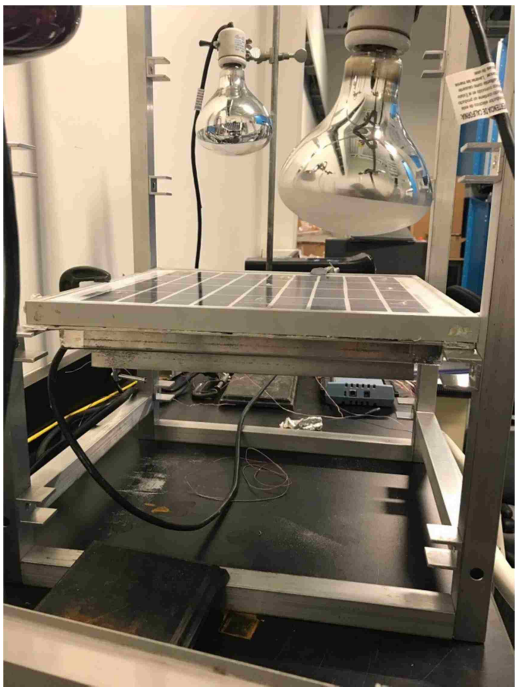

(b)

Figure 4.5: PV-PCM system (a) with external fins, (b) placed in the frame

4.1.4 Lamp system used for incident radiation

Three heat bulbs (Figure 4.6), 250 W each, have been used for producing incident radiation on the panels. In addition to visible light, heat lamps have considerable amount of thermal heating (infrared or IR) component suitable for the present research objective of thermal regulation. However, as discussed later, on the flip side, they also produce less power for a given intensity of incident radiation.

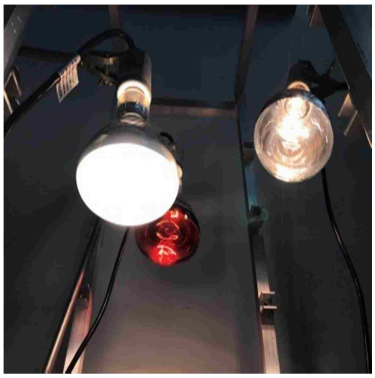

Figure 4.6 Heat bulbs

4.1.5 Instrumentation and accessories

The variables being measured and the measuring instruments including a rheostat are summarised in Table 4.1

Table 4.1 Variables measured and mode of control

Variable measured	**Instruments/Accessories used**	**Mode of data measurements/ control**
Cell temperature	T-type thermocouple	Continuous through DAQs
Incident radiation	Pyranometer	Discrete and manual
Voltage	Multimeter	Discrete and manual
Current	Multimeter	Discrete and manual
	Variable load bank (Rheostat)	Continuous control of load

The specifications of the instruments are furnished below.

1. **Thermocouple –**

   T type thermocouple: 11 nos**.**

   Standard error for T-type thermocouple: $\pm 1^0$C

2. **Pyranometer (Figure 4.7 a) – 1 no.**

Model:	TES 132
Make:	TES Electrical Electronics Corporation, Taiwan
Range:	0-2000W/m^2
Resolution:	1 W/ m^2
Spectral resolution:	400-1000 nm
Accuracy:	Within ±10 W/m^2 or ±5% , whichever is greater in sunlight, additional temperature induced error of ±0.38 W/$m^2/^0$C above 25^0C
Sampling rate:	1 time/sec

3. **Multimeter (Figure 4.7 b) -2 nos.**

Model:	FLUKE series 70 multimeters (73 and 77 III)
Make:	Fluke Corporation
Voltage accuracy:	Upto 320 V ± (0.3%+1)
Current accuracy;	Upto 320 mA ± (1.5%+2)

4. **Variable load bank (Rheostat) – 1 no.**

   A rheostat **(**Figure 4.7 b) is used as a variable load bank for the V-I characteristics of the panel during the experiment.

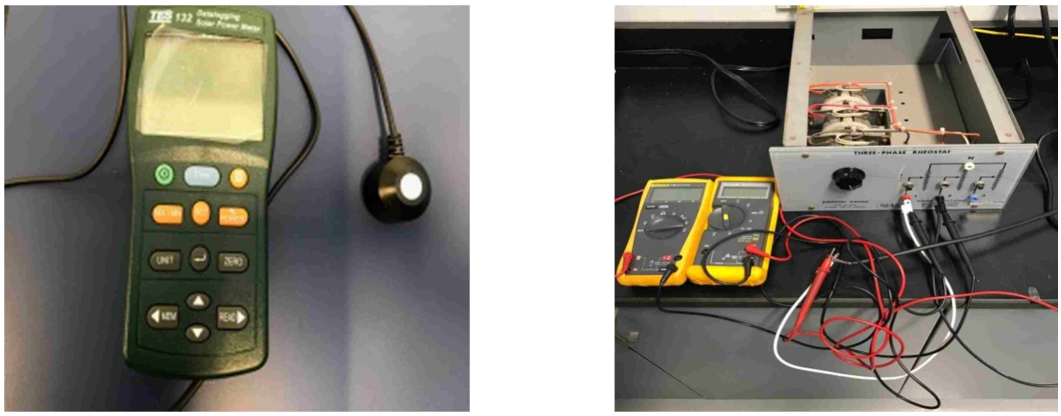

(a) **(b)**

Figure 4.7 (a) Pyranometer and (b) Multimeter and Rheostat

4.1.6 Data acquisition system (DAQs)

Thermocouple data are logged through DAQs system procured for the purpose. Figure 4.8 shows the DAQ and the wiring connection for the purpose.

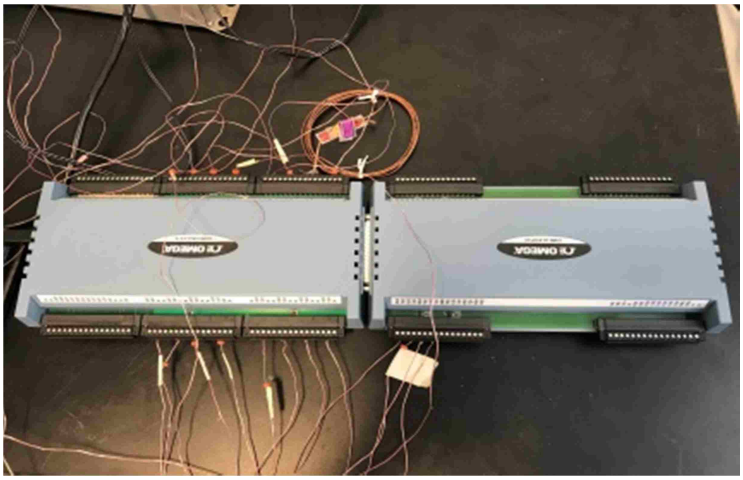

Figure 4.8 Data Acquisition System

The complete specifications for the DAQ are as follows.

Data Acquisition (DAQ) Card: OMB-DAQ-2416

Supplied by: OMEGA ENGINEERING Inc.

Analog Input Characteristics

Number of channels: 32 single-ended or 16 differential (software-selectable per channel) Type of A/D converter (ADC): Successive approximation

Resolution: 24 bits

Max sampling rate: 3750 Samples/sec

Input signal ranges (Bipolar) for Thermocouple: ±0.78125 V

CJC sensor accuracy (condition 0-55^0 C) ±0.5^0 C max

Integration of DAQs with LabVIEW$^{(R)}$ software for data acquisition control and storage had to be done through dedicated programming done in this study as the DAQs of OMEGA company and LabVIEW$^{(R)}$ of National instruments had different protocols for data handling.

4.1.7 Phase Change Material (PCM)

Paraffin wax type of organic material has been a very widely used type of PCM for many applications. This is because of their wide choice of melting temperature and easy availability. For the purpose of the present study, a commercially available paraffin wax type PCM is used. Figure 4.9 shows a sample of the PCM used in the present study.

Figure 4.9 MICRONAL® 5528 X paraffin PCM used in the study

The properties of the PCM used as furnished by manufacturer are as follows

Type – Paraffin wax branded MICRONAL® 5528 X

Manufacturer- Microtek Laboratories Inc., Ohio, USA

Thermo-Physical properties

Mean Particle Size; 50-400 μm

pH value: 8.5 ± 0.5

Density 300-400 kg/m^3

Phase Change (Melting) 28 °C ± 1°C

Phase Change (Crystallization) 25 °C ± 1°C

Heat of Fusion' 160 kJ/kg

4.1.8 Circulating fan

A circulating fan was used for cooling the PV panel to obtain different steady state temperatures of the panel for a constant incident intensity of radiation.. This was achieved by placing the fan at different distances away from the panel.

4.2 Estimation of error and uncertainty

The various errors and uncertainties in the measurement of the parameters and variables are obtained by applying the methods of uncertainty analysis. Checking for precision error (also called random error) errors was done for each measured parameters based on 5 random measurements for each.

According to rule of Root Sum Squares (RSS) in uncertainty analysis, the resultant uncertainty is given by,

$$U_{parameter} = \sqrt{B_{parameter}^2 + P_{parameter}^2} \quad ..(4.1)$$

where $B_{parameter}$ and $P_{parameter}$ denote the bias and precision error of the parameter.

Based on 5 data points student's t-distribution at 95% confidence level, is the t- distribution $t_{5,95}$ is found to be 2.776. This value is subsequently used for finding the random error. Random error, $P_{parameter}$ is given by,

$$P_{parameter} = 2.776\ x\ \frac{Standard\ deviation}{\sqrt{no.\ of\ samples}} \quad ..(4.2)$$

Equations 4.1 and 4.2 have been used throughout for calculating total and random errors.

i. Temperature measurement with thermocouple and DAQ

Standard error for T-type thermocouple, B_1: $\pm 1^0$C

DAQ error including CJC error, at 1 Sample/s (as per DAQ manual) B_2: $\pm 0.5^0$C)

Resultant Bias Error, $B_T = \sqrt{B_1^2 + B_2^2} =$ $\pm 1.12^0$C

The standard deviation for random measurement = $\pm 0.25^0$C

Random error, P_T $\pm 0.31^0$C

Thus, the uncertainty in temperature measurement $U_T = = \sqrt{B_T^2 + P_T^2}_T =$ $\pm 1.16^0$C.

Considering a nominal temperature (on the lower side) of 30^0C, the relative uncertainty become, U_T/T =±3.87%

ii. Incident radiation intensity measurement by pyranometer

The Pyranometer used in the experiment had

i) Minimum accuracy, B_1 ±10 W/m^2

ii) Resolution error, B_2 = 1/2 of instrument resolution =±0.5 W/m^2

Thus, bias error of the pyranometer, $B_P = \sqrt{{B_1}^2 + {B_2}^2} =$ ± 10.0125 W/m^2

In absence of any repetitive experiment, random error (Ur) is taken as zero and

uncertainty in incident radiation becomes, $U_G = \sqrt{{B_P}^2 + {U_r}^2} = B_P =$ ± 10.0125 W/m^2

Standard deviation = ±6.25 W/m^2

Uncertainty, U_G = ±12.67 W/m^2

The relative uncertainty is given by U_G/G= ±1.76%

iii. Voltage and current measurement by multimeter

Voltage accuracy, B_{1v}: Upto 320 V = ± (0.3%+1)

Voltage resolution, B_{2v} = ± 0.1 V

Current accuracy, B_{1c}; Upto 320 mA = ± (1.5%+2)

Current resolution, B_{2c} = ± 0.1 mA

For the current experiment, maximum voltage obtained has been 21.3 V and maximum current 510 mA. As such, the maximum bias errors for measurement of voltage (B_V) and current (B_C) are as follows:

$B_V = \sqrt{{B_{1v}}^2 + {B_{2v}}^2} = \pm 1.068$ V

$B_C = \sqrt{{B_{1c}}^2 + {B_{2c}}^2} = \pm 8.651$ mA

Standard deviation for random test for voltage= ±0.54 V

Random error for voltage, P_v = ±0.67 V

Total uncertainty in voltage, U_v= ±1.26 V

Standard deviation for random test for current = ±10.65 mA

Random error for current, P_c = ±8.26 mA

Total uncertainty in current, U_c = ±11.96 mA

The relative uncertainties for voltage and current are ±5.27% and ±3.1%, respectively.

iv. Uncertainty in the calculated values of power

From the rule of uncertainty, if a parameter Y is dependent on $X_1, X_2, \ldots, X_n$, the uncertainty of Y is determined using the RSS as follows.

v. $$U_Y = \pm\sqrt{\left(\frac{\partial Y}{\partial X_1} U_{X_1}\right)^2 + \left(\frac{\partial Y}{\partial X_2} U_{X_2}\right)^2 + \cdots + \left(\frac{\partial Y}{\partial X_n} U_{X_n}\right)^2} \quad ..(4.3)$$

where, U_{X_i} , $i = 1 \ldots n$ denotes the uncertainties of the variables X_i

Relative uncertainty is given by

$$\frac{U_Y}{Y} = \pm\frac{\sqrt{\left(\frac{\partial Y}{\partial X_1} U_{X_1}\right)^2 + \left(\frac{\partial Y}{\partial X_2} U_{X_2}\right)^2 + \cdots + \left(\frac{\partial Y}{\partial X_n} U_{X_n}\right)^2}}{Y} \quad ..(4.4)$$

Power, is calculated using the formula,

$P = VI$ ..(4.5)

Thus, using Equations (4.4) and 4.5, the uncertainty in the values of electrical power can be calculated from the measured values of voltage, V (in Volts) and current, I (in mA) as follows.

$$\frac{U_P}{P}(\%) = \pm\frac{\sqrt{(VU_C)^2+(IU_V)^2}}{P} \text{x}100 \quad ..(4.6)$$

Considering the maximum anticipated values of power to be 16 W and inserting the appropriate values of B_V and B_C, the maximum expected uncertainty (in absence of random error) in power is obtained as,

$U_P/P\ (\%) = \pm 4.53\ \%$

vi. Uncertainty in the calculated value of panel area

The uncertainty U_A in measurement of area A of the PV panel is obtained as follows.

$$A = LxH \quad ..(4.7)$$

where L and H are the length and breadth of the panel as measured with a meter steel rule with least count of 1 mm.. As such, accuracy ($B_{accuracy}$), resolution ($B_{resolution}$) and total bias error in length measurement of L and H are calculated as follows.

$B_{accuracy} = \pm 1$ mm

$B_{resolution} = B_{accuracy}/2 = \pm 0.5$ mm

$$B_{steel\ rule} = B_L = B_H = \pm\sqrt{\left(B_{Haccuracy}\right)^2 + (B_{resolution})^2} = \pm 1.12 \text{ mm}$$

Standard deviation with random test = ±1.2 mm

Random error, $P_{length} = \pm 1.49$ mm

The expected uncertainty in length measurements are,

$U_L = \pm 1.86$ mm

From Equation 4.4,

$$U_A = \pm\sqrt{(LU_L)^2 + (HU_L)^2} \quad ..(4.8)$$

For the measured size (L=292.9 mm and H=317.5 mm), the relative uncertainty in area,

$$\frac{U_A}{A}(\%) = \pm\frac{\sqrt{(LU_H)^2+(HU_L)^2}}{A} \text{x}100 = 0.86\ \%$$

vii. Uncertainty in the calculated values of panel efficiency

Efficiency (η) of a solar panel is calculated from the equation as furnished below.

$$\eta = \frac{P_{max}}{AG} \quad ..(4.9)$$

and, hence, using Equation 4.2, the expression for uncertainty in efficiency becomes,

$$U_\eta = \pm\sqrt{\left(\frac{U_{P_{max}}}{AG}\right)^2 + \left(-\frac{P_{max}}{AG^2}U_G\right)^2 + \left(-\frac{P_{max}}{A^2G}U_A\right)^2} \quad ..(4.10)$$

Inserting the experimental nominal values of G (720 W/m^2), P_{max} (16 W), A (0.093 m^2) and the other uncertainty values already calculated , the uncertainty in the calculated values of efficiency is found to be,

Relative uncertainty, $\frac{U_\eta}{\eta}$ = ± 4.67%.

Table 4.2 furnishes the uncertainties in the measured values of the parameters and variables as well as the computed values of variables using measured values.

Table 4.2 Uncertainty values in measurement/calculation

Parameters/Variables	Maximum Uncertainty
Temperature	±3.87 %
Voltage	±5.92 %
Current	±3.10 %
Incident Radiation	± 1.76 %
Area of panel (calculated)	±0.86%
Power (calculated)	± 4.54%
Efficiency (calculated)	± 4.67%

4.3 Details of experimentation

The experimentation consists of both thermal and electrical measurements under the following conditions.

i) Experimentation with only solar panel

   a) Electrical characteristics and efficiency in dependence of cell temperature under different steady state temperature conditions
   b) Time evolution of PV cell temperature

ii) Experimentation for thermal regulation with PV-PCM system

   a) Experiment with solar panel-PCM (PV-PCM) without fins in the container for time evolution of temperature

   b) Experiment with PV-PCM and internal fins for time evolution of temperature

   c) Experiment with PV-PCM with a combinations of internal and external fins for time evolution of temperature

All the measurements for the experimentations as above were taken under a constant intensity of incident radiation (720 W/m^2) as the maximum obtainable intensity for the present set up. During all experiments with temperature evolution study, electrical load was applied throughout to incorporate the effect of electrical energy out on the energy absorption by the cell in increasing its temperature. Electrical load was applied and controlled through a rheostat type resistance load.

The incident radiation was measured with pyranometer placed at nine different locations as shown in Figure 4.10. The temperature values on the surface of the cell were measured with T-type thermocouples placed at the same nine locations as shown in Figure 4.2(a) and Figure 4.10. The locations are chosen to take care of the possible non-uniformity in the distribution of incident radiation and consequent temperature distribution on the solar panel. A reasonably good uniform distribution of incident radiation intensity and temperature over the solar panel was obtained with the lamp system and presented in Chapter 5 (Figures 5.1 and 5.2).

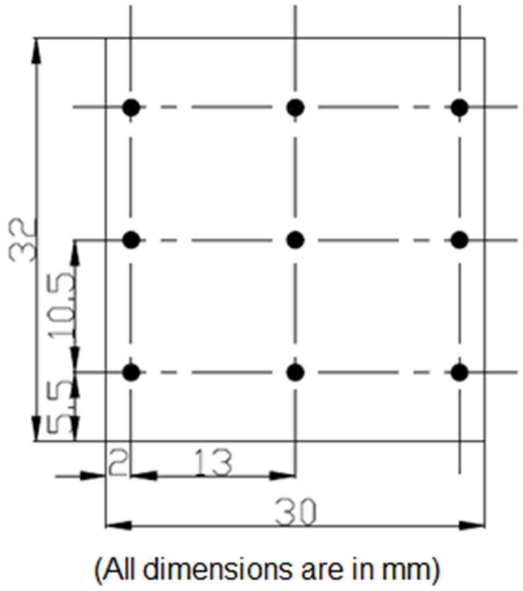

Figure 4.10 Locations of thermocouple and pyranometer measurement on the PV panel

Experimental details for the above-mentioned modules are discussed in the next sections to follow.

4.3.1 Experimentation with only solar panel

In this series of experimentation, measurements for V-I characteristics were carried out. The experimental data are used to find the P-V characteristics, temperature correlation and temperature coefficient (β) for conversion efficiency

Electrical measurements were carried out for V-I characteristics at different steady state temperature conditions. This was done to determine the temperature effect of efficiency considering the irradiation level to be constant. In the present experimental set up developed for the study, for a constant average condition of intensity of incident radiation, four different steady state temperatures were obtained by forced cooling of the panel employing a circulating fan. Different operating temperature could be established by placing the fan at correspondingly different distances, a priori marked, away from the panel. The incident radiation was provided by three lamps put over the solar panel at a suitable height as shown in Figures 4.5 and 4.6. The temperature values on the surface of the cell were measured with T-type thermocouples placed at nine locations as shown in Figure 4.2(a) and Figure

4.9. A methodology is adopted for calibrating the conditions required for obtaining different steady state temperature in a separate exercise of experimentation for the purpose so that during the actual electrical measurement experiment, the experimental condition for the steady conditions can be recreated. Described below are the methodologies adopted for calibration of cooling fan location as well as electrical parameter experimentation under steady state temperature conditions for the PV cell only.

i) Methodology and steps for calibrating the conditions required for obtaining steady state temperature

1. The PV panel is placed at the lowest level of the frame to produce relatively uniform intensity of radiation onto the top of the frame, due to more possible interception of heat flux from the diverging cone of light ray from the bulbs. The spatial variations of intensity for all conditions were found to be within ±2.5%. of the mean of The spatial variations of intensity for all conditions were found to be within ±2.5% of the mean of 720 W/m^2 with standard deviation of 10.44 W/m^2, as discussed in Chapter 5. This level of intensity was kept constant for all experimental cases.
2. The heat bulbs are switched on
3. The thermocouples with the DAQs are put into operation for recording of the PV temperature
4. The temperature data are monitored for steady state conditions and steady state temperature noted.
5. Next, a circulating fan is placed at an arbitrary distance a little away (1.5 m) from the panel centre and switched on to produce forced air cooling of the panel.
6. Under this condition, the PV panel temperature would come down and the steady state temperature noted.
7. If the new steady state temperature is about 10-12^{0}C lower than the previous steady state value, the position of the fan is marked on the table on which it was kept.
8. Next the circulating fan is placed nearer to the panel to obtain a still lower value of steady state temperature.
9. Steps 7 is repeated
10. Steps 8 and 9 repeated one more time

Thus, four different steady state values are obtained (one without fan and three with fan) and the conditions for achieving this, later during measurement for electrical characteristics experiment, are calibrated in terms of noting the positions of the fan and marking prominently, where the fans would be subsequently placed to produce the desired steady state temperatures of the panel. The fan speed remained the same producing a flow pattern presumably the same. As the ultimate objective was to obtain different levels of stead state temperature, the fan-induced flow velocity over the panel was not measured for its distribution as its effect is reflected through the temperature distribution, which was measured through thermocouples

ii) Methodology and steps for electrical measurements

Equipment and instruments for the measurement of electrical parameters used are as follows.

1. Solar cell
2. Multimeter – 2 nos.
3. Variable load bank (rheostat)
4. Insulated wire with alligator clips
5. Light source
6. Light intensity meter (Pyranometer) – 1 no.
7. Circulating cooling fan

A circuit for the measurement is made as per the circuit diagram shown in Figure 4.11. The two multimeters are used- one for measurement of voltage and the other for current. The objective is to obtain V-I characteristics of the PV module for different at steady state operating temperatures.

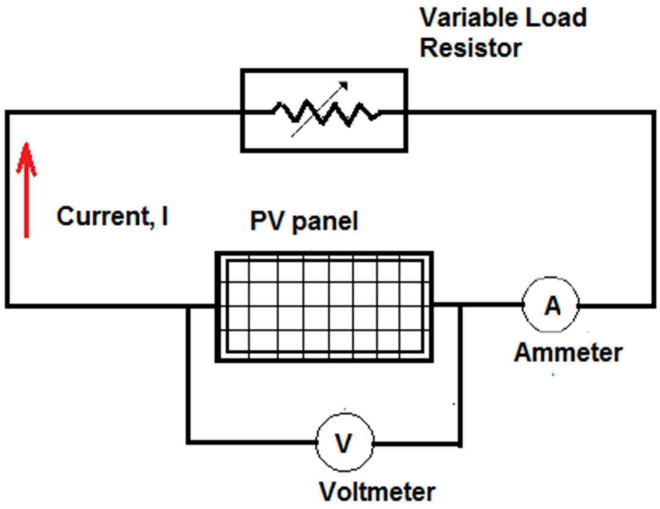

.Figure 4.11 Circuit for electrical measurements.

At each steady state temperature condition, the power output was varied through the rheostat and corresponding voltage and current were measured by two numbers of multimeters, one for each. The electrical measurement methodology and steps are described as follows.

The sequence of steps for the electrical measurement is as follows.

1. Thermocouples are pasted on the PV panel at the nine locations without data recording connection.
2. The circuit is set up as per Figure 4.9 without load connection
3. Lamps are switched on
4. After waiting for about half an hour assuming steady state condition of intensity of light has been achieved, the light intensity measurement is started and the pyranometer placed at one of the nine locations. The reading is noted.
5. Pyranometer measurements for all other locations are obtained serially and noted
6. Thermocouple measurements and DAQs started to check for subsequent steady state condition for temperature
7. After steady state condition is reached, electrical measurements start
8. Output terminals of the PV panel are short circuited by a wire and the short circuit current and voltage recorded.

9. Variable load resistance is then connected starting from lower resistance and increasing to higher ones in instalments so that the panel voltage increases from zero towards open circuit condition when the load resistance is very high. At each load condition, the voltage and current values are recorded.
10. The DAQ data for the temperature stored for the steady state temperature value.
11. The electrical connections are switched off.
12. The thermocouple and DAQs are put off.
13. So far, the panel was allowed to heat up under normal surrounding ambient condition. Now, a different steady state temperature condition with the same setting of bulbs is obtained with the help of cooling fan. The cooling fan is placed at one of the already marked places (described earlier) and the fan switched on
14. Steps from serial no. 6 to 12 are repeated for each of the three marked locations of the fan.
15. At the end of the experiment, pyranometer measurements were again taken to observe if there were any discrepancies in the readings due to any possible fluctuation in the supply voltage for the lamps. Throughout the entire experimentation, the time variation of intensity reading was less than 0.5%.

4.3.2 Experimentation for thermal regulation with PV-PCM system

The experiment was carried out by placing the solar panel within the frame as shown in the Figures 4.2 and 4.4. No screen mesh were placed as all experiments for thermal regulation were designed to be carried out at incident radiation close to 750 W/m^2 (used in many literature work) and the maximum intensity that could be achieved in the set up was 720 W/m^2 as observed during electrical characteristic measurements in module (a) above. The temperature rise in PV is not expected to be very rapid and as such, a sampling rate for temperature measurement was set at 1 sample per second and stored in the computer. The experiment was carried out till an acceptable steady state temperature condition is reached. Variable load resistor setting was kept corresponding to maximum power delivery at G=720 W/m^2 as obtained from experimental setting during experimentation of module (a). This ensures a real life situation for load during PV heating delivering maximum power all the time during thermal measurement.

The ambient temperatures remained within the range of 21^0C to 23^0C throughout the course of experimentation. The time evolution of the solar cell temperature was recorded for processing.

The different modules under this series of experiments are described in the following subsections.

4.3.2.1 PV-PCM without fins

The setting for incident radiation, rheostat setting for maximum power load and the sequence of pyranometer and other measurements were kept the same as in module (i)..

The PCM container was fitted to the back of the PV cell (Figures 3.6, 4.4 and 4.5) and molten PCM poured through the inlet feeding funnel and inlet piping system and filled near the top of the long pipe bend. The long bend at the inlet ensures that the PCM container is always full of PCM and the PV back surface consequently had always PCM in its contact for heat transfer. The PCM was allowed to cool to the ambient temperature when it solidified before the experimental runs were taken. The presence of PCM makes the system take a longer time to come to steady state and hence, for practical reasons, the readings were taken during a period of about 3-4 hours.

4.3.2.2 PV-PCM with internal fins

The settings for incident radiation and rheostat were kept the same. Experimental procedures and measurement protocols are the same as in (ii). In this module of experimentation, the PCM container used was fitted with internal fins placed longitudinally at the internal side of the back plate of the container. Experiments were carried out with both configurations of 6 and 12 of internal fins in the back surface of the container. Using internal fins within the PCM was done to increase the effective thermal conductivity of PCM. Two configurations of fins (6 and 12 internal fins.) were chosen to investigate the effect of number of internal fins on thermal regulation. The measurement steps are the same as in module *(i)*. Time evolution of the solar cell temperature is recorded as before.

4.3.2.3 PV-PCM with internal and external fins

The settings for all parameters were kept the same as in the previous modules. Experimental procedures are the same as in iii) above except that the PCM container used was fitted with 6 nos. of internal fins in the inside of the back surface as well as 12 nos. of rectangular fins fitted on the external surface of the container back plate. This was done to increase the effective thermal conductivity of PCM (by internal fins) as well as to enhance heat transfer away to the ambience through the back plate external surface fins.. The measurement steps are the same as in module (i). Time evolution of the solar cell temperature was recorded as before. Electrical load connection with the rheostat setting corresponding to maximum power setting was maintained as in modules (i), (ii) and (iii).

Chapter 5: Results and Discussion

As a part of the present study, electrical characteristics of the PV panel at hand were obtained experimentally at different operating temperatures of the panel. The conversion efficiency of the PV cell in dependence of temperature has been obtained from the V-I characteristics. The efficiency correlation with temperature and temperature coefficient, β, are obtained from the plot of efficiency with temperature.

Experiments for thermal regulation study, as described in Chapter 4, were initially carried out with reference cell only. After appropriate data reduction and data processing, the corresponding results are compared with established results available in literature are also presented in Figure 5.6 for comparison.

To assess the relative efficacies of PV-PCM systems i) without fins, ii) with 6 internal fins, iii) with 12 internal fins, iv) with 6 internal fins and 12 fins fitted at the external surface of the container back plate and v) the reference system (PV only), experiments are carried out to obtain the temperature evolution history for each case and discussed.

Various thermal regulation performance indicators are used for different configurations of PV/PV-PCM system and discussed.

The heat loss rate and rate of heat absorption for the PV reference cell and different configurations of PV-PCM systems are calculated following the analyses as described in Chapter 3 and presented.

5.1 Data reduction and processing

i) Intensity of incident radiation (G)

Intensity of incident radiation from the heat bulbs on the cell surface was measured by pyranometer. The intensity was recorded at the locations as in Figure 4.10. The representative incident radiation of PV cell at any instant of time is computed as the arithmetic mean of the measured intensities at the nine locations, which was 720 W/m^2.. The standard deviation of the spatial distribution is 10.44 W/m^2 about the mean. The maximum spatial variation has been less than ±2.08% about the mean. A typical intensity mapping on the PV surface is shown in Figure 5.1..

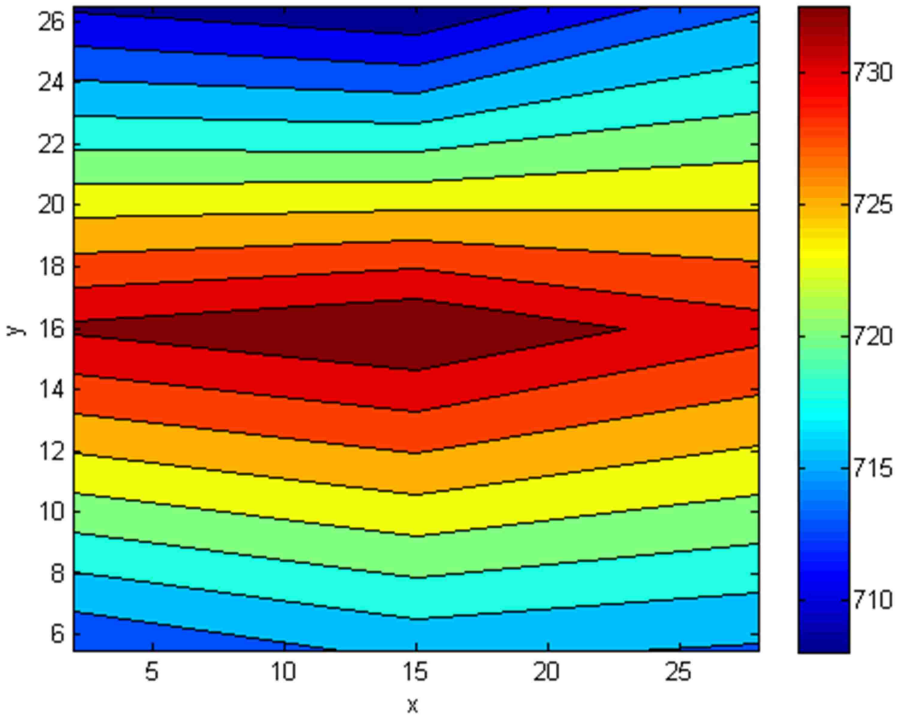

Figure 5.1 Typical incident heat flux distribution on the PV cell front surface ($G_{average}$=720 W/m^2)

ii) PV cell temperature (T)

Cell front surface temperatures were measured at 9 (nine) locations (shown in Figure 4.10) on the cell surface by thermocouples using DAQs and logged on to the computer as detailed in Chapter 4. The sampling rate was kept at 1 sample per

second as temperature rise was considered gradual enough. As a matter of fact, temperature evolution as revealed by plots in subsequent graphs justifies the consideration. Figure 5.2 shows thermal mapping of the PV cell surface under steady state (mean temperature of 49.7 ^{0}C) as obtained from a typical discrete data of temperature measurements at nine locations. The representative temperature of PV cell at any instant of time is computed as the arithmetic mean of the temperatures at the nine locations (Figure 4.10). The maximum spatial variation has been less than ±7.8% about the mean. The standard deviation of the spatial distribution is 2.48 ^{0}C about the mean.. Temperature at the back of the PV cell was found to be equal to the front surface of the cell to the first decimal digit. This is because of very negligible resistance (Section 3.6.2) of the PV component layers.

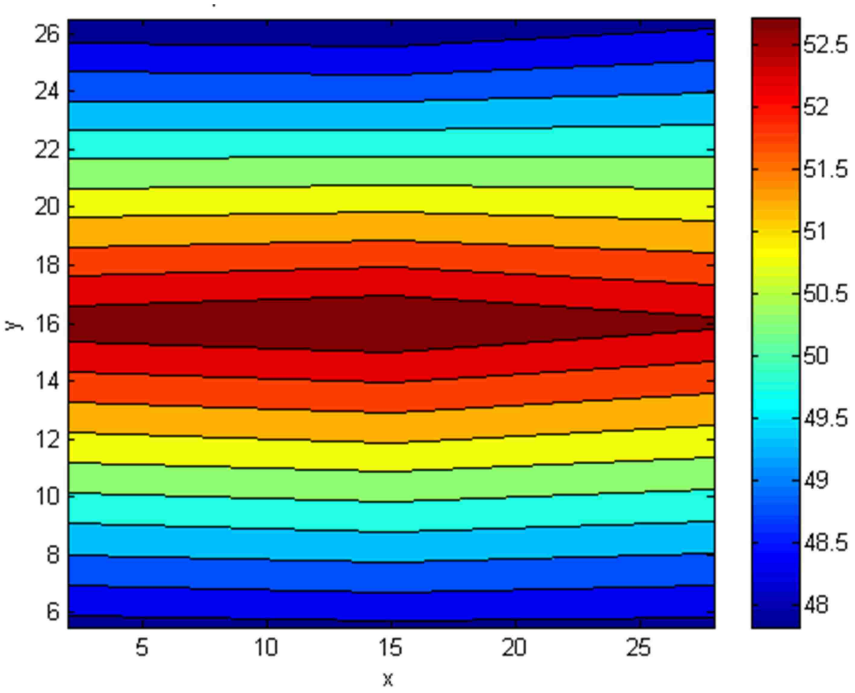

Figure 5.2 Typical temperature distributions on the PV cell front surface at an instant of time during PV heating
(G=720 W/m^2)

The origin coordinates indicated in the contour map of Figures 5.1 and 5.2 correspond to the actual geometrical coordinate (2,5.5) of the lowermost left corner location (where measurements were taken) with respect to the zero origin of the

actual working panel (Figure 4.10). The straight line contours as obtained with MATLAB for both heat flux and temperature distribution appear to be due to relatively smaller number of data points (9 only) available for interpolation as provided for the purpose from experimental measurements,

The spatial variation of both intensity of radiation and temperature distribution indicate are considered fairly uniform and the locations of measurement as in Figure 4.10 prove satisfactory.

iii) Electrical measurements

The voltage and current measurements were obtained with the help of the variable load resistor and two multimeters as described in Chapter 4. These were used for plotting the V-I characteristics. Power output (P) was calculated by multiplying the voltage with the current and the corresponding P-V characteristics were plotted. The conversion efficiency was computed by dividing the power out by the input power which is the mean of the incident radiation intensity as measured by the pyranometer. The reference efficiency for the PV cell was calculated from the experimental data extrapolating to 25^0C.

5.2 V–I characteristics and Conversion Efficiency

Experiments were conducted to investigate the effect of cell temperature on the efficiency of the cell at four different steady state temperature conditions under a constant incident radiation of 720 W/m^2. The correlation of efficiency with cell operating temperature and temperature coefficient of efficiency were obtained from the experimental data.

Figure 5.3 (a & b) depicts the V-I characteristics and the power curve thereof for different steady state temperature. For a constant incident radiation intensity, the power output ($P_{out} = \eta\ G\ A$) is linearly proportional to the incident radiation provided temperature remains the same (i.e. η becomes essentially constant). The maximum power output of the test cell is 15 W at 1000 W/m^2 and 25^0C (from cell data sheet under Standard Test Conditions). One of the present experimental conditions of G=720 W/m^2 and T= 30.6^0 C, has a relatively small deviation from the standard test condition of temperature of 25^0 C. Therefore, the maximum power output for the present condition can be taken to be proportional to the intensity of

radiation and hence should be 10.8 W (= 15 x 720/1000), approximately. However, it is observed (Figure 5.3) that the maximum power output for the particular experimental condition is 7.36 W, which is about 32% less. Any error in the multimeter measurements notwithstanding, the major source of such large deviation may be attributed to the fact that the incident radiation in the experiment provided with heat lamps possibly does not have the spectrum of solar radiation, especially lacking the visible light range of the electromagnetic spectrum and hence the conversion is much less in comparison. Determination of the heat bulb spectrum could not be carried out in the ambit of the present study. It is also observed that the maximum power condition based on which efficiency of a PV cell is computed occurs almost at the same voltage although shifting a bit towards higher voltages with lower temperature which is also the general trend as found in literature. Open circuit voltage is known to increase a little with decrease in temperature as also revealed in Figure 5.3. As expected from standard literature data, the short circuit current I_{sc} is also obtained as almost independent of temperature. However, experimental I_{sc} (about 500 mA) is much lower than the STC I_{sc} for the cell which is 940 mA. This is chiefly because of the difference in intensities as well as spectrum in the present experiment in comparison to STC quantities.

Conversion efficiency as a function of the cell operating temperature is shown in Figure 5.4. Efficiency values are computed from the results of the electrical measurements as in Figure 5.3. The experimental efficiency values do not compare favourably with those value at standard test conditions (1000 W/m^2 and 25^{0}C) because the incident radiation in the present experiment does not simulate the solar radiation spectrum as explained earlier. However, as expected, efficiency falls with increase in operating temperature. By using the value of η_{ref} as 12.07% (obtained by extrapolating the experimental correlation to the STC temperature of 25^{0}C), the temperature coefficient value of β ($\beta = \frac{1}{\eta_{ref}}\frac{d\eta}{dT}$) is calculated as 0.33%/K which is a little lower than the standard literature value range of 0.40% to 0.50%/K. This is thought to be due to the lower share of visible range of radiation in the experimental spectrum compared to the IR component. Thus, increasing the temperature should have lower influence on the conversion efficiency decrease and hence a lower value of β is obtained in the experiment compared to the value when there is solar spectrum in the incident radiation.

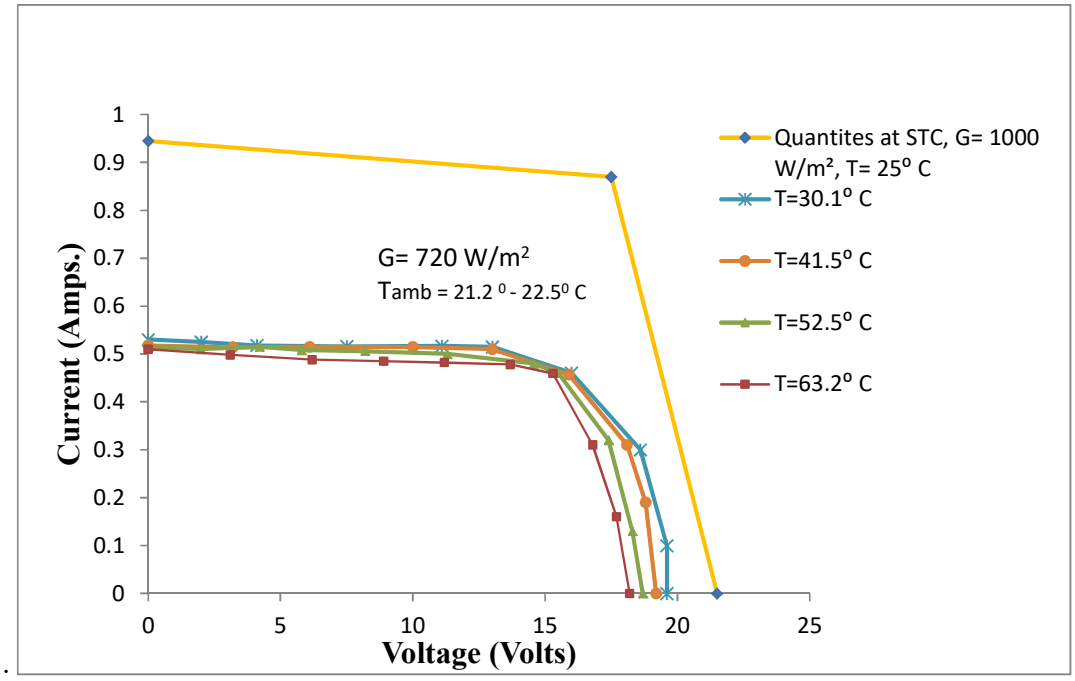

(a)

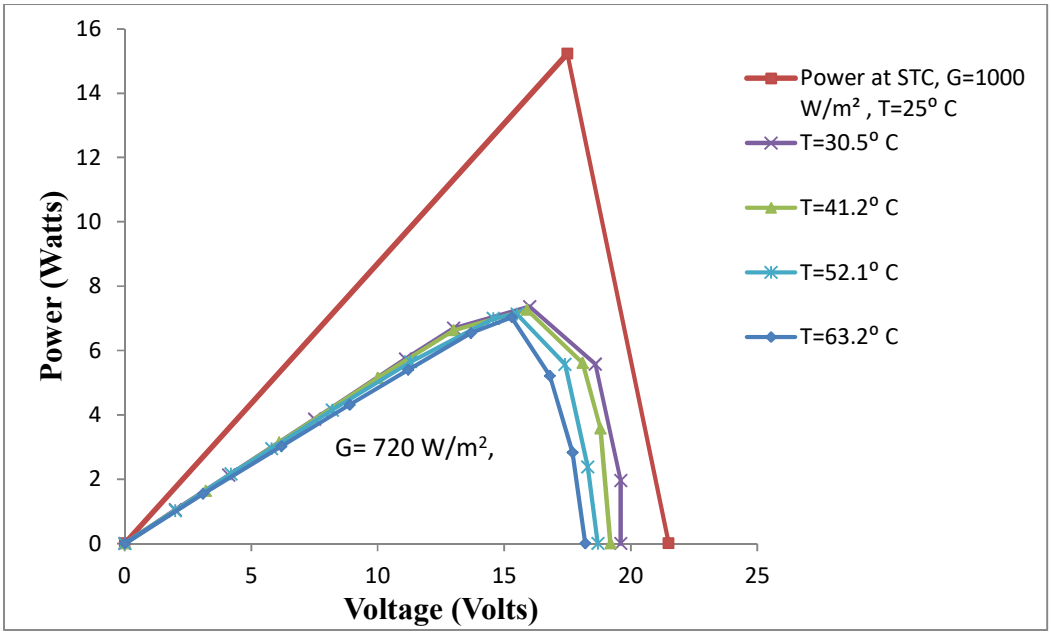

(b)

Figure 5.3 (a) V-I characteristics and (b) P-V characteristics for the panel

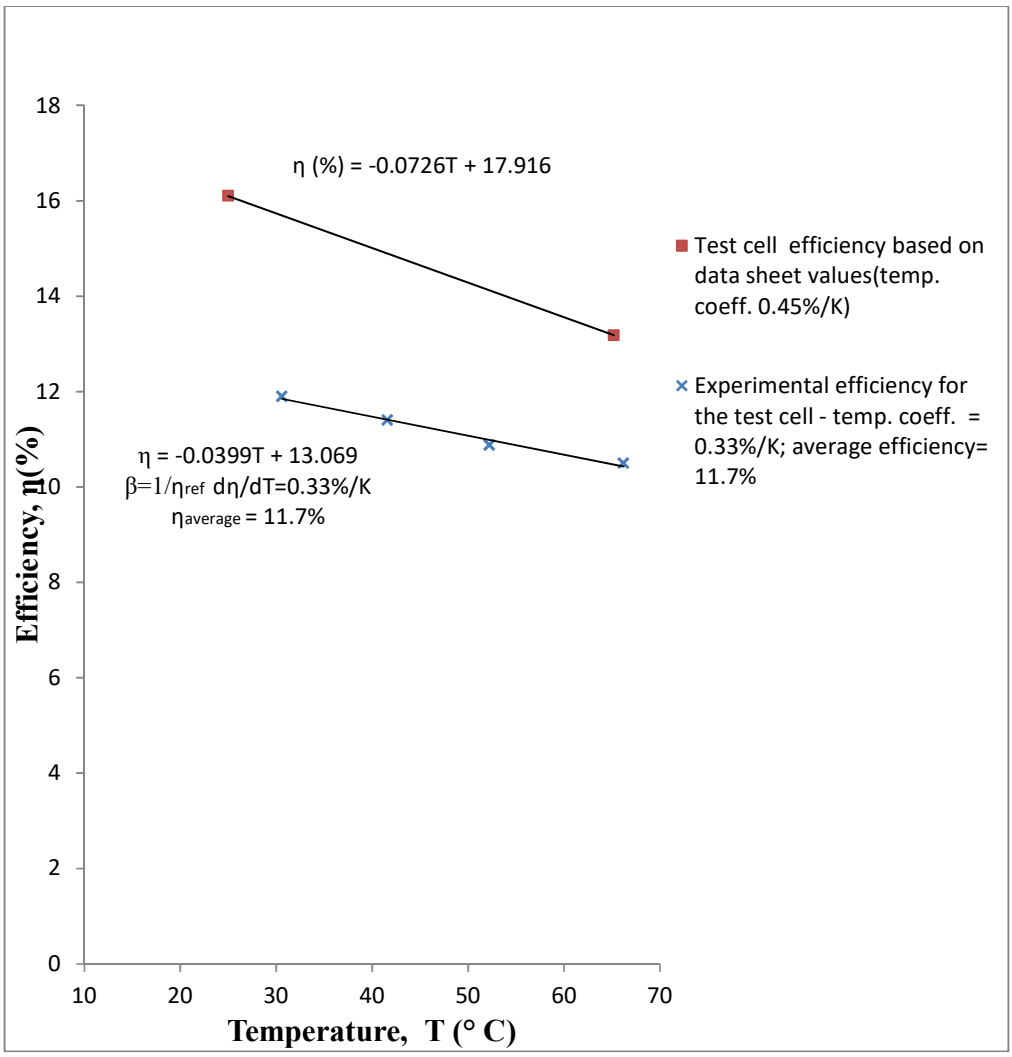

Figure 5.4 Efficiency vs. temperature of the experimental cell

From the best fit line, the conversion efficiency (%) correlation is obtained as

$$\eta(T) = 0.0399\,T + 13.069 \quad \text{.. (5.1)}$$

Although, the correlation is obtained for the experimental temperature range of 30 ^{0}C-63 ^{0}C, since the correlation fit is linear (as also established in literature), the same correlation can be used for extrapolating either way for other temperature conditions also.

The best fit line for the STC condition as obtained from the manufacturer data (using three data points for maximum power, short circuit current and open circuit voltage) is also shown in Figure 5.4.

The reference efficiency needed for calculating the temperature coefficient, β (Equation 3.3), is normally obtained from the PV manufacturer's data of the values of current and voltage provided for the maximum power condition under Standard Test Condition of 1000 W/m^2. Using the slope of the STC efficiency plot as in Figure 5.4 and the reference efficiency, the temperature coefficient value for the cell is calculated as 0.45%/K, However, since in the present investigation, the illumination spectrum is possibly different compared to STC solar spectrum, the STC reference efficiency value would lead to a wrong value of temperature coefficient for the present experiment. As such, experimental reference efficiency at 25^0C (STC temperature) is calculated from the efficiency correlation as obtained from the experimental results by extrapolating it to the temperature of 25^0C. The temperature coefficient (β) as calculated from the efficiency plot, is found out as 0.33%/K. This value is about 26.7% less than the temperature coefficient at STC as per STC coefficient value of 0.45%/K.

5.3 Results for the PV reference system

In general, as the incident radiation falls onto the panel, a part of the incident radiation is reflected, a part is transmitted through; a part is absorbed as infra-red and other electromagnetic radiation energy. A part of the absorbed energy is converted to electrical energy while the rest appears as thermal energy inside the cell and heats it up. The panel exchanges heat with surrounding media both at the front and back surfaces as convection and long wave radiation heat. The balance of these energy exchanges establishes the operating temperature of the panel at any instant of time. The energy exchange and heat dissipation phenomena are described in Chapter 3. Here, the results of the present experimental study are presented and compared with literature data.

The plots in Figure 5.5 show a comparison of the experimental results in the present study and the results of experiment in the literature for the time-temperature history of PV heating.

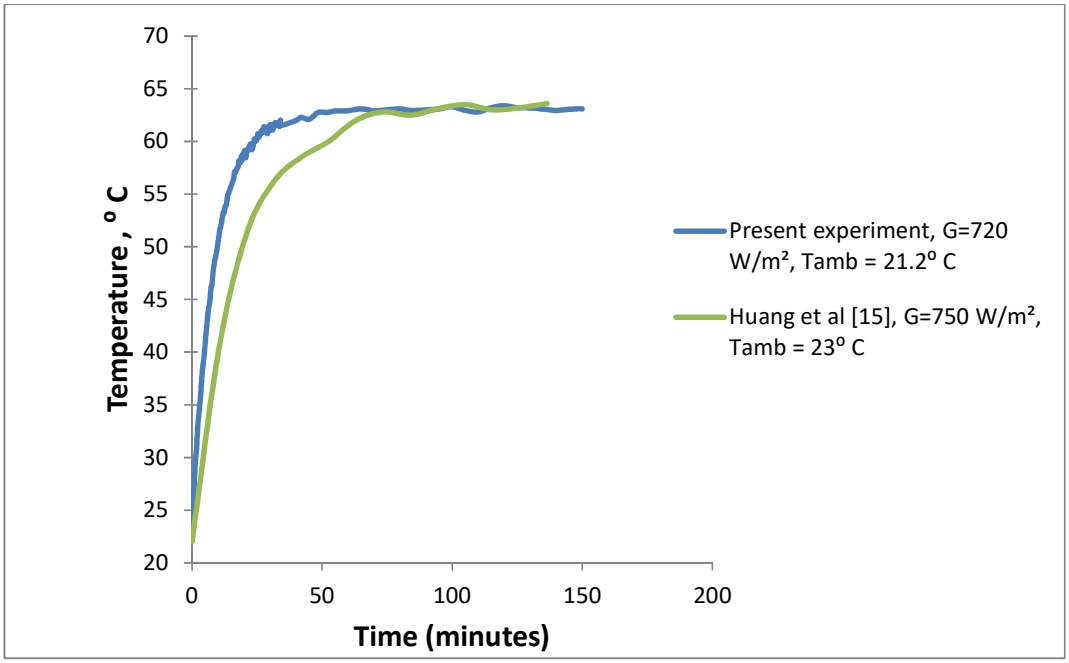

Figure 5.5 Temperature history for the PV cell only (present experiment and literature data)

It is observed that the steady state temperatures for both the current experiment and standard experimental results are practically the same (about 63^0C). However, the theoretical analysis predicts about 29.7% higher a value of steady state temperature. This could be due to possible errors in the values of heat transfer coefficient used for the PV surfaces as well as error due to neglecting radiation exchanges.

The transient response for the present experiment is about 40 min and in Huang et al [15], it is 70 min. The initial slope for the present experiment is higher than that in Huang et al [15] because the reference [15] plot is for a an incident radiation of 750 W/m^2, while the plot for the present experiment corresponds to a lower value of 720 W/m^2 in the present experimental radiation, coming from heat bulbs, thus comprising a good amount of thermal (IR) spectra causing a higher heating effect and faster increase in temperature.

5.4 Results for the PV-PCM system

One of the major objectives of the present study is to investigate the effect of incorporating fins at the back plate of the PCM container both inside and outside in longitudinal

orientation as well the number of fins (or fin spacing) so placed on thermal regulation of PV panel.

The detailed scheme of the experimentation has been described in Chapter 4. The time evolution of temperature was investigated for five different systems as follows.

1. Experiment with PV only
2. Experiment with PV-PCM without fin
3. Experiment with PV-PCM with 6 nos. of internal fins.
4. Experiment with PV-PCM with 12 of internal fins
5. Experiment with PV-PCM with 6 nos. of internal fins and 12 nos. external fins.

5.4.1 Experimentation without fins

Time history of PV temperature of the PV-PCM system without fins is presented in Figure 5.6 and compared with literature results. For assessing a general improvement (Figure 2.1) in thermal regulation by the use of PV-PCM, the temperature plot for PV only is also incorporated in Figure 5.6. It clearly shows that using a PV-PCM system substantially improves temperature regulation when the temperature with PV-PCM (no fins) rises to about 45^0C for around 4 hours while the PV alone system rises to about 63^0 C within almost an hour.

The literature results with fins are also shown in Figure 5.6 to indicate the efficacy of fins in enhancing the effective thermal conductivity of PCM, thereby improving thermal regulation. All the plots have three distinct regions. The initial rising part correspond to the sensible heating of the solid PCM in contact with the PV back plate, the second relatively flat zone which correspond to a melting phase of the PCM in contact combined with a sensible heating of the part of the PCM that has melted in contact with the PV and the third zone where the temperature rises again (finally coming to a steady state if sufficient time could be given) when the PCM in contact has melted and sensible heating of the liquid PCM continues. In the plot with fins, the rise in temperature is much less. The temperature of the PCM in contact with the cell (i.e. the temperature of the PV) increases slowly after initial sensible heating when phase change starts. This is due to increased heat transfer by virtue of enhanced effective conductivity of the PCM. Heat is quickly transferred from the

first layer of PCM to the interior of the PCM and hence the melting duration of the PCM is small and so also is the heating rate of the first layer of PCM.

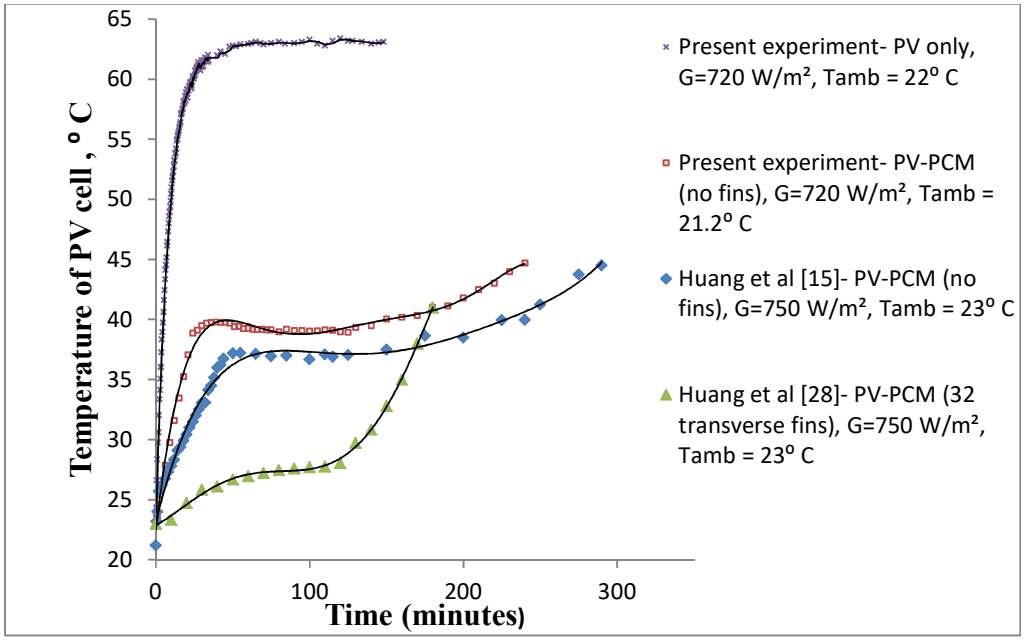

Figure 5.6 Thermal regulation in the present study (without fin) and literature experimental results (without and with fins)

It is observed that the experimental results of the present study compare quite well with established literature data. However, the present PV-PCM system indicates a steeper rise of temperature and simultaneous higher levels of temperature during the initial phase. This could be attributed to the facts that, as earlier discussed in Section. 5.4.1, the incident radiation spectra for the present experiment contains higher quantum of Infrared component so that the heating effect is more than that in Huang et al [15]. Also, the PCM used in the present study had about 2.5 times higher thermal diffusivity $(k/\rho C_p)$ of 3.33×10^{-10} m^2/s, compared to that used by Huang et al [15] of 1.71×10^{-10} m^2/s, in the solid phase. Further, The PCM used in the present experiment had a slightly higher melting point (28^0C) compared to 26.6^0C of the PCM used in [15]. In addition, the initial temperature of the present experiment is about 1.9^0C more than that as in [15].

The phase transition duration is more or less same in the two cases. The PV temperature rises again in the third phase of sensible heating of the liquid PCM in both the case as expected. However, in the present experiment, the rate of rise is more than that in reference

[15]. This can again be attributed to the higher thermal diffusivity of the PCM as used in the present study.

Further, it is observed that while the reference PV cell attains a temperature of 60^0 C within 20 minutes (Figure 5.6), the PV-PCM system in the present experiment maintains a temperature below 45^0C for about 160 minutes. A comparative statement of results for some performance markers are presented in Table 5.2.

Steady state temperature in the course of the experiment with PV-PCM could not obtained as the duration of individual experiment was not more than four hours (excluding initial setting etc.) for practical constraints. For a constant value of incident radiation as done in the present and literature experiment and literature, it is thus worthwhile to investigate the effect of PCM on PV temperature for a few hours only, probably up to complete melting and for some more time beyond to allow sensible heating of the liquid PCM. This is because the major objective of the present study has been to investigate the relative efficacy of different configurations of PCM system used.

The efficacy of putting fins is clearly indicated in Figure 5.6, when 32 nos. of transverse fins were provided on the interior side of the front plate on which the PV lamina was pasted as in reference [15, 28] even though the rate of rise is more than the other two cases as the average conductivity of PCM has increased. However, this is acceptable as the temperature plot for this case crosses the other temperature plot only after 3 hours and by this time actual incident solar radiation will probably change to some lower value.

5.4.2 Experimentation with fins

It is observed from References [15, 28] that the PV temperature remains substantially low with incorporation of fins placed in a transverse direction. The fins were placed in transverse direction as shown in Figure 1.16. The results in reference [15, 28] indicate that the transverse fins would hinder the natural convection flow within the PCM during phase change and during liquid phase sensible heating periods, thereby offsetting some benefit. For the present study, therefore, longitudinal fins were designed. The fins were fitted on the internal surface of the back plate of the PCM container as the container front was open and fitted with the backside frame of a commercially available PV panel. This arrangement was conceived to facilitate retrofitting of PCM container to existing panels at site. In turn, this

arrangement has two apparent consequences. One is that the fins are not in direct contact with the PV panel and separated by a layer of PCM while the second is that, the fins can conduct heat not only into the bulk of PCM (increasing the effective conductivity) but also to the back plate of the container with which the fins are attached. The first consequence results in an initial slow heating of the PCM in contact with the PV panel due to poor conductivity of the PCM and thus due to less heat transferred from the PV panel to the PCM, the panel temperature should rise relatively to higher value at the initial stage. The second consequence is a favourable one as the fins would conduct heat to the back plate which, in turn, transfers the heat to the surrounding ambience.

The above argument is vindicated with reference to Figure 5.7. Two sets of experiment with 6 internal (fins spacing 23.6 mm) and 12 internal fins (fin spacing 44 mm) were conducted to investigate the effect of fin spacing Fin parameters used in the present study and reference [28] for comparison are furnished in Table 5.1

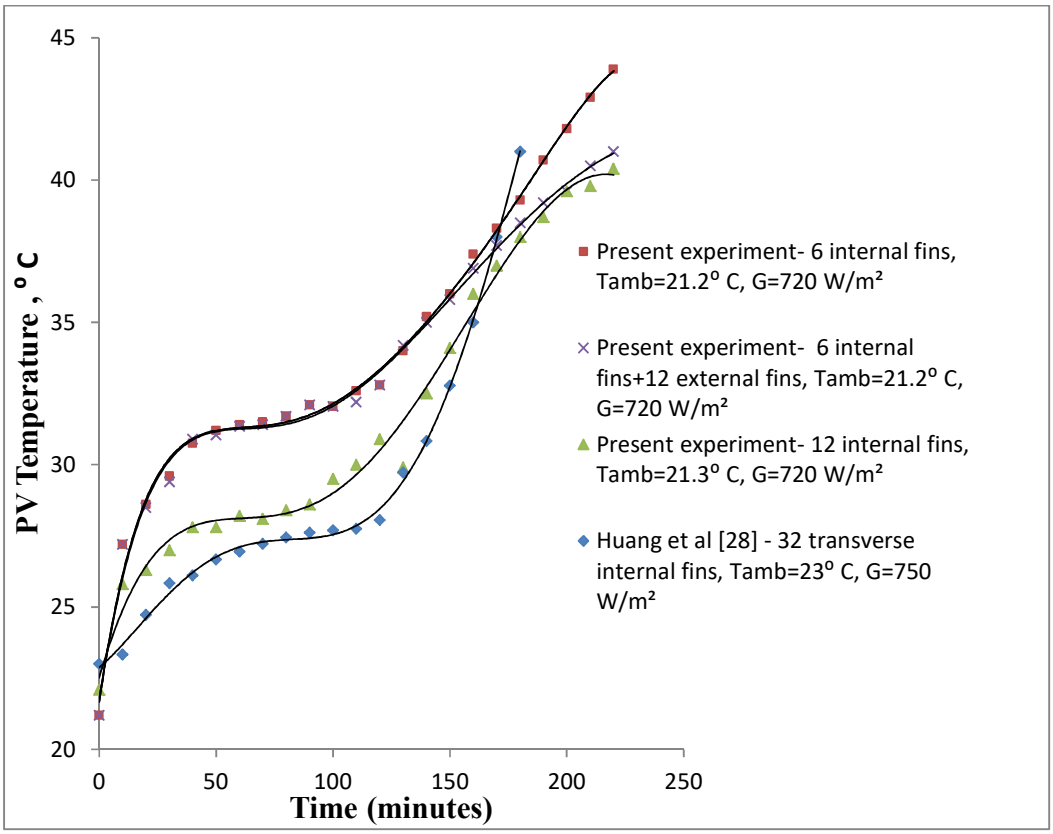

Figure 5.7 Thermal regulation (with fins) in the present study and literature experimental results

Table 5.1 Fin parameters for the present study and literature work

Description	Orientation of fins	No. of fins	Fin spacing
Present experiment 1	Longitudinal – inside the PCM container back plate	6 internal	44.0 mm
Present experiment 2	Longitudinal – inside the PCM container back plate	12 internal	23.6
Present experiment 3	Longitudinal – both inside and outside the PCM container back plate	6 internal + 12 external	44.0 mm internal +23.6 mm external
Huang et al[28]	Transverse- inside the front plate in contact directly with the PV	32 internal	4.0 mm

It is observed (Figure 5.7) that increasing number of fins (or reducing fin spacing) considerably improves overall thermal regulation of the PV up to a period possibly when all the PCM has melted. However, both in case of present experimentation and reference [15, 28], it is observed that beyond some point of time and temperature, the cases with higher number of fins leads to a steeper rise in temperature in the third zone of heating (sensible heating of liquid PCM all through). In case of Huang et al [15, 28] after all the PCM has melted, the fins which are an integral part of the front plate of the PCM container, the effective area of heat transfer from the PV to the adjacent liquid PCM increase and, this time in absence of any phase change, further heats up the PCM at a faster rate than in absence of the fins. As there is no direct contact of these fins with the back plate only the liquid PCM with poor conductivity transfers heat through back plate to the ambience and thus a large number of fins becomes a little counterproductive. However, in actual scenario, varying solar intensity may not allow this condition to continue for long. On the other hand, the rate of increase is lower during the third phase of liquid PCM sensible heating for the present experimental configuration of fins. This is possibly due to the fact that although the fins are a small distance (5 mm) away from the PV cell backing plate, they are in direct contact with the PCM container back plate contributing in dissipating the PCM heat through external dissipation more effectively during later part of sensible heating of the PCM.

Plots for temperature evolution for the present experimental cases are comprehensively shown in Figure 5.8 for better comprehension. The trends for different configurations are

already discussed when introduction of PCM drastically enhances thermal regulation with 12 internal fins showing the best results.

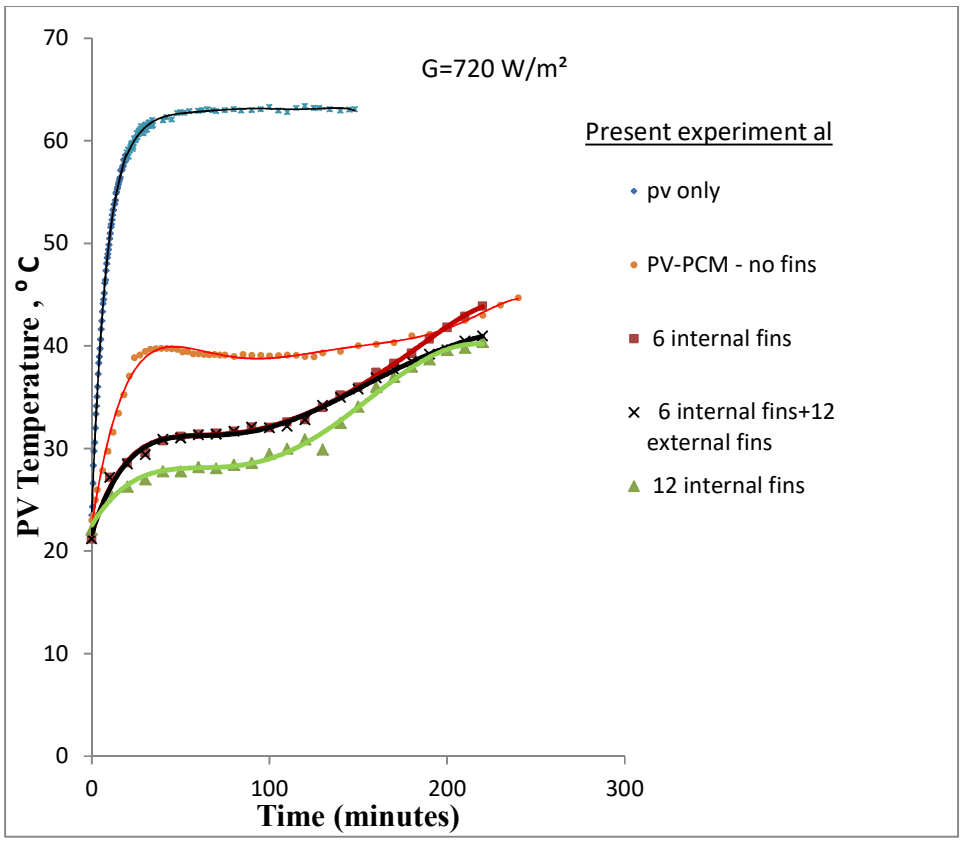

Figure 5.8 Temperature evolution for the configurations employed in the present study

The influence of fins in augmenting back plate dissipation was examined by placing 12 fins on the exterior surface of the back plate in conjunction with 6 internal fins. As is evident from Figure 5.8, such arrangement did not make much difference in comparison to the case with only 6 interior fins, as expected, till possibly all the PCM has melted. This is because unless the PCM in contact with the back plate melts the full efficacy of the exterior fins may is not be in place. But as soon as all the PCM has possibly melted, it is observed that the rate of temperature rise in the third sensible heating zone decreases compared to the case with only 6 interior fins.

A comparison of thermal regulation performance can be in terms of the average temperature during certain period of time for each configuration. The average temperatures are

calculated by determining the area under relevant curves in Figures 5.6 and 5.7 and dividing the areas with corresponding time interval as follows,

$$\bar{T} = \frac{1}{t_2 - t_1} \int_{t_1}^{t_2} T dt \quad ..(5.2)$$

The function T(t) for each curve is found from a best fit polynomial curve for the corresponding experimental points and integrating it for the limits of time. The results are furnished in Table 5.2 and Figure 5.9.

Table: 5.2 Comparison table for average PV surface temperature

Configuration	Conditions for first 90 minutes		Conditions for first 150 minutes		Conditions for first 220 minutes	
	$T_{average}$	% deviation	$T_{average}$	% deviation	$T_{average}$	% deviation
PV only	58.90	0.00	60.58	0.00	62.2 (extrapolated)	0.00
PV-PCM	37.28	-36.70	38.08	-37.14	39.08	-37.17
PV-PCM- 6 internal fins	29.84	-49.34	31.31	-48.31	34.09	-45.19
PV-PCM- 12 internal fins	29.77	-49.45	31.24	48.435	33.20	-46.62
PV-PCM- 6 internal+12(external fins)	27.21	-53.80	28.64	-52.73	31.61	-49.18
Literature [28]-32 transverse fins	26.000	-55.85	27.22	-55.06	32.06 (extrapolated)	-48.46

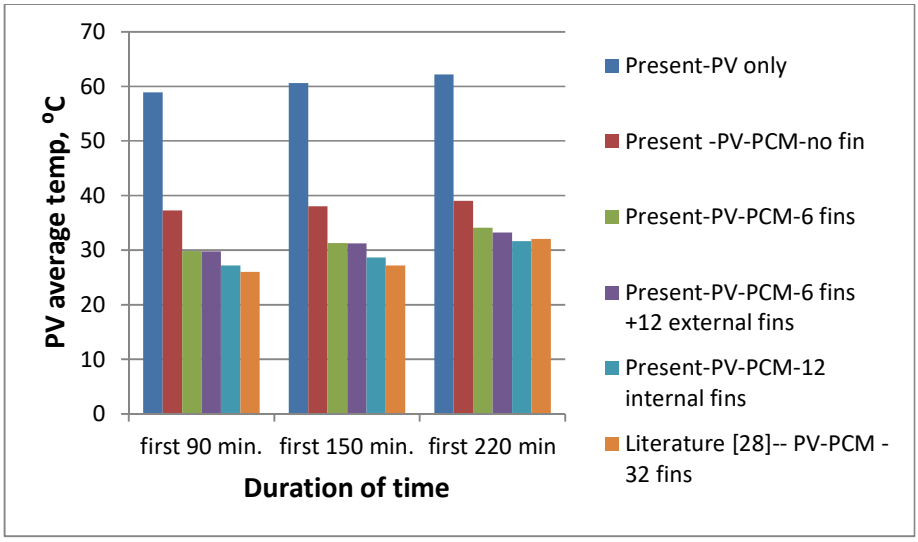

Figure 5.9 Column chart for comparison of average temperatures

From Table 5.2 and Figure 5.9, it is evident that there has been a substantial decrease in PV temperature for PV-PCM system (about 37%) and PV-PCM systems with fins (about 50% or more with 12 internal fins). Though, initially, the average temperature for PV-PCM systems with 6 fins and 6+12 fins system are almost the same, the effect of 12 external back fins are evident during later part of PV heating. The reduction in average cell temperature with only 12 longitudinal internal fins becomes 49.1%., as the heating process continues to 220 minutes. This could be due to contact of the internal fins with the back plate, as in the present study.

Thermal regulation performance is also investigated by obtaining time for which the PV temperature remains within a temperature range. Longer the time it remains within a given temperature, better will be what is known as thermal regulation. Such durations for which a PV remains within certain temperature have been obtained using the data of Figures 5.6 and 5.7 and presented in Table 5.3 and Figure 5.10. It is observed that initial thermal regulation is very good for the cases when present PV/PCM system uses 12 fins and the PV/PCM system as in Reference [28] using 32 fins when the PV temperature remains within 30^0C and within 35^0C. This is expected because of the presence of more number of fins. However, for the present PV/PCM system with both 6 internal fins and 6 internal fins plus 12 external fins cases, there is a major improvement in thermal regulation almost by the

same amount when the PV temperature remains less than 35^0C. During this period possibly near the completion of phase change in the bulk of PCM, the external fins do not contribute to the dissipation of heat because the solid PCM layer in contact with the back plate will still have a temperature of 28^0C (melting point of PCM) till the finish of melting and hence the back plate will not dissipate much heat to the external ambience which is at about 22^0C. However, when the phase change is complete and sensible heating has started these external fins would start dissipating more heat and as we see the column chart in Figure 5.9, the case with external fins has quite good thermal regulation when PV temperature is less than 40^0C (a temperature zone when sensible heating of PCM has already started). However, in standard literature [15,28] and most interestingly, the case of PV/PCM system in reference [28] with no fins, the thermal regulation drastically increases, even more than the case when 32 fins are fitted, when possibly phase change is over and possible sensible heating is in progress.

For the period when PV temperature remains within 40^0C, the present experiment with 6+12 fin configuration (200 minutes) compares almost same with that with 12 fins (220 minutes). This is possibly due to the increased effect of back plate external surface heat dissipation in the former case with external fins.

Table 5.3 Comparison of thermal regulation period

References	Fin spacing	Approx. duration of time PV temperature remains within 30^0 C, minutes	Approx. duration of time PV temperature remains within 35^0 C, minutes	Approx. duration of time PV temperature remains within 40^{0C}, minutes
Present experiment (reference cell only)	N.A.	2	3	4
Present experiment PV-PCM (without fins)	N.A.	10	20	30
Huang et al [15,28] PV-PCM (without fins)	N.A	20	40	225
Present experiment PV-PCM (6 internal fins)	44 mm	30	140	160
Present experiment PV-PCM (12 internal fins)	23.6 mm	110	155	220
Present experiment PV-PCM (6 internal fins+ 12 external fins)	44 mm internal+ 23.6 mm external	30	140	200
Huang et al [15,28] PV-PCM (32 nos. transverse fins)	4 mm	135	160	175

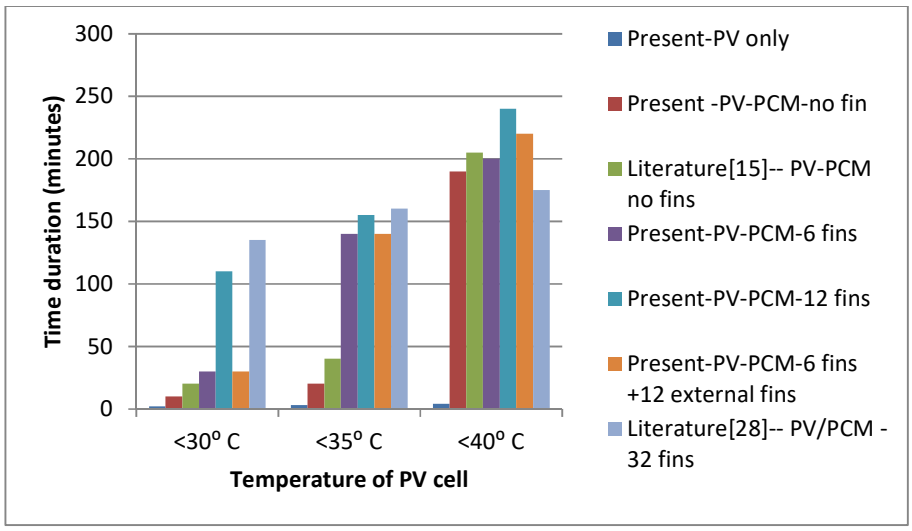

Figure 5.10 Column chart for comparison of thermal regulation period

5.5 Electrical output, heat loss and heat absorption

In order to assess the effect of PCM on the electrical power, heat dissipation and heat absorption each of them are calculated from the experimental data following the discussion in Chapter 3. Each of them is calculated on the basis of unit area of the cell. This would facilitate comparison of present data with those for a PV cell of any size.

5.5.1 Electrical output

During the experiment for temperature evolution of PV and PV-PCM systems, electrical load has been kept applied all the time. However, the electrical power output has been computed for each time-temperature condition from the efficiency correlation (Equation 5.1). The electrical power output at any instant of time, for a given panel temperature T, is given by,

$P_{output} = \eta\ (T)\ GA$ Watt ..(5.3)

For unit area this becomes,

P_{output} /A= Electrical energy flux out = $\eta\ (T)\ G\ W/m2$ ..(5.4)

The efficiency values $\eta\ (T)$ are calculated from the correlation using from the experimental data of panel temperatures. Panel temperatures are stored in computer using the DAQs from thermocouple measurements.

Electrical power per unit area is calculated using Equation 5.3 from measured values of temperature in DAQs, incident solar radiation and efficiency correlation. The electrical energy flux as calculated is subsequently used in the energy conservation and energy budget analysis. Results for the electrical output flux for different systems are shown in Figure 5.11. Table 5.4 furnishes comparative results for average electrical power output for different configurations. The average power output is determined in the same way as average temperature as in Equation 5.2.

It is observed that by incorporating PCM in the PV cell, electrical output has increased quite substantially (by about 12 %). Out of different PCM configuration, the 12 internal fins indicate the best output (increase by 14.72%). Combination of 6 internal and 12 external fins performs better than with only 6 internal fins, as expected. The improvement is more prominent during later part of PV –PCM heating when heat dissipation through back plate becomes larger. However, if further time is allowed when all the PCM has melted and all configurations are being heated up the effect of enhanced heat dissipation by external fins should be prominent and PV temperature should come down resulting in increase in electrical output.

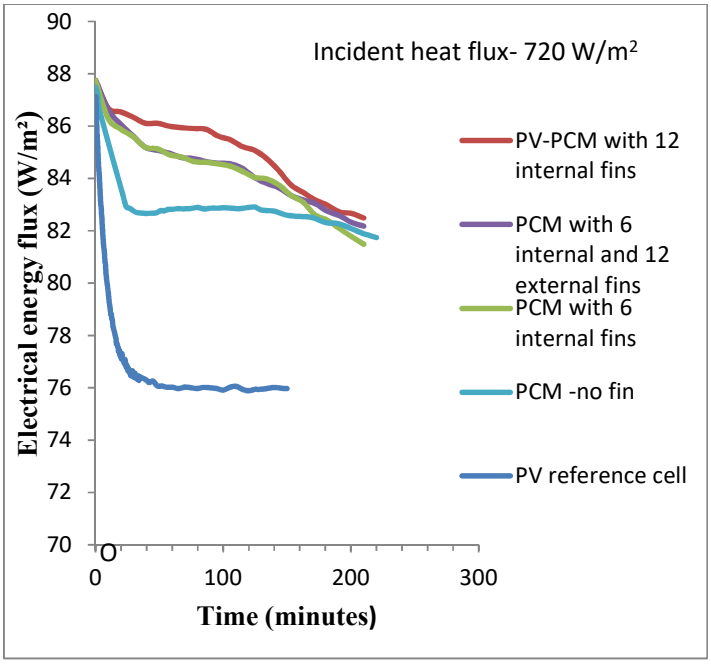

Figure 5.11 Electrical energy flux output with time for different PV systems

Table: 5.4 Comparison of average power generation

Configuration	Conditions for first 90 minutes		Conditions for first 150 minutes		Conditions for first 220 minutes	
	Average power $(W/m^2)_e$	% increase	Average power (W/m^2)	% increase	Average power (W/m^2)	% increase
PV only	75.52	0.00	73.98	0.00	74.00 (extrapolated)	0.00
PV-PCM	83.38	10.42	83.16	12.41	82.87	11.99
PV-PCM- 6 internal fins	85.39	13.08	84.90	14.76	84.08	13.62
PV-PCM- 12 internal fins	86.26	14.23	85.77	15.95	84.90	14.72
PV-PCM- 6 internal+12(external fins)	85.46	13.16	84.94	14.81	84.22	13.81

5.5.2 Heat loss and heat absorption

As discussed in Chapter 3, the heat loss and absorption rates for different PV systems are computed from Equations 3.5 and 3.6 using experimental PV surface temperature data. Figures 5.12 and 5.13 typically show the heat loss and heat absorption fluxes during the period of heating in the experiment for PV reference cell only and PV-PCM system with 12 internal fins, respectively..

Figure 5.12 indicates that for the PV reference cell, initially the cell gets heated up and the rate of heat absorption is much more than the heat dissipation rate because the cell surface temperature does not rise as quickly. As the cell surface temperature increase, its losses (convection and radiation losses) also increase when the loss rate subsequently become more than the absorption rate. As the cell approaches steady state the absorption rate of heat becomes zero as expected and the dissipation rate, which is a function of cell temperature, therefore also becomes constant with electrical power remaining relatively constant.

Energy budget for a PV-PCM system is shown in Figure 5.13, typically for the configuration with 12 nos. of internal fins only. The trend will be similar for other fin configuration as well. In case of a PV-PCM system, the rate of increase of panel temperature is much less compared to PV reference case as there is absorption of latent heat by the PCM. The heat loss, as a result, does not increase appreciably while the PCM continues to absorb heat mostly in the latent heat form. Finally when the PCM has melted, the sensible heat raises the temperature and heat dissipation rate increases at a faster rate and the heat absorption rate starts falling till possibly following the behaviour of a PV reference cell as in Figure 5.10.

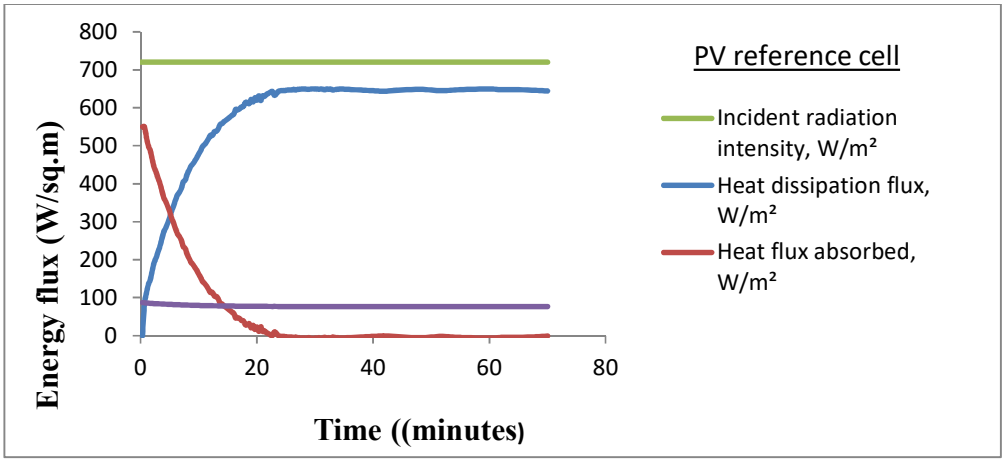

Figure 5.12 Energy budget with time for a PV reference cell

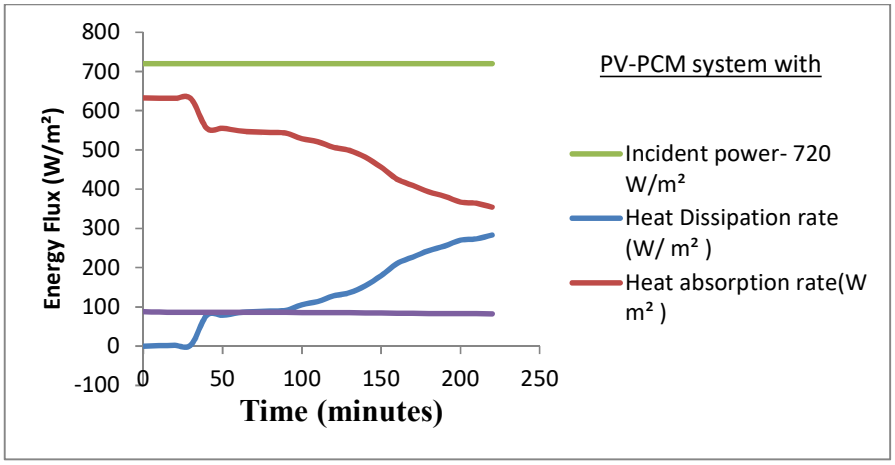

Figure 5.13 Energy budget with time for a PV-PCM system

Chapter 6: Conclusions and Recommendations

6.1 Conclusions

Thermal regulation of PV cells is **experimentally** investigated in the present study using paraffin wax as the phase change material. PCM container suitable for retrofitting is developed for the purpose. Longitudinal fins are fitted on the interior and exterior surfaces of the container back plate to enhance effective conductivity of the PCM as well as to enhance heat dissipation from the back plate to the ambience. The salient observations and conclusions regarding the present study can be listed as follows.

1. An efficiency correlation with temperature was developed experimentally to study the deterioration in electrical performance of the PV cell. The correlation is given as:

   $$\eta\,(T) = 0.0399\,T + 13.069.$$

   The temperature coefficient, β was determined out from the correlation and was found to agree well with the standard temperature coefficient value of a silicon PV cell.

2. The time evolution of a PV panel temperature (PV- only system) as obtained from the present experiment matches very closely with experimental results found in the literature.

3. Incorporation of PCM in the PV panel significantly improved thermal regulation by limiting the PV temperature for a period of time longer by an order of magnitude.

4. Internally finned PV-PCM systems show marked improvement in thermal regulation over PV-PCM system without fins by increasing the effective thermal conductivity of the PCM

5. Thermal regulation in PV-PCM system with internal fins increases with a decrease of fin spacing.

6. Incorporation of external fins at the back surface of an internally finned PCM container aids/ improves thermal regulation during the latter part of the temperature rise when the PCM in contact with the back plate has melted starting sensible heating there. However, they may not be as effective if the incident radiation changes over time precluding a long enough time available for sensible heating of the PCM liquid in contact with the back plate.

7. Present arrangement of internal fins fitted at the inner face of the back plates and extending into the PCM form the container back side compares very well in the performance of thermal regulation with those fitted at the back of the front side of the PCM container and extending into the PCM from PV panel side as used in standard literature work.

8. Thermal performance of present arrangement of only 12 longitudinal fins compares very favourably with those in literature with 32 numbers of transverse fins and this is possibly due to inhibition of buoyancy driven flow of the melt pool inside the PCM and law of diminishing return with increasing number of fins due to less amount of PCM mass, for the latter case.

9. Analysis for duration of time a PV-PCM system remains below different temperature limits as used in the present work appears to be very helpful in comparison of performance of different PV-PCM systems and can assist in choice and design of systems under varying incident flux condition.

10. Energy budget analysis for heat dissipation and heat absorption carried out in the present work provides a good basis for comparison of thermal performance of PV systems

11. Power output at a given panel temperature of the present PV panel are lower than the corresponding values with the value of incident radiation as expected with the manufacturer data. Temperature coefficient also is less than as expected. This is thought to be due to possible deviation of the spectrum present heat lamp system from the solar spectrum. As such, spectrum of incident radiation would play a major

role in the electrical and thermal performance of the cell at any particular value of incident intensity.

12. The design of the present PV-PCM container lends itself for retrofitting to existing solar panel installations.

It may thus be concluded that the present investigation has indicated quite a few important findings and directions for improved thermal regulation using PCM. It can therefore be considered to be of significant importance to efficient utilisation of PCM in thermal regulation of existing and future PV solar power generation systems. One of the primary concerns for the industrial application is some form of trade off of cost of PCM and implementing PV-PCM system and the benefits derived out of it vis-a-vis other cooling methods. Some of the findings in this study would help in such decision making for a given particular application.

6.2 Recommendations

The observations from the present study are thought to assist in further research and investigations in the field of thermal regulation of PV system using PCM. . The results and conclusions arrived at here can be verified and improved by widening the range of parameters used in the present study. They can also be improved through designing PCM containers with fins of different spacing, orientations, and shape.

However, as an initial effort to make an experimental system for the purpose, many features and aspects could not be incorporated in the present investigation. Therefore future researchers utilizing the present experimental setup may be well suggested to make the following additions and modifications in order to carry out more comprehensive investigation.

1. Similar experiments with different categories of PCM with different depth of PCM in the container should provide more insight as to the role of PCM on the thermal regulation phenomenon
2. The illumination system needed to be improved with system for holding the lamps preferably with electronic control for adjusting intensity in addition to the already devised easy way by inserting wire mesh screens

3. Sampling rate of 1 sample per second which is the minimum rate for the DAQ acquired for the present investigation, turned out to be a too high rate for the type of time history required for the present investigation leading to a huge number of data. A DAQ with a wider range of choice of sampling rate can be helpful.

4. DAQ system may be employed for measurement of both incident radiation and electrical measurement during the course of an experimentation run.

5. An arrangement for tilting the PV-PCM system along with the illumination system may be devised to investigate the effect of natural convection both inside and outside the container.

6. Different spectral composition of incident radiation may be used in the experimentation to investigate the spectral effect on thermal and electrical performance of a PV cell. This, in addition, may throw some light on the possibility of simulating solar radiation with a low cost simulator.

7. PCM with variation in thermal diffusivities may be tried to see its effect on the temporal variation of PV temperature

8. A comprehensive melting-solidification model using CFD for the PCM with the different configurations of fins needs to be employed to have better understanding of the thermal behaviour of the PCM and the fin configurations chosen.

References

[1] "World Energy Outlook 2016", Publication of International Energy Agency (IEA).

[2] http://www.alternative-energy-tutorials.com/solar-power/photovoltaics.html

[3] By Nick84 - http://commons.wikimedia.org/wiki/File:Solar_spectrum_ita.svg, CC BY-SA 3.0, https://commons.wikimedia.org/w/index.php?curid=24648395, License link: Creative Commons Attribution-Share Alike 3.0 Unported license.

[4] http://www.samlexsolar.com/learning-center/solar-panels-characteristics.aspx

[5] Biwole P, Eclache P, Kuznik F. (2011), "Improving the performance of solar panels by the use of phase-change materials." Proceedings of the World renewable energy congress

[6] Sandberg M. (1999), "Cooling of building integrated photovoltaics by ventilation air." Proceedings of the first international forum on natural and hybrid ventilation, Sydney, Australia.

[7] Hasan A, McCormack SJ, Huang MJ, Norton B (2010). "Evaluation of phase change materials for thermal regulation enhancement of building integrated photovoltaics." Sol Energy, **84**: 1601–12.

[8] Krauter, S., (1994). "Actual optical and thermal performance of PV modules". Proceedings of the 1st World Conference on Photovoltaic Energy Conversion (Joint Congress of IEEE/ PVSEC/EUPVC). Waikoloa, Hawaii (USA), December, **1**, 734–737.

[9] Raziemska, E. (2003). "The effect of temperature on the power drop in crystalline silicon solar cells." Renewable Energy **28**, 1–12.

[10] Batagiannis P, Gibbons C. (2001) "Thermal assessment of silicon-based composite materials used in photovoltaics." Proceedings of renewable energy in maritime Island climates conference, Belfast, UK.

[11] Skoplaki E, Palyvos J A. (2009). "On the temperature dependance of photovoltaic module electrical performance.: A review of efficiency /power correlations." Sol Energy; **83**:614–24.

[12] Zondag HA, de Vries D W, Steenhoven AAV, Helden WGJV, Zolingen RJCV. (1999),. "Thermal and electrical yield of a combi-panel.":Proceedings of ISES World Congress. Israel:Jerusalem;.p.96–101.

[13] Kern E C Jr., Russell M C.(1978) "Combined photovoltaic and thermal hybrid collector systems;", 13th Photovoltaic Specialists Conference, IEEE, Washington, D.C.,USA, 1153-1157.

[14] https://www.1-act.com/

[15] Huang M J, Eames P C, Norton B (2004). "Thermal regulation of building-integrated photovoltaics using phase change materials." Int J Heat Mass Transf; **47**: 2715–33.

[16] Yang HX, Marshall RH, Brinkworth BJ. (1996) "Validated simulation for thermal regulation of photovoltaic wall structures." Proceedings of the 25th IEEE PV Specialists Conference, Washington DC;.

[17] Brinkworth BJ, Marshall RH, Ibarahim Z.A. (2000) "Validated model of naturally ventilated PV cladding." Sol Energy; **69:** 67–81.

[18] Fossa M, Ménézo C, Leonardi E. (2008) "Experimental natural convection on vertical surfaces for building integrated photovoltaic (BIPV) applications." Exp Ther Fluid Sci; **32**, 980–90.

[19] Yun GY, McEvoy M, Steemers K., (2007) "Design and overall energy performance of a ventilated photovoltaic façade", Sol Energy;**81:** 383–94.

[20] Anderson W G, Dussinger P M, Sarraf D B, Tamanna S. (2008), "Heat pipe cooling of concentrating photovoltaic cells.":Proceedings of the 33rd IEEE photo- voltaic specialists conference PVSC'08;.1–6.

[21] Brogren M, Karlsson B.(2002), "Low-concentrating water-cooled PV-thermal hybrid systems for high latitudes." Proceedings of the conference record of the 29th IEEE 2002 photovoltaic specialists conference; .1733–1736.

[22] Krauter S. (2004), "Increased electrical yield via water flow over the front of photovoltaic panels." Sol Energy Mater Sol Cells **82**:131–138

[23] Wilson E. (2009), "Theoretical and operational thermal performance of a 'wet' crystalline silicon PV module under Jamaican conditions." Renew Energy; **34**:1655–1660.

[24] Tonui J K and Tripanagnostopoulos Y. (2007), "Improved PV/T solar collectors with heat extraction by forced or natural air circulation." Renew Energy;**32**: 623–37.

[25] Ben Xu, Li P, Chan C. (2015), "Application of phase change materials for thermal energy storage in concentrated solar thermal power plants: A review to recent developments." Applied Energy, **160**: 286–307

[26] Huang M J. (2002), "The application of CFD to predict the thermal performance of phase change materials for the control of photovoltaic cell temperature in buildings." (Ph.D. thesis). UK: University of Ulster;

[27] Huang M J, Eames P C, Norton B (2006). "Comparison of a small-scale 3D PCM thermal control model with a validated 2D PCM thermal control model." Sol Energy Mater Sol Cells; **90**:1961–72.

[28] Huang M J, Eames P C, Norton B (2006). "Phase change materials for limiting temperature rise in building integrated photovoltaics." Sol Energy; **80**: 1121–30.

[29] Huang, M.J., McCormack, S. J., Eames P.C. and Norton, B. (2008). "The effect of phase change material crystalline segregation on the building integrated photovoltaic system thermal performance.":Proceedings of the World Renewable Energy Congress.

[30] Huang M J, Eames P C, Norton B, Hewitt N J (2011). "Natural convection in an internally finned phase change material heat sink for the thermal management of photovoltaics." Sol Energy Mater Sol Cells;**95**(7):1598–603.

[31] Maiti S, Banerjee S, Vyas K, Patel P, Ghosh P K (2011). "Self regulation of photovoltaic module temperature in V-trough using a metal–wax composite phase change matrix." Sol Energy; **85**:1805–16

[32] Tan L (2013). "Passive cooling of concentrated solar cells using phase change material thermal storage [Doctor of Philosophy, Ph.D.]. Aerospace, Mechanical and Manufacturing Engineering." Melbourne, Australia: RMIT University, http:// research bank.rmit.edu.au/view/rmit:160452;.

[33] Karthick A., Murugavel K K, Ramanan P (2018), "Performance enhancement of a building-integrated photovoltaic module using phase change material", Energy, **142** 803-812

[34] Atkin P, Farid M M (2015). "Improving the efficiency of photovoltaic cells using PCM infused graphite and aluminium fins", Solar Energy, **114** 217–228

[35] Smith CJ, Forster PM, Crook R (2014). "Global analysis of photovoltaic energy output enhanced by phase change material cooling." Appl Energy; **126**:21–28.

[36] Huang MJ, Eames PC, Norton B (2000). "The application of computational fluid dynamics to predict the performance of phase change materials for control of photovoltaic cell temperature in buildings." In:Sayigh AAM, editor. World renewable energy congress VI. Oxford:Pergamon;. 2123–2126.

[37] Huang MJ, Eames PC, Norton B (2007). "Comparison of predictions made using a new 3D phase change material thermal control model with experimental measurements and predictions made using a validated 2D model." Heat Transf Eng ; **28**:31–7.

[38] Biwole PH, Eclache P, Kuznik F (2013). "Phase-change materials to improve solar panel's performance." Energy Build; **62**:59–67.

[39] Biwole PH, Eclache P, Kuznik F (2011). "Improving the performance of solar panels by the use of phase-change materials. In: Proceedings of the world renewable energy congress." Linkoping, Sweden.

[40] Sarwar J, McCormack SJ, Huang MJ, Norton B (2010). "Experimental validation of CFD modelling for thermal regulation of photovoltaic panels using phase change material." In: Proceedings of the international conference on solar heating, cooling and buildings EuroSun, 28 September–1 October2010, Graz, Austria.

[41] Park J, Kim T, Leigh S-B (2014) Application of a phase-change material to improve the electrical performance of vertical-building-added photovoltaics considering the annual weather conditions. Sol Energy; **105**:561–74.

[42] Cellura M, Ciulla G, Brano VL, Marvuglia A, Orioli A. A Photovoltaic panel coupled with a phase changing material heat storage system in hot climates. In: Proceedings of the 25th conference on passive and low energy architecture PLEA. Dublin; 22–24 October, 2008.

[43] Ciulla G, Brano VL, Cellura M, Franzitta V, Milone D (2012). "A finite difference model of a PV–PCM system." Energy Procedia; **30**: 198–206.

[44] Lo Brano V, Ciulla G, Piacentino A, Cardona F (2013). "On the efficacy of PCM to shave peak temperature of crystalline photovoltaic panels: an fdm model and field validation." Energies; **6**:6188–210.

[45] Lo Brano V, Ciulla G, Piacentino A, Cardona F (2014). "Finite difference thermal model of al atent heat storage system coupled with a photovoltaic device: description and experimental validation." Renew Energy; **68**:181–93.

[46] Tanuwijava A, Ho C, Lai C-M, Huang C-Y (2013). "Numerical investigation of the thermal management performance of MEPCM modules for PV applications." Energies;**6**:3922–36

[47] Hasan A, McCormack SJ, Huang MJ, Norton B (2008). "Experimental design for integrating phase change materials into building integrated photovoltaics for thermal control." In: Proceedings of the 4th photovoltaic science, applications and technology conference. Bath: UK (PVSAT-4);

[48] Hasan A, McCormack SJ, Huang MJ, Norton B (2007). "Phase change materials for thermal control of building integrated photovoltaics:: experimental design and findings." Proceedings of the 22nd European photovoltaic solar energy conference and exhibition. Milan:Italy.

[49] Malvi CS, Dixon-Hardy DW, Crook R (2011). "Energy balance model of combined photovoltaic solar-thermal system incorporating phase change material." Sol Energy; **85**(7):1440–6.

[50] Huang JM (2011). "The effect of using two PCMs on the thermal regulation performance of BIPV systems.", Sol Energy Mater Sol Cells; **95**:957–63.

[51] Jeon J, Lee J-H, Seo J, Jeong S-G, Kim S (2013). "Application of PCM thermal energy storage system to reduce building energy consumption." J Therm Anal Calorim;**111**::279–88.

[52] Khudhair AM, Farid MM (2004). "A review on energy conservation in building applications with thermal storage by latent heat using phase change materials." Energy Convers Manag;**45**:263–75.

[53] Kurnia JC, Sasmito AP, Jangam SV, Mujumdar AS (2013). "Improved design for heat transfer performance of a novel phasec hange material (PCM) thermal energy storage (TES)", Appl Therm Eng;**50**:896–907.

[54] Regin AF, Solanki SC, Saini JS (2008). "Heat transfer characteristics of thermal energy storage system using PCM capsules-:a review." Renew Sustain EnergyRev;**12**:2438–58.

[55] Zalba B, Marín JM, CabezaL F, Mehling H (2003). "Review on thermal energy storage with phase change: materials, heat transfer analysis and applications." Appl Therm Eng; **23**:251–83.

[56] Hasan A, McCormack SJ, Huang MJ, Norton B (2007). "A brief review of phase change materials with an experimental design for use in thermal control for building integrated photovoltaics." Proceedings of the 3rd Photovoltaic science, applications and technology conference (PVSAT-3).Durham:UK;

[57] Hasan A, McCormack S, Huang M, Norton B (2009). "Phase change materials for thermal control of building integrated photovoltaics:characterisation and experimental evaluation." Proceedings of the 11th international conference on thermal energy storage, Stockholm international Fairs, Stockholm: Sweden.

[58] Hasan A, McCormack SJ, Huang MJ, Norton B (2014). "Characterization of phase change materials for thermal control of photovoltaics using differential scanning calorimetry and temperature history method". Energy Convers Manag;**81**:322–9.

[59] Makki A, Omer S, Sabir H (2015). "Advancements in hybrid photovoltaic systems for enhanced solar cells performance." Renew Sustain Energy Rev;**41**: 658–84.

[60] Hasan A, McCormack SJ, Huang MJ, Norton B (2007). "Phase change materials for thermal control of building integrated photovoltaics: experimental design and findings." Proceedings of the 22nd European photovoltaic solar energy conference and exhibition. Milan:Italy.

[61] "ELEC3205 ELECTRICAL ENERGY SYSTEMS & MANAGEMENT", School of Electrical and Information Engineering, University of Sydney

[62] https://www.cleanenergyreviews.info/blog/solar-panel-components-construction

[63] https://www.pveducation.org/pvcdrom/design-of-silicon-cells/anti-reflection-coatings

[64] Simons R E (2001) "Simplified Formula for Estimating Natural Convection Heat Transfer Coefficient on a Flat Plate." Electronics Cooling, **7**(3)

[65] Cengel Y A and Ghajar A J. (2011). Heat and Mass Transfer- Fundamentals and Applications, 4th Ed., McGraw Hill Education (India) Private Limited.

Appendix-A

View factor for radiation

The Figure A1 models the PV cell kept within the laboratory. It is observed that the surroundings completely encloses the PV cell i.e. all the radiation energy emitted by the PV cell (object 1) is received by the surroundings (object 2). However, the converse is not true.

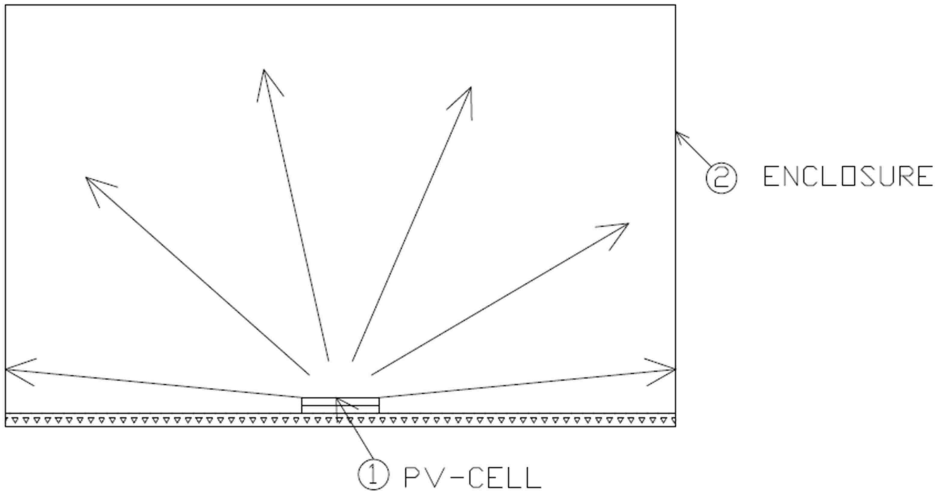

Figure A-1 Surrounding environment completely enclosing the PV cell

A_1 and ε_1 are the surface area and emissivity of the PV panel while A_2 and ε_2 are the surface area and emissivity of the enclosure.

The view factor, $F_{1\text{-}2}$ defined by the fraction of energy emitted by the object 1 as received by the body is given as,

$$F_{1-2} = \frac{Radiant\ energy\ emitted\ by\ body\ 1\ which\ is\ eceived\ by\ body\ 2}{Total\ Radiant\ energy\ emitted\ by\ body\ 1}$$

$$= \frac{Radiant\ energy\ emitted\ by\ body\ 1\ which\ is\ eceived\ by\ body\ 2}{A_1 \varepsilon_1 \sigma T_1^4}$$

and

$$F_{2-1} = \frac{Radiant\ energy\ emitted\ by\ body\ 2\ which\ is\ eceived\ by\ body\ 1}{Total\ Radiant\ energy\ emitted\ by\ body\ 2}$$

For the enclosure, since object 2 fully encloses 1, all the energy emitted by 1 is received by object 2 and hence $F_{1\text{-}2}$ =1.

$F_{2\text{-}1}$ is found out using reciprocal theorem which states that for any two bodies exchanging radiation heat, [1]

$$A_1 F_{1\text{-}2} = A_2 F_{2\text{-}1} \quad \text{(A-1.0)}$$

A_1 and A_2 are the emitting surface areas of 1 and 2.

Hence,

$$F_{2-1} = \frac{A_1}{A_2} F_{1-2} \quad \text{(A-1.1)}$$

For the completely enclosed body 1, $F_{1-2} = 1$

Thus,

$$F_{2-1} = \frac{A_1}{A_2} \quad \text{(A-1.2)}$$

Thus,

$$F_{2-1} = \frac{A_1}{A_2} = \frac{Radiant\ energy\ emitted\ by\ body\ 2\ which\ is\ eceived\ by\ body\ 1}{Total\ Radiant\ energy\ emitted\ by\ body\ 2}$$

Total radiant energy emitted by the body 2 is $A_2\ \varepsilon_2 \sigma T_2^4$.

Hence Radiant energy emitted by 2 and received by 1 = $\frac{A_1}{A_2} A_2 \epsilon_2 \sigma T_2^4 = A_1 \epsilon_2 \sigma T_2^4$

Normally the emissivity, ε_2 of surrounding air is considered 1 (black body assumption).

It follows that the radiation energy from 2 reaching Surface of body 1 is $A_1 \sigma T_2^4$.and the corresponding part absorbed by it is $\epsilon_1 A_1 \sigma T_2^4$

Therefore, the net heat loss from the surface at 1 due to radiation exchange

= Radiation out – radiation in = $A_1 \varepsilon_1 \sigma T_1^4$ -$\epsilon_1 A_1 \sigma T_2^4 = \epsilon_1 A_1 \sigma (T_1^4 - T_2^4)$

For the present investigation, $T_1 = T_{surface,\ PV}$, $T_2 = T_{surrounding}$, A_1=A (top surface area of the panel) and $\epsilon_1 = \epsilon_{glass}$

Appendix-B

Calculation for heat conduction through PV/PV-PCM

The calculations for steady state heat conduction through resistance network circuit for a PV and PV-PCM system are detailed as follows.

The equivalent resistance can be computed using the data for the PV cell in Table 3.1 and work out to be,

$R_{equiv.,\,PV} = 0.0036$ K/W

Under steady state condition and neglecting any radiation loss (for the purpose of this analysis only), the total convection loss is equal to the incident radiation. Any electrical output is also assumed zero. The convection heat loss from the top surface is h_1 ($T_1 - T_{ambience}$) while that from the bottom surface is h_2 ($T_2 - T_{ambience}$). It is initially assumed that $T_1 \approx T_2$, the ratio of back to front surface heat dissipation becomes equal to h_2/h_1. Table 3.1 shows that with $h_1 = 8.0$ W m^{-2} K^{-1} and h_2=2.0 W m^{-2} K^{-1} i.e. h_2/h_1 is only ¼. Thus, 20% of the total heat dissipation takes place at the back surface, if only convection loss is considered. Since, under steady state, total dissipation is equal to incident radiation, G, the heat flow out through the back surface is 0.2xG. From continuity of heat flux as applied at the point 2 in the circuit (Figure 3.7), the heat flux through the PV, q_x, is given by

$q_x = 0.2$ G. (B-.1.0)

Using an incident heat flux (G) data of 720 W/m^2 (from present experiment), temperature difference (T_1-T_2) between front and back surfaces of the PV cell under steady state condition can be calculated from Equation 3.12 as,

$(T_1\text{-}T_2)_{PV} = q_x \times R_{equiv.,\,PV} = (0.2 \times 720) \times 0.00036$ K$= 0.5\ ^0$C.

Thus, under steady state condition the temperature at the back of the PV cell is practically the same as that on the front top surface.

Even if we relax the earlier assumption that $T_1 \approx T_2$ while estimating the ratio of back surface convection heat to front surface convection heat, it will change the ratio very insignificantly and the final result of the temperature difference will not be affected materially

With reference to Figure 3.7, addition of PCM implies an additional layer of resistance R_6 in series in the circuit. Using Table 3.1 and Equation 3.11, the additional resistance, due to PCM layer, R_6 is calculated as

R_6=0.111 K/W

It is observed that this resistance is quite high compared to PV only resistance of 0.0036 K/W.

The equivalent resistance for the PV-PCM system is thus

$R_{equiv., PV\text{-}PCM}$ = 0.00036+0.11111= 0.11147 K/W

Following the same reasoning for apportionment of heat flow through the PV-PCM system as for the PV reference only system (Art. 3.6.2), the temperature difference (T_1-T_2) between front and back surfaces of the PV-PCM under steady state condition can be calculated as

$(T_1\text{-}T_2)_{PV\text{-}PCM} = q_x \times R_{equiv., PV\text{-}PCM}$ = (0.2 x720) x 0.11147 = 16.05 ^{0}C.

It is observed that the temperature difference between the front and the back surface for a PV panel is negligibly small (0.5^{0}C) for conduction of heat flow through the bulk of the PV layers at any instant of time. This is because the thermal resistance for the PV cell as a whole is very small (due to the very small thicknesses of the layers and hence the temperature of the front surface and back surface of the PV cell are practically same and the temperature distribution through the PV cell is uniform at any instant of time throughout the bulk of the PV cell.

Thus, it may be concluded that the heat flow through the PV cell faces very little resistance to heat flow in the bulk of the material. However, the final heat flow out during the transient heating time will also depend upon the heat dissipation from the PV cell surfaces and hence it can be said that heat transfer can be enhanced (thereby limiting the PV cell temperature rise), if heat dissipation can be improved from the surfaces. This indicates that placement of fins at the external back surface of the PV cell can be useful. However, this arrangement needs a change in the manufacturing process which would integrate the fins at the back with the PV cell. Further, this arrangement is not applicable for thousands of PV solar units already in operation. The resulting temperature control with this arrangement may also be not as effective.

Vita Auctoris

Name: **Joyjit Ghosal**

Place of Birth: **Kolkata, India**

Education: **Master of Applied Science, University of Windsor, Canada, 2019**